X-622-66-307

NASA TM X-55587

AN ATLAS OF STRATOSPHERIC MEAN ISOTHERMS DERIVED FROM TIROS VII OBSERVATIONS

FACILITY FORM 602

N67 11365 (ACCESSION NUMBER)	(THRU)
85 (PAGES)	1 (CODE)
TMX-55587 (NASA CR OR TMX OR AD NUMBER)	20 (CATEGORY)

GPO PRICE $ ______

CFSTI PRICE(S) $ ______

Hard copy (HC) 2.50

Microfiche (MF) .75

ff 653 July 65

BY
JAMES S. KENNEDY
CAPTAIN, USAF

JULY 1966

NASA
GODDARD SPACE FLIGHT CENTER
GREENBELT, MD.

X-622-66-307

AN ATLAS OF STRATOSPHERIC MEAN ISOTHERMS DERIVED FROM TIROS VII OBSERVATIONS

James S. Kennedy*
Captain, USAF

GODDARD SPACE FLIGHT CENTER
Greenbelt, Maryland

*Air Weather Service member temporarily attached to Goddard Space Flight Center.

N67-11365

ABSTRACT

The TIROS VII Meteorological Satellite, launched 19 June 1963, was equipped with a medium resolution scanning radiometer. One of the spectral regions observed, the 15 micron region, largely measured the emission from the stratosphere. The spatial and temporal variations of the observed 15 micron emission were found to correspond closely to major thermal patterns of the stratosphere. The data have been compiled and mapped on a series of ten-day mean charts, normally at five-day intervals, covering the 13-month period subsequent to launch. The charts comprise data from regions of the globe normally inaccessible to conventional means and are presented as a guide to stratospheric behavior during the period of June 1963 to July 1964.

Author

CONTENTS

LIST OF ILLUSTRATIONS

LIST OF TABLES

AN ATLAS OF STRATOSPHERIC MEAN ISOTHERMS DERIVED FROM TIROS VII OBSERVATIONS

1. INTRODUCTION

The TIROS VII weather satellite, launched 19 June 1963, included a five-channel scanning radiometer among its complement of meteorological sensors. One of the radiometric channels was sensitive in the 15 micron spectral region where atmospheric emission is predominately due to the 15 micron vibration-rotation band of carbon dioxide. The primary goal of the 15 micron experiment was to examine the suitability of the spectral region for horizon sensing (Bandeen et al., 1963). The advantages inherent in the 15 micron region are: (1) the very short unit optical depths of the troposphere minimize the effect of tropospheric phenomena, specifically clouds, on the outgoing emission, and (2) carbon dioxide is the only major absorber in the 5 to 30 micron region, the region which encompasses the bulk of atmospheric emission, which is present in sensibly constant mixing ratios at altitudes of significant emission.

Implicit in the aforementioned properties of the 15 micron region is the fact that variations in observed emission are due primarily to horizontal variations in the temperature field at levels of significant emission. It will be shown that most of the emission reaching the satellite originates in the stratosphere. Thus a mapping of observed emission duplicates, to a large extent, the major thermal patterns of the stratosphere.

While the extension of in situ measurements of upper atmosphere parameters, especially since the International Geophysical Year of 1957, has been accelerated, large areas of sparse data exist even in the Northern Hemisphere. The Southern Hemisphere, except for localized areas, is a major data gap. Therefore, we feel that even relatively unconventional means such as the remote measurements by the 15 micron channel of TIROS VII, should be studied to the fullest extent to explore the behavior of hitherto forbidden areas. To quote Prof. V.P. Starr, ". . . many new conceptions concerning the operation of the atmosphere are to be looked for at the borderline of measurability" (Starr and Wallace, 1964).

The TIROS VII 15 micron data have been compiled into a series of ten-day, global mean-temperature charts covering a period of 13 months. The following sections will examine in more detail the physical significance of the 15 micron sensor and describe the manner in which the charts were constructed.

2. 15 MICRON RADIOMETER

The 15 micron channel of the five-channel scanning radiometer was sensitive from 14.8 to 15.5 microns. The field of view of the instrument was five degrees between the half-power points. From the mean satellite altitude of 635 km, the minimum instantaneous area viewed as projected on the earth was about 2400 sq km when the optical axis was normal to the surface.

The optical axis of the radiometer was at a fixed angle of 45 degrees from the spin axis of the satellite. The radiometer viewed in two colinear directions, 180 degrees apart, known as floor side and wall side. At least one side was exposed to outer space at all times, providing a check point of absolute zero. The spinning motion of the satellite at the rate of about 10 rpm, combined with the orbital motion with the spin axis approximately fixed with respect to inertial space, produced a rather complicated pattern of scanning (Allison and Warnecke, 1964; also Staff Members, 1964, Vol. 1, App. B). The orbital inclination of the spacecraft was 58.2 degrees, prohibiting observations poleward of about 60 degrees latitude.

A detailed description of the components of the radiometer and its method of operation is contained in the TIROS VII Radiation Data Catalog and Users' Manual (Staff Members, 1964). The emphasis here is on the relation of the measurements to stratospheric temperatures.

It is possible to decompose the total outgoing radiation into contributions as a function of altitude based on the radiative properties of carbon dioxide and the spectral response of the radiometer (Nordberg *et al.*, 1965). Figure 1 shows the results for four model atmospheres and two extremes of nadir angle. ψ (h) expresses the weight given to various altitudes.

While the weighting curves are rather blunt and broad, it may be seen that most of the outgoing energy originates in the region from 10 to 35 km. The absolute maxima at low nadir angles is at about 23-25 km which corresponds to roughly a pressure of 25-35 mb. Figure 1(c) shows that the weighting functions shift upward somewhat at larger nadir angles. To reduce the dependence of the observations on nadir angle, only measurements made with nadir angles of 40 degrees or less were used in this study.

At low nadir angles, more than 96 percent of the total outgoing intensity originates at levels above 10 km. Cloudiness, therefore, does not greatly affect the observed energy. The effect of cloudiness would be the greatest for a tropical atmosphere at zero degree nadir angle, due to the high tropopause and large difference between surface and tropopause temperature. Since the Tropics is a

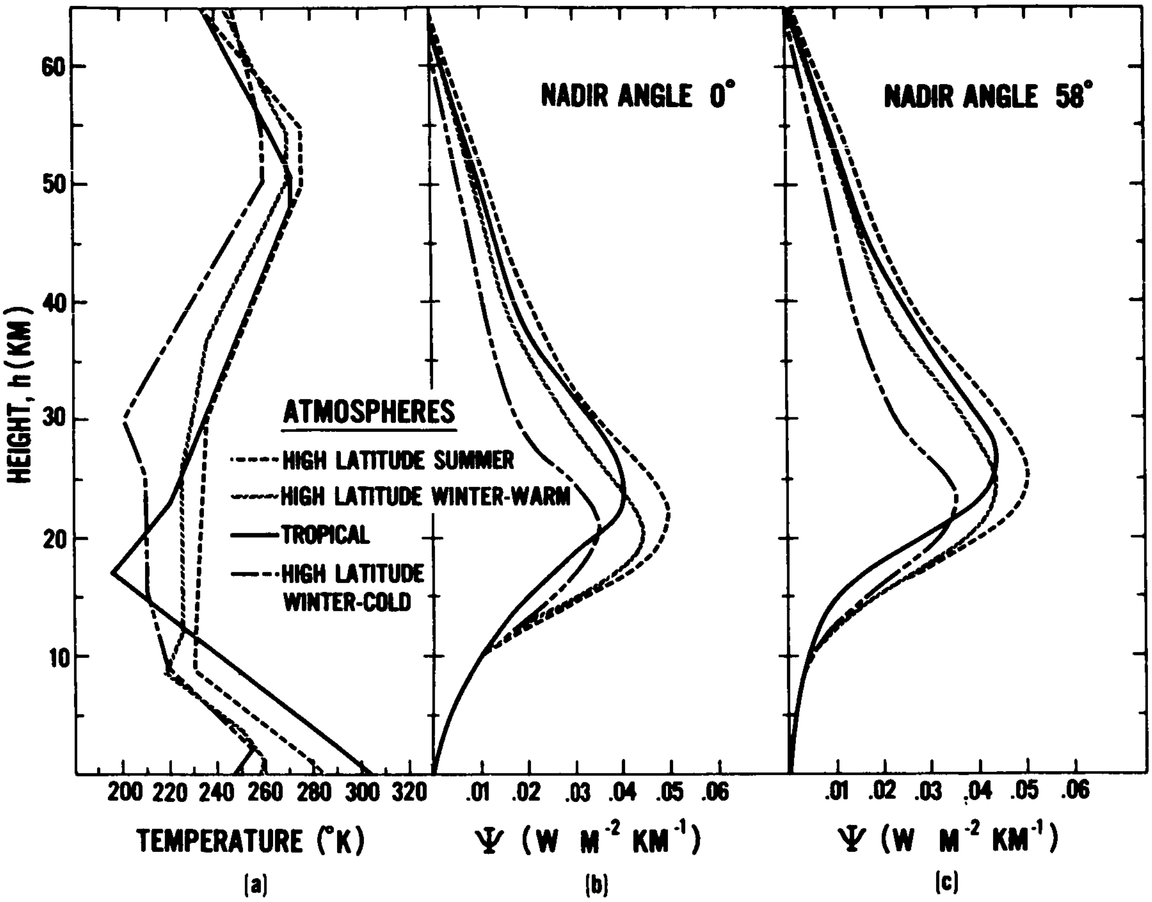

Figure 1. (a) Typical temperature profiles based on proposed supplements to the "U.S. Standard Atmosphere 1962" for 60° North summer, 60° North winter (warm and cold) and 15° North (b) Weighting functions $\psi(h)$, applying to the measured outgoing radiance; nadir angle = 0° (c) Weighting functions, $\psi(h)$, applying to the measured outgoing radiance; nadir angle = 58°

region of persistent high cloudiness, the effect of clouds was calculated from radiative transfer theory to obtain a limiting "worst case" (Kunde, 1966). The result was found to be that an overcast at the tropopause would reduce the derived mean temperature by only three degrees Kelvin as compared with clear skies. At higher latitudes, the effect is much less. Due to the very weak horizontal temperature gradients in the tropical stratosphere, cold pockets associated with areas of persistent high cloudiness are frequently found. The lower readings may be partially due to actual colder stratospheric temperatures caused by cloudy insulation of the stratosphere from tropospheric heat sources.

The observations at higher latitudes are more physically meaningful in the context of stratospheric dynamics partly because the effect of cloudiness is nil but more importantly, because the lapse rates from 10 to 30 km are nearly isothermal as shown in Figure 1(a). Weighted mean temperature patterns at high latitudes will correspond more nearly to true temperature patterns at a given level than in the Tropics where there is a sharp discontinuity at the tropopause. An added complication in the Tropics is the double reversal of the horizontal poleward temperature gradient from troposphere to lower stratosphere and from lower stratosphere to mid-stratosphere.

The energy received by the radiometer was converted into units of equivalent blackbody temperature (T_{BB}). Equivalent blackbody temperature is defined as the temperature of an isothermal blackbody filling the field of view (as in the laboratory calibration) which would cause the same response from the radiometer as does the generally non-Planckian spectral distribution of the radiation emerging from the top of the atmosphere in the direction of the satellite. Since a vertically-weighted-mean temperature does not easily fit into the framework of existing conventional measurements, we feel that the global patterns produced from 15 micron data are much more meaningful than the absolute values of equivalent blackbody temperature. The next section describes the manner in which the 15 micron data are displayed.

3. DATA DEFICIENCIES

While knowledge of stratospheric behavior from existing conventional measurements was the prime consideration in the format of the data, modifications and compromise were necessitated by the following factors: (1) progressive degradation of the radiometer, (2) low signal-to-noise ratio of the radiometer, (3) errors in geographically locating the data, (4) gaps in global coverage.

3.1 Degradation

The radiometer did not have onboard calibration except for a zero degree reference when viewing outer space. The performance of the instrument was checked by computing mean quasi-global temperatures as a function of time. (The quasi-globe is that portion of the earth viewed by TIROS VII, roughly 65 N to 65 S latitude.) It was found that the mean temperatures decreased sharply during the first 30 days after launch and decreased at a much slower rate thereafter. The cause is unknown. In addition, the wall side and floor side recorded different readings for the same target viewed a few minutes apart. The difference between wall and floor side measurements increased with time and was also found to be a function of the temperature of the viewed region. Corrections were determined by fitting smooth curves through the global mean wall and floor side temperatures and correcting back to temperatures shortly after launch. A detailed description of the degradation is contained in the TIROS VII manual (Staff Members, 1964). Briefly each measurement was modified by applying a correction, ΔT, in the form,

$$\Delta T_{f,w}(t) = a_{f,w}(t) + b_{f,w}(t) T_{f,w} \quad (1)$$

where
- f = Floor Measurement
- w = Wall Measurement
- a, b = Correction Factors
- t = Time
- T = Uncorrected Observed Temperature

The correction factors, a and b, were determined from degradation nomograms in the TIROS VII manual (Staff Members, 1965, Vol. 3). The time scale of the degradation was sufficiently slow that the factors could be computed for the mid-date of any map and used for all data included in the map, usually that observed over a 10-day period. The degradation of the instrument casts some doubt on the validity of the absolute value of the measurements but does not greatly affect the final temperature patterns.

3.2 Signal-To-Noise Ratio

The 15 micron channel measurements were characterized by a random noise component with an rms amplitude of about 5 degrees Kelvin. The noise component was largely eliminated by time and spatial averaging which will be described later.

3.3 Geographic Location

Depending on the angle between the spin axis and local vertical, the radiometer scans the earth in one of three distinctive patterns (Allison and Warnecke, 1964). When the spin axis is nearly vertical, the radiometer traces a helical pattern on the ground which does not cross the horizon, known as closed mode. When the spin axis is nearly horizontal, the radiometer scans the earth alternately from floor and wall sides, known as the alternating open mode. At intermediate angles, which constitute the major portion of the total data, the radiometer describes a series of open arcs, all traced by either the floor or wall side, known as the single open mode.

In the single open mode the horizon is traversed twice during each rotation of the satellite, and the known length and time of the scan enable the data to be precisely located. In the closed mode, the spin rate of the spacecraft must be interpolated from the single open mode data measured just prior and subsequent to the closed mode. Since the spin rate varies somewhat due to magnetic torques and other factors, the data are subject to misplacement. In the alternating open mode, the computer distinguishes between the alternate floor and wall side measurements by the respective lengths of the earth-viewed portion of the scans. Midway through the alternating mode sequence, the floor and wall scans are approximately equal and the computer is apt to mislabel the scans, resulting in a gross mislocation of data.

As mentioned in a previous section, the computer was instructed to reject all data with nadir angles greater than 40 degrees to minimize changes in the weighting curves. To avoid mislocation of data, a proviso was added that all scans with minimum nadir angles occurring within the scan greater than 38 degrees be rejected completely. All ambiguous portions of the alternating mode cycle were thus eliminated as well as most of the closed mode.

3.4 Data Coverage

The orbital inclination of the satellite, 58.2 degrees, prohibited measurements poleward of approximately 60 degrees latitude. Limitations in acquiring the data from the spacecraft resulted in additional gaps within the confines of the quasi-globe. Of the nearly 15 orbits per day experienced by TIROS VII, a maximum of nine orbits can be interrogated by the three Command and Data Acquisition stations in North America during any given interrogation day. The interrogation day includes all orbits interrogated in the series of nine consecutive orbits which come within range of the acquisition stations during each 24-hour period. The interrogation day often occurs on two seperate calendar days. The orbits acquired on one interrogation day are compiled on one Final Meteorological Radiation Tape (FMRT).

Two regions of the quasi-globe are never viewed, Central Siberia and southern South America. On most days, less than the optimum nine orbits are acquired. In the latter half of the 13 months of mapped 15 micron data, rarely are more than four orbits acquired per interrogation day. To fill out the quasi-globe and also to overcome random noise, several FMRT's, usually ten, were combined to produce one map. The rationale for ten-day maps will be covered in the next section.

4. MAPPING PROCEDURES

While grouping and altering the 15 micron data were necessitated by technical deficiencies as outlined in the previous section, ultimately, the characteristic spatial and time scales of the major stratospheris phenomena must be considered to arrive at a meteorologically useful product. In brief, the stratosphere above 20 km is characterized by large scale, slow moving disturbances superimposed on a zonal current. Teweles (1963) has shown that most of the eddy activity is explained by zonal wave numbers one through four. Boville (1960), using 25 mb temperature data from Resolute, N.W.T., performed a spectral analysis and found that most of the variance is found in the seasonal shift of temperature, with a secondary maximum in the 16 to 32 day range associated with baroclinic waves. The findings of these authors guided the choice of length and time parameters.

A Mercator map base was selected for the data display as being most suitable for the quasi-globe. The data were gathered on a rectangular grid of equispaced points, each grid point being assigned the average value of all observations falling within its square of influence. The spacing of grid points was constant at five degrees of longitude in the zonal direction and variable, ranging from five degrees of latitude at the equator to about 2.5 degrees at latitude 60 degrees, in the meridional direction. The zonal grid spacing permits the resolution of disturbances up to wave number 36; however, spatial filtering was employed to filter such high wave numbers.

The long time scale of stratospheric phenomena enabled us to compile the data into ten-day mean charts at five-day intervals. Actually, the FMRT, rather than the calendar, was our basic time unit and the charts comprise 9 to 11 FMRT's depending on circumstances. During the course of the 13 months of observation, there were days or groups of days when no data were recorded. The FMRT's included in a chart were then either expanded or contracted to avoid overlapping such periods. The days of no data also prohibited the maintenance of a constant five day interval between charts throughout the 13 months. The term mean chart is somewhat of a misnomer. Certain areas of the quasi-globe may have been sampled once, daily, or not at all during the period of a chart. Slow moving stratospheric disturbances and strong spatial smoothing are the two factors which mitigated the random sampling of data.

The use of about ten days of data helped to overcome two of the major data deficiencies: data gaps and random noise. Throughout much of the 13 months of observation, a ten-day period comprises 50 to 70 orbits, and even during data-poor periods, 20 to 30 orbits. The average temperature at an individual grid point usually comprised hundreds, often thousands of observations.

After the data had been gathered on the grid array, two factors were dealt with before analysis could begin. First, all grid points of the quasi-globe did not have an assigned temperature. Any average temperature comprising less than 40 observations was rejected because of random noise. Since an electronic curve plotter was used for analysis, a complete field of data was required. The grid array was completed by linear interpolation across data gaps in a zonal direction. This method approximates the technique a human analyst would employ.

Second, the temperature field contained many short wave perturbations which were considered to be noise. Partially, the perturbations were due to the quantization of mean temperatures into integer values by the computer. An electronic curve plotter cannot selectively ignore such minor variations and therefore the temperature was smoothed by a two dimensional spatial filter.

The filter was designed to leave the longest wavelengths unchanged in amplitude and phase and eliminate the shortest wavelengths. The filter was constructed following the method of Wallington (1962).

Basically, two different filters each having three weights in the meridional direction and nine weights in the zonal direction were passed over the grid array and the weighted temperature was assigned to the central value. The same result could have been derived in one step using a five-by-seventeen filter but would have had to be modified when the operator included external grid points. Using two three-by-nine filters in succession resulted in the loss of only the northernmost and southernmost line of data. Since the data are cyclic with period 2π in the zonal direction, the array was equivalent to a hollow cylinder with only the top and bottom lines of data being external points.

The first filter had a weight array as follows:

0.002	-0.043	0.354	-1.358	2.342	-1.358	0.354	-0.043	0.002
0.004	-0.086	0.708	-2.716	4.684	-2.716	0.708	-0.086	0.004
0.002	-0.043	0.354	-1.358	2.342	-1.358	0.354	-0.043	0.002

The second filter was,

0.002	0.012	0.031	0.051	0.058	0.051	0.031	0.012	0.002
0.004	0.024	0.062	0.102	0.116	0.102	0.062	0.024	0.004
0.002	0.012	0.031	0.051	0.058	0.051	0.031	0.012	0.002

Both filters are symmetrical in the meridional and zonal directions to eliminate any phase shift of the filtered harmonics. By taking the Fourier transform of the filter weights, it is possible to compute the response of the filter as a function of wavelength (Holloway, 1958). The wavelength response is shown in Figure 2 for the equivalent five-by-seventeen filter. Note that for the longest zonal harmonics the response is near unity, indicating that they are unaffected by the filtering. At a wavelength of three grid intervals, the zonal response is negative, indicating a 180 degree phase shift. The response, however, is only 10

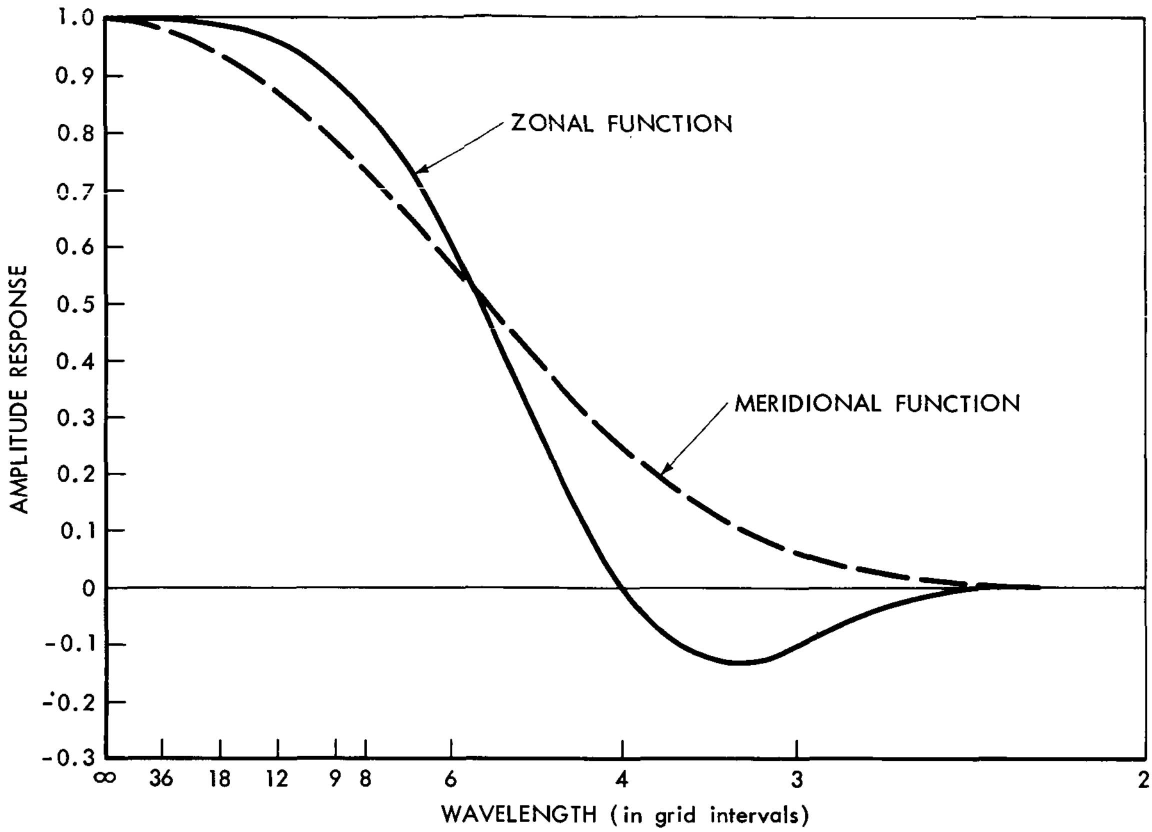

Figure 2. Amplitude Response of the Spatial Smoothing Operator in the Meridional and Zonal Directions as a Function of Wavelength

percent and disturbances at this wavelength were largely eliminated. Zonal disturbances at wavelengths of two and four grid intervals were eliminated completely.

After the smoothing operation, the data were analyzed by an electronic curve plotter at intervals of two degrees Kelvin. The resulting charts are presented in the next section.

5. TEN-DAY MEAN CHARTS

The TIROS VII 15 micron data have been compiled and mapped on a series of seventy-three ten-day mean charts, normally at five-day intervals, covering the 13-month period from launch (19 June 1963) to 16 July 1964. The charts are numbered such that in general a series of successive and contiguous ten-day charts (without time overlap) is made up of either the odd-numbered charts or the even-numbered charts. However, the phase of the two sets is staggered such that the beginning points in time of the maps of say the odd-numbered set occur at the midpoints in time of the maps of the even-numbered set or vice versa.

Because of occasional interrogation problems resulting in a failure to acquire the data successfully, the pattern of time-continuity is broken at several points in both sets of charts. The odd-numbered set is the more nearly continuous, suffering only one-to-three day breaks surrounding the five entries of "NO DATA ACQUIRED" in Table I, plus an eight-day break during the interval 5-12 May 1964. The even-numbered set suffers five extensive breaks in the intervals identified by entries of "NO DATA ACQUIRED" in Table I, plus a seven-day break during the interval 10-16 May 1964. Hence, though the final chart is numbered 78, there are five fewer actual charts represented because of the indicated intervals where no data were acquired. The degradation-corrected measurements on the charts are given in terms of equivalent blackbody temperatures (T_{BB}). All measurements were made in the nadir angle range $0° - 40°$. Other pertinent data concerning the charts are documented in Table I.

ACKNOWLEDGMENTS

This project was conducted under the guidance and supervision of Mr. William R. Bandeen, Head of the Planetary Radiations Branch, Goddard Space Flight Center. The treatment of the vast amount of data was facilitated by Mr. Robert T. Hite, Head of the branch computing section, ably assisted by Mr. Gary Wolford and Mr. Walter Musial.

The efforts of these individuals are hereby gratefully acknowledged.

Table I
Documentation Data Concerning 15 Micron Charts

CHART NO.	DATES (INCL.)	FMRT REELS	ORBITS (INCL.)	TOTAL NO. OF ORBITS	CORRECTION FACTORS (cf EQUATION 1)				PAGE
					a_w	b_w	a_f	b_f	
1	19 Jun-28 Jun 63	333-342	0001-0136	56	13.2	-0.047	-23.0	0.098	13
2	23 Jun-2 Jul 63	337-346	0058-0192	55	12.4	-0.042	-24.0	0.107	14
3	29 Jun-7 Jul 63	343-351	0146-0270	47	10.8	-0.033	-26.0	0.115	15
4	3 Jul-12 Jul 63	347-356	0205-0343	60	9.4	-0.025	-26.2	0.118	16
5	8 Jul-17 Jul 63	352-361	0277-0416	64	7.8	-0.012	-27.0	0.120	17
6	13 Jul-22 Jul 63	357-366	0350-0489	67	5.4	0.0	-27.5	0.125	18
7	18 Jul-26 Jul 63	362-370	0423-0547	60	5.6	0.0	-28.2	0.128	19
8	22 Jul-31 Jul 63	366-375	0481-0620	62	5.6	0.0	-28.2	0.128	20
9	27 Jul-5 Aug 63	371-380	0554-0692	50	5.8	0.0	-28.6	0.130	21
10	31 Jul-9 Aug 63	375-384	0613-0751	46	5.9	0.0	-29.0	0.131	22
11	5 Aug-13 Aug 63	381-389	0702-0821	44	6.0	0.0	-29.2	0.132	23
12	9 Aug-18 Aug 63	384-394	0744-0896	52	6.0	0.0	-29.5	0.134	24
13	14 Aug-23 Aug 63	390-399	0831-0970	52	6.2	0.0	-30.0	0.135	25
14	18 Aug-27 Aug 63	394-403	0890-1028	59	6.4	0.0	-30.1	0.137	26
15	24 Aug-1 Sep 63	400-408	0977-1101	49	6.5	0.0	-30.5	0.140	27
16	27 Aug-5 Sep 63	403-412	1021-1160	53	6.7	0.0	-30.8	0.141	28
17	2 Sep-11 Sep 63	409-418	1109-1246	56	6.9	0.0	-31.1	0.143	29
18	6 Sep-15 Sep 63	413-422	1167-1306	52	7.1	0.0	-31.5	0.145	30
19	12 Sep-20 Sep 63	419-427	1255-1379	47	7.3	0.0	-32.0	0.147	31
20	16 Sep-25 Sep 63	423-432	1313-1450	52	7.6	0.0	-32.1	0.148	32
21	21 Sep-30 Sep 63	428-437	1387-1525	51	7.8	-0.001	-32.6	0.150	33
22	26 Sep-5 Oct 63	433-442	1461-1597	57	8.0	-0.002	-33.0	0.152	34
23	30 Sep-9 Oct 63	437-446	1517-1655	61	8.2	-0.003	-33.3	0.153	35
24	5 Oct-14 Oct 63	442-451	1591-1729	53	8.4	-0.004	-33.7	0.155	36
25	10 Oct-19 Oct 63	447-456	1664-1801	56	8.8	-0.006	-34.0	0.157	37
26	15 Oct-24 Oct 63	452-461	1736-1875	56	9.0	-0.007	-34.5	0.159	38
27	19 Oct-28 Oct 63	456-465	1794-1933	58	9.4	-0.009	-34.9	0.161	39
28	24 Oct-2 Nov 63	461-470	1867-2006	56	9.7	-0.010	-35.2	0.163	40
29	29 Oct-7 Nov 63	466-475	1940-2094	57	10.0	-0.011	-35.9	0.165	41
30	3 Nov-12 Nov 63	471-480	2013-2166	52	10.4	-0.013	-36.2	0.166	42
31	7 Nov-16 Nov 63	475-484	2086-2225	42	10.7	-0.014	-36.7	0.168	43
32	13 Nov-22 Nov 63	481-490	2176-2312	50	11.2	-0.016	-37.1	0.170	44
33	17 Nov-27 Nov 63	485-495	2234-2379	55	11.4	-0.017	-37.7	0.173	45
34	NO DATA ACQUIRED								
35	1 Dec-10 Dec 63	496-505	2437-2575	37	12.5	-0.021	-39.0	0.178	46
36	6 Dec-15 Dec 63	501-510	2512-2647	43	12.9	-0.022	-39.5	0.181	47
37	10 Dec-19 Dec 63	505-514	2568-2706	48	13.2	-0.023	-40.0	0.183	48
38	NO DATA ACQUIRED								
39	22 Dec-31 Dec 63	515-525	2743-2891	43	14.0	-0.026	-41.5	0.190	49
40	NO DATA ACQUIRED								
41	2 Jan-11 Jan 64	526-536	2909-3055	52	15.1	-0.030	-43.0	0.197	50
42	6 Jan-15 Jan 64	531-540	2977-3110	48	15.4	-0.031	-43.6	0.199	51
43	11 Jan-20 Jan 64	536-545	3050-3187	46	16.0	-0.033	-44.2	0.202	52
44	16 Jan-25 Jan 64	541-550	3126-3261	61	16.2	-0.034	-45.0	0.207	53
45	20 Jan-29 Jan 64	545-554	3181-3314	66	16.7	-0.036	-45.6	0.210	54
46	NO DATA ACQUIRED								
47	31 Jan-9 Feb 64	555-564	3341-3475	63	17.5	-0.039	-47.3	0.217	55
48	5 Feb-14 Feb 64	560-569	3414-3553	62	18.0	-0.041	-48.2	0.220	56
49	9 Feb-18 Feb 64	564-573	3472-3611	67	18.5	-0.043	-49.1	0.225	57
50	14 Feb-23 Feb 64	569-578	3545-3684	63	19.0	-0.045	-50.1	0.229	58
51	19 Feb-28 Feb 64	574-583	3620-3757	49	19.5	-0.047	-51.3	0.234	59
52	24 Feb-4 Mar 64	579-588	3691-3830	38	20.0	-0.049	-52.0	0.237	60
53	28 Feb-8 Mar 64	583-592	3750-3888	43	20.4	-0.051	-53.1	0.241	61
54	4 Mar-13 Mar 64	588-597	3827-3961	53	20.9	-0.053	-54.2	0.246	62
55	9 Mar-18 Mar 64	593-602	3896-4033	55	21.3	-0.055	-55.3	0.250	63
56	14 Mar-23 Mar 64	598-607	3969-4107	63	22.0	-0.058	-56.5	0.255	64
57	18 Mar-27 Mar 64	602-611	4027-4165	64	22.4	-0.060	-57.5	0.260	65
58	23 Mar-1 Apr 64	607-616	4100-4238	63	22.8	-0.062	-58.6	0.264	66
59	28 Mar-6 Apr 64	612-622	4173-4326	72	23.7	-0.065	-59.8	0.270	67
60	1 Apr-10 Apr 64	617-626	4246-4384	61	24.0	-0.067	-61.2	0.275	68
61	6 Apr-15 Apr 64	622-631	4319-4457	54	24.7	-0.070	-62.5	0.280	69
62	10 Apr-19 Apr 64	626-635	4377-4516	52	25.2	-0.072	-63.8	0.285	70
63	16 Apr-25 Apr 64	632-641	4466-4603	42	25.6	-0.074	-65.0	0.290	71
64	20 Apr-29 Apr 64	636-645	4525-4661	32	26.0	-0.076	-66.3	0.296	72
65	25 Apr-4 May 64	641-650	4598-4734	22	26.8	-0.079	-67.8	0.301	73
66	30 Apr-9 May 64	646-655	4671-4805	25	27.3	-0.081	-69.2	0.307	74
67	13 May-22 May 64	658-667	4861-4997	58	28.7	-0.087	-73.1	0.322	75
68	17 May-27 May 64	662-671	4917-5070	51	29.3	-0.090	-74.5	0.328	76
69	21 May-1 Jun 64	667-676	4990-5143	40	29.8	-0.092	-75.6	0.333	77
70	27 May-6 Jun 64	672-681	5077-5216	40	30.6	-0.095	-77.5	0.341	78
71	1 Jun-11 Jun 64	677-686	5150-5289	40	31.4	-0.098	-79.1	0.348	79
72	6 Jun-15 Jun 64	682-691	5224-5361	35	32.0	-0.100	-80.9	0.355	80
73	11 Jun-21 Jun 64	687-696	5296-5447	31	32.4	-0.102	-82.7	0.362	81
74	NO DATA ACQUIRED								
75	24 Jun-2 Jul 64	697-706	5479-5609	23	34.2	-0.109	-86.8	0.380	82
76	28 Jun-7 Jul 64	702-711	5544-5683	26	34.5	-0.110	-88.0	0.387	83
77	2 Jul-11 Jul 64	706-715	5605-5740	27	35.2	-0.113	-90.0	0.392	84
78	7 Jul-16 Jul 64	711-720	5678-5813	26	36.0	-0.116	-92.2	0.402	85

REFERENCES

Allison, L. J., and G. Warnecke, 1964: "Examples of Certain Data Reduction and Mapping Procedures Utilizing TIROS III Five-Channel Radiometer Data". Goddard Space Flight Center Document X-651-64-132, 30 April 1964, 38 pp.

Bandeen, W. R., B. J. Conrath and R. A. Hanel, 1963: Experimental confirmation from the TIROS VII meteorological satellite of the theoretically calculated radiance of the earth within the 15-micron band of carbon dioxide, J. A. S., 20, 609-614.

Boville, B. W., 1960: The Aleution Stratospheric Anticyclone. Jn. Met, 17, 329-336.

Holloway, J. L., 1958: Smoothing and filtering of time series and space fields, Adv. in Geophysics, 4, 351-389.

Kunde, V. G., 1966: unpublished personal communication.

Nordberg, W., W. R. Bandeen, G. Warnecke, and V. G. Kunde, 1965: Stratospheric temperature patterns based on radiometric measurements from the TIROS VII satellite. pp. 782-809 in Space Research V Ed. by P. Muller, North-Holland Publishing Company, Amsterdam.

Staff Members, 1964: TIROS VII Radiation Data Catalog and Users' Manual, Vol. 1, Goddard Space Flight Center, Greenbelt, Maryland, 30 September 1964, 256 pp.

Staff Members, 1965: TIROS VII Radiation Data Catalog and Users' Manual, Vol. 3, Goddard Space Flight Center, Greenbelt, Maryland, 15 October 1965, 269 pp.

Starr, V. P. and M. Wallace, 1964: Mechanics of eddy processes in the tropical troposphere, Pure and Applied Geophysics, 58, 138-144.

Teweles, S., 1963: Spectral Aspects of the Stratospheric Circulation During the IGY. Planetary Circ Proj Rpt No. 8, Meteor. Dept., Mass. Inst. of Tech., 191 pp.

Wallington, C. E., 1962: The use of smoothing or filtering operators in numerical forecasting. Q.J.R.M.S., 88, 470-484.

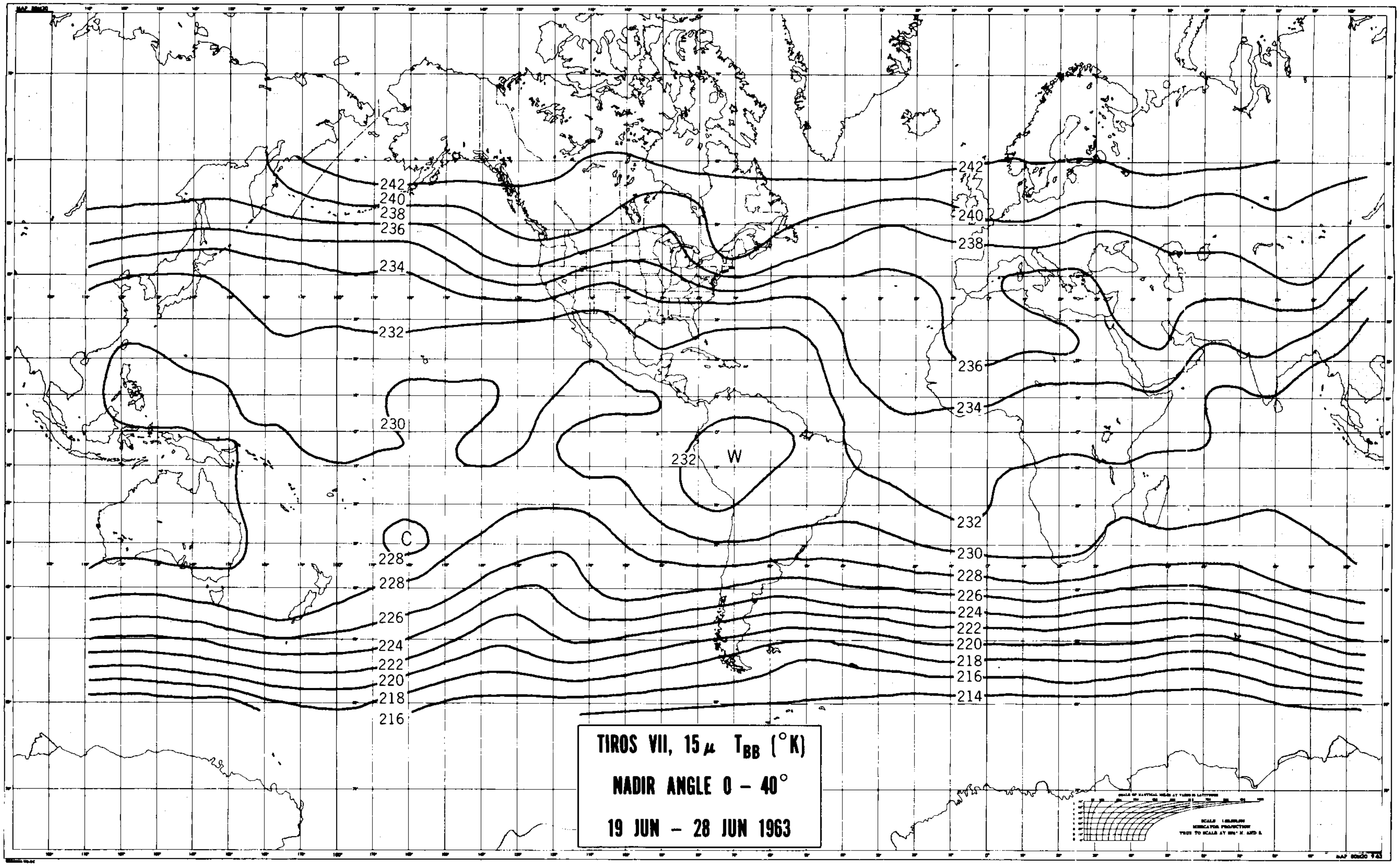
TIROS VII, 15μ T_{BB} (°K)
NADIR ANGLE 0 – 40°
19 JUN – 28 JUN 1963
242
240
238
236
234
232
230
228
226
224
222
220
218
216
214
W
C

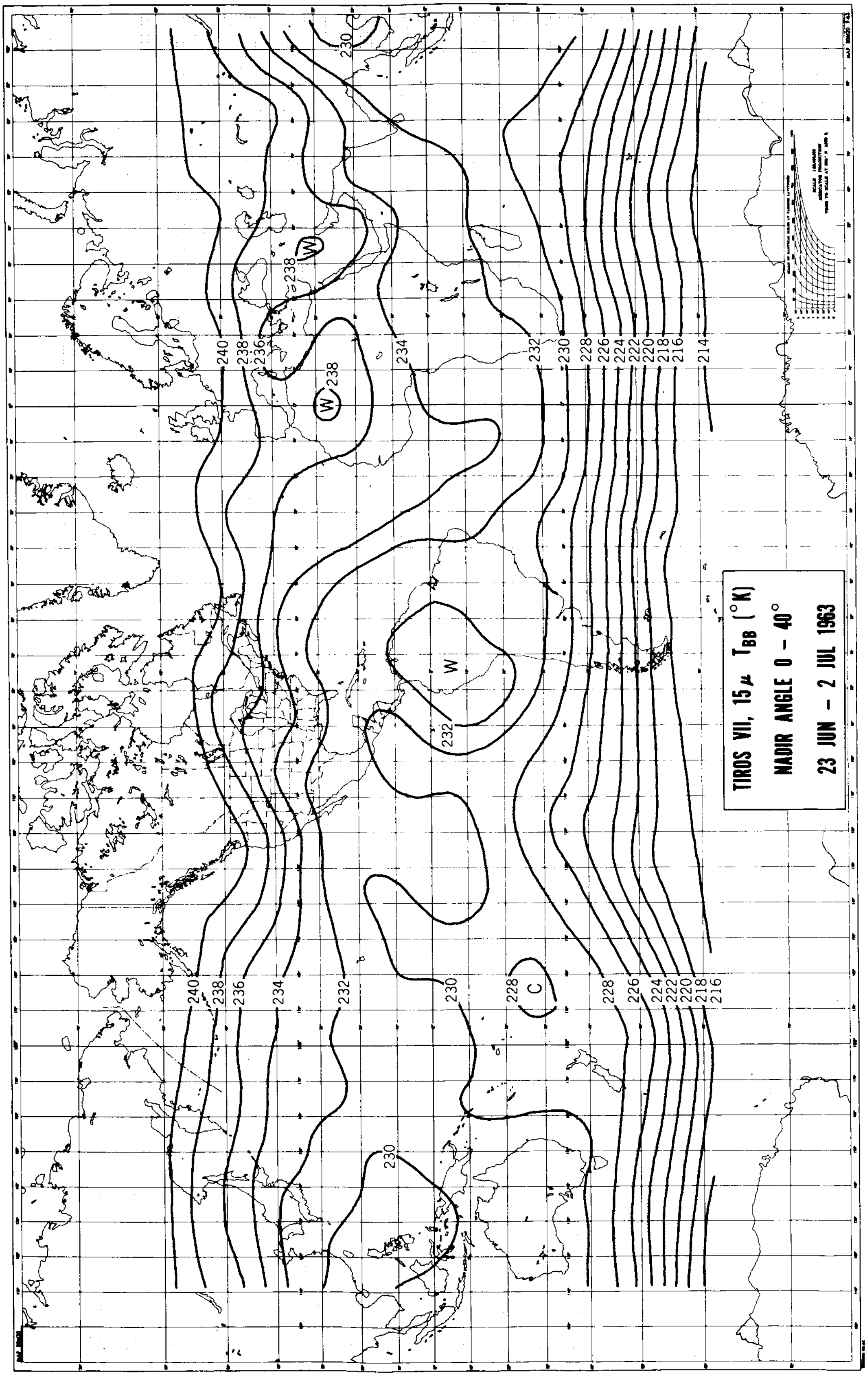
TIROS VII, 15μ T_{BB} (°K)
NADIR ANGLE 0 – 40°
23 JUN – 2 JUL 1963
240
238
236
234
232
230
228
226
224
222
220
218
216
214
W
C

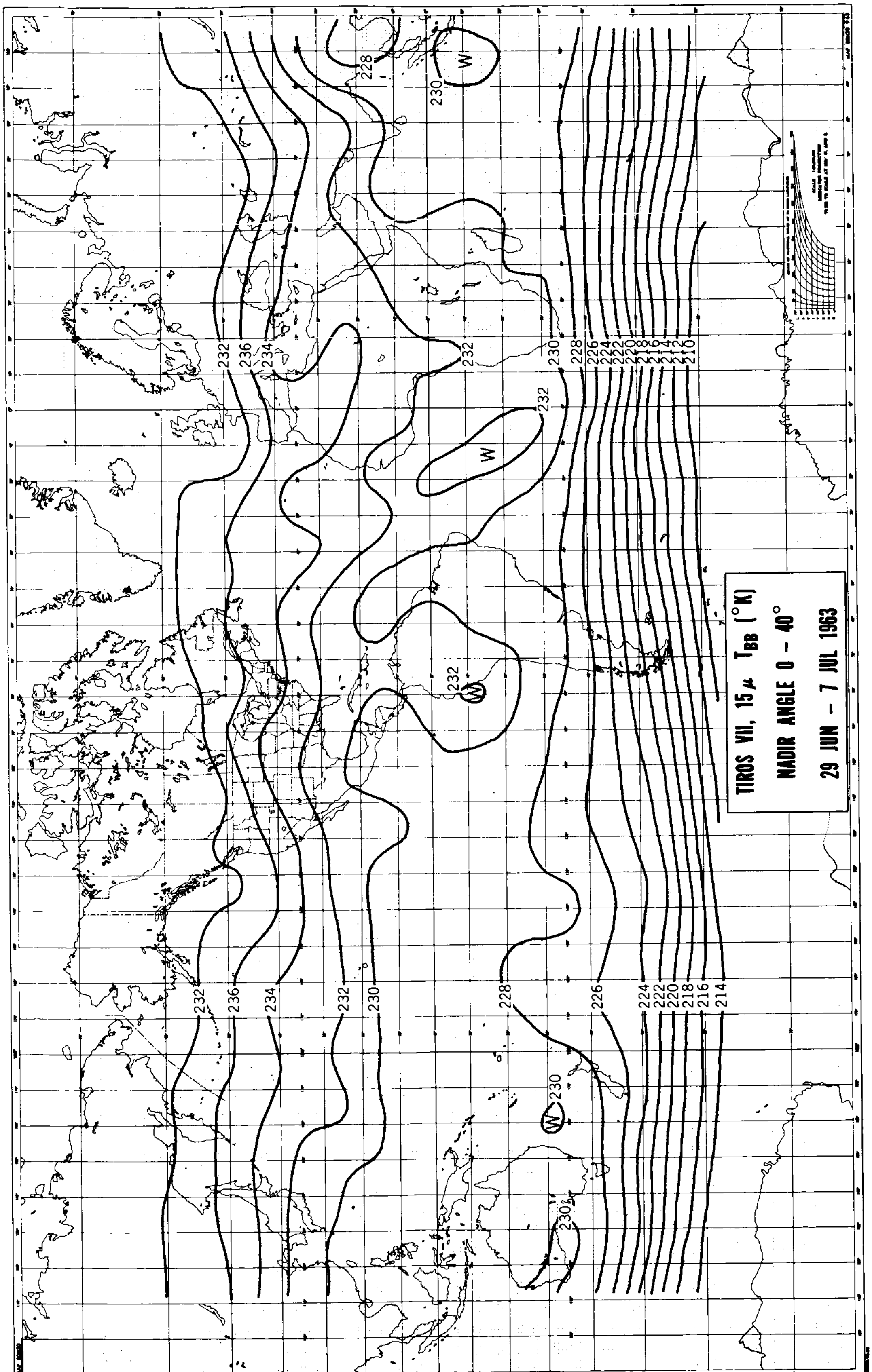
TIROS VII, 15μ T_{BB} (°K)
NADIR ANGLE 0 – 40°
29 JUN – 7 JUL 1963

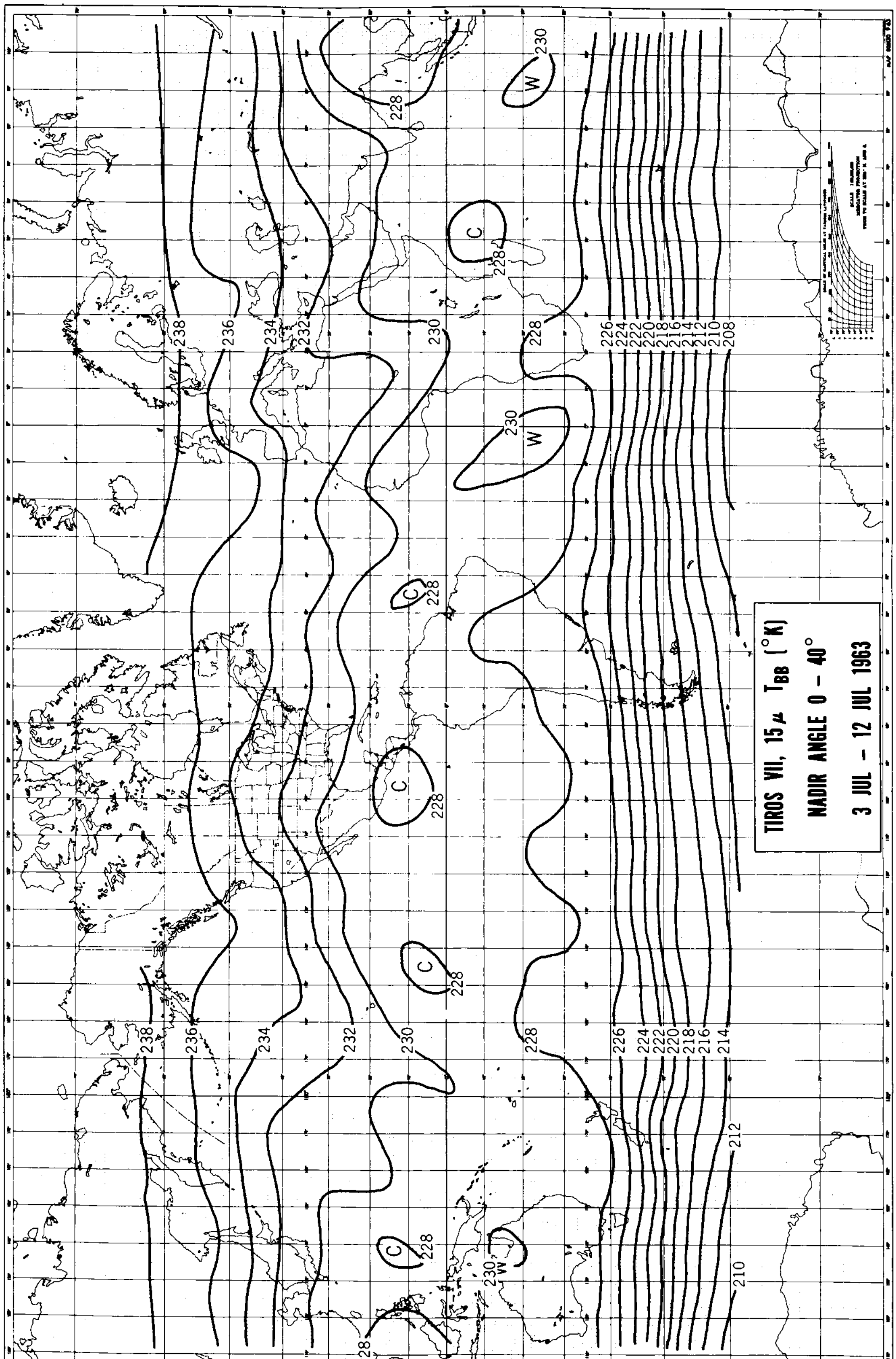
TIROS VII, 15μ T_{BB} (°K)
NADIR ANGLE 0 - 40°
3 JUL - 12 JUL 1963
238
236
234
232
230
228
226
224
222
220
218
216
214
212
210
208
C
W

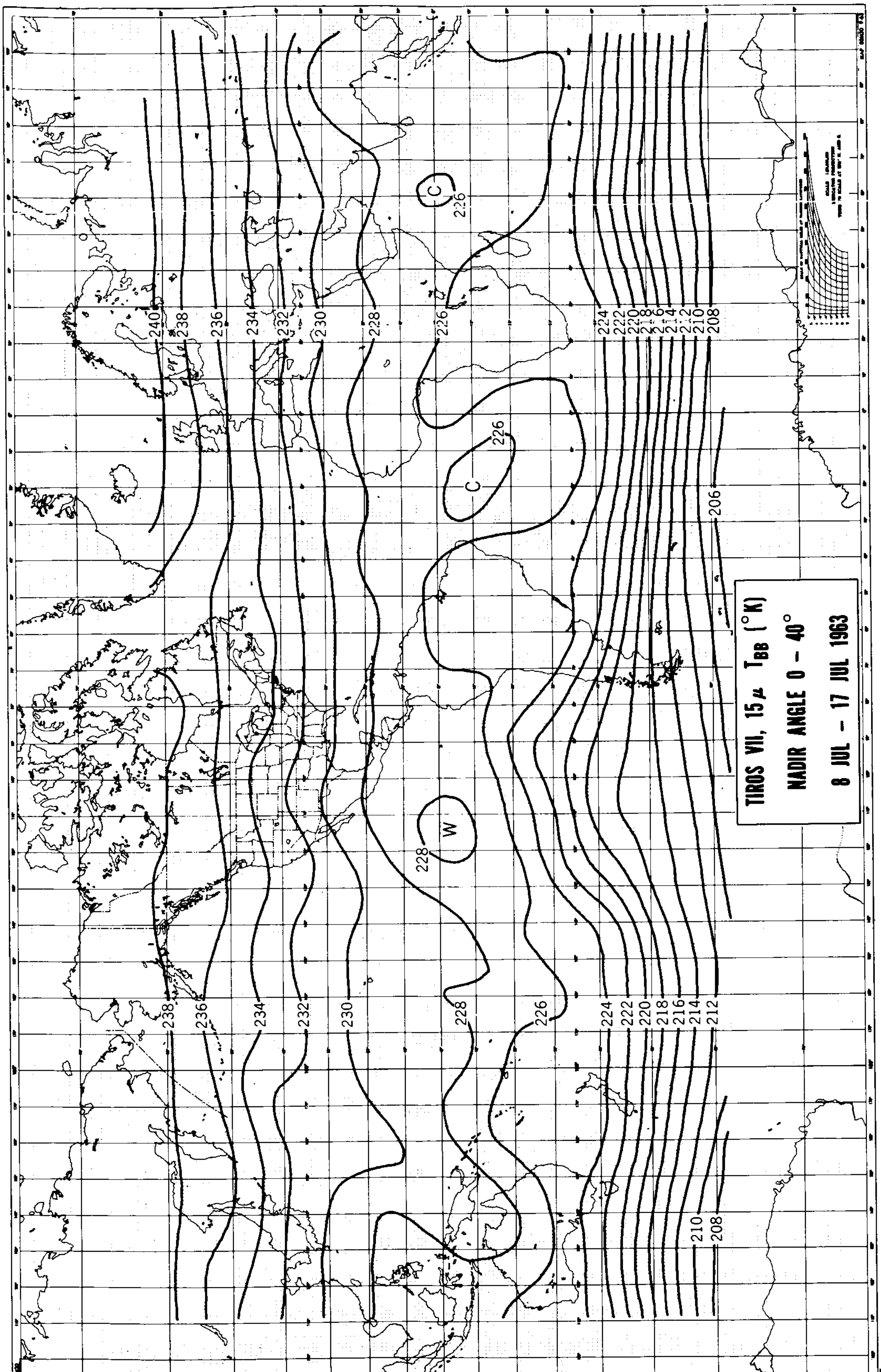
TIROS VII, 15μ T_BB (°K)
NADIR ANGLE 0 – 40°
8 JUL – 17 JUL 1963
240
238
236
234
232
230
228
226
224
222
220
218
216
214
212
210
208
206
C
W

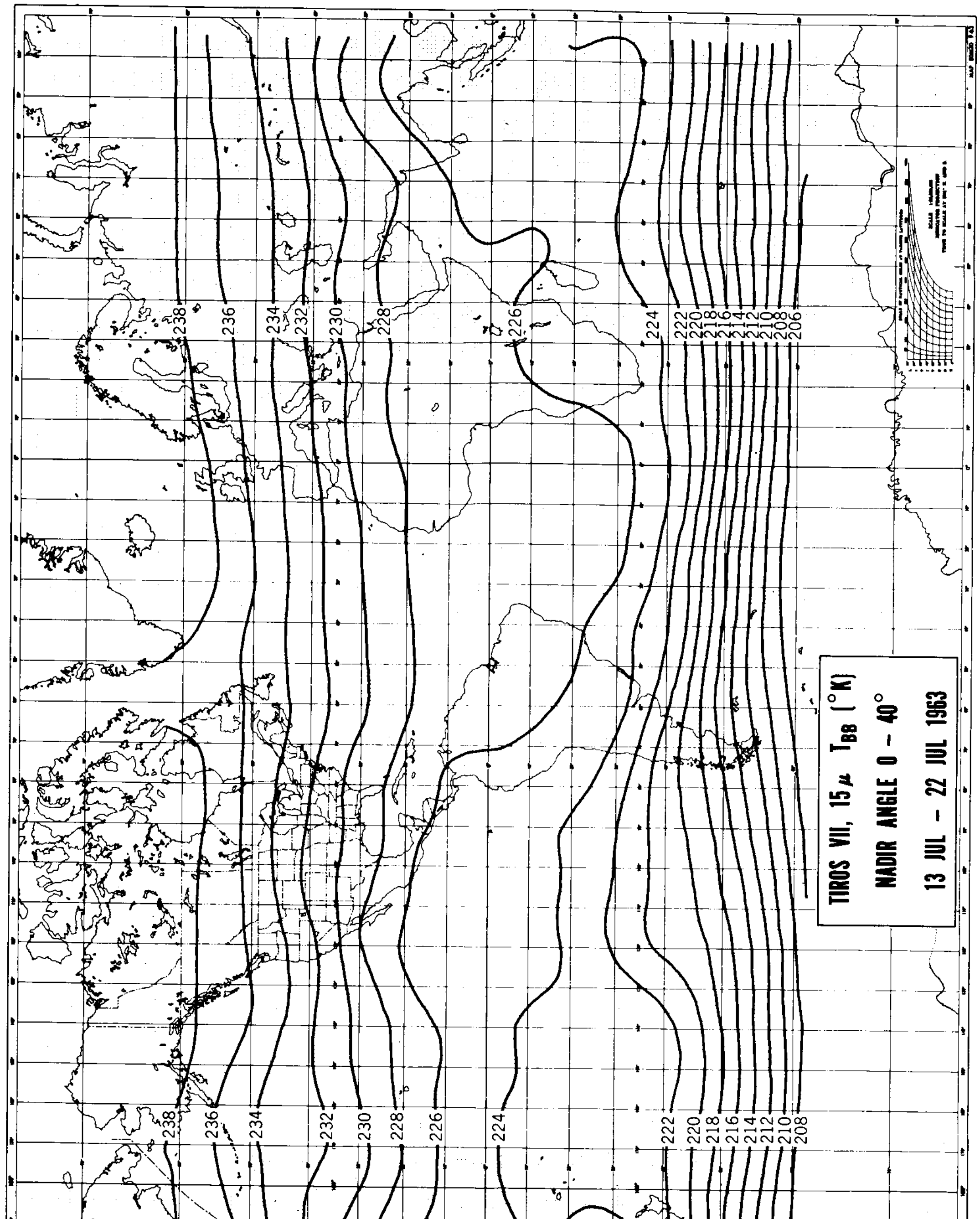
TIROS VII, 15μ T_{BB} (°K)
NADIR ANGLE 0 – 40°
13 JUL – 22 JUL 1963
238
236
234
232
230
228
226
224
222
220
218
216
214
212
210
208
206

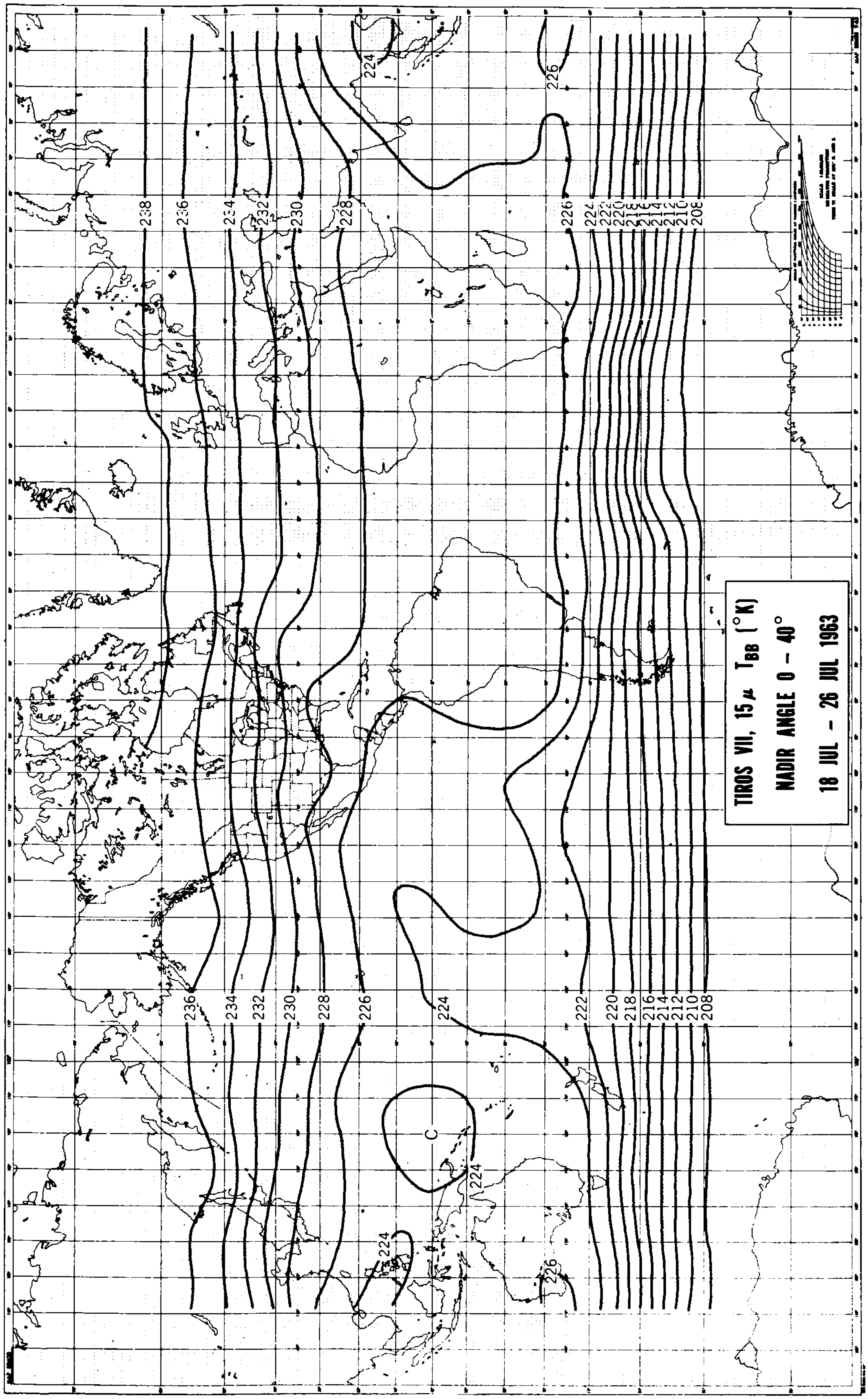
TIROS VII, 15μ T_BB (°K)
NADIR ANGLE 0 – 40°
18 JUL – 26 JUL 1963
238
236
234
232
230
228
226
224
222
220
218
216
214
212
210
208
C

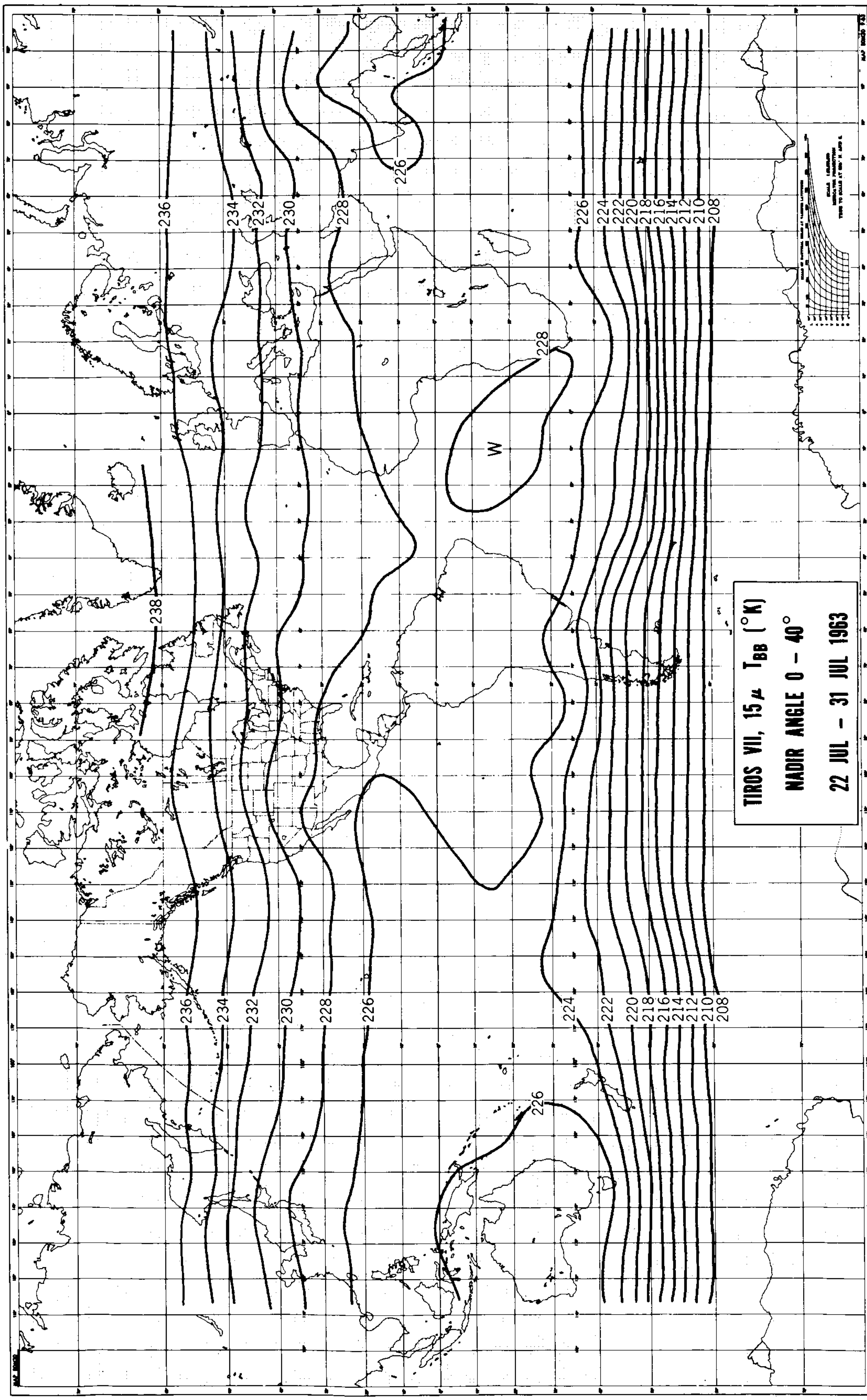
TIROS VII, 15 μ T_{BB} (°K)
NADIR ANGLE 0 - 40°
22 JUL - 31 JUL 1963
236
234
232
230
228
226
224
222
220
218
216
214
212
210
208
238
W

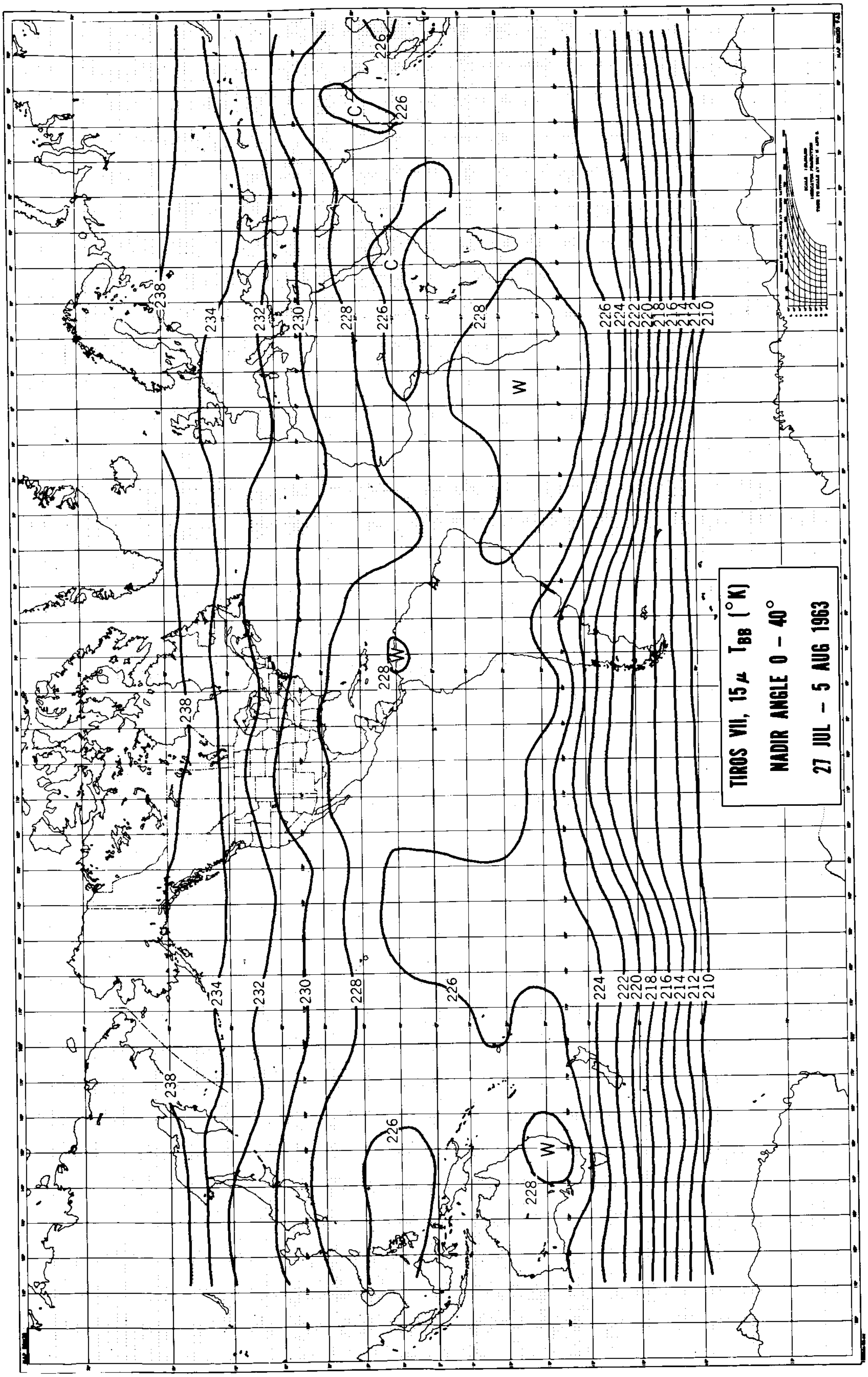
TIROS VII, 15 μ T_BB (°K)
NADIR ANGLE 0 – 40°
27 JUL – 5 AUG 1963

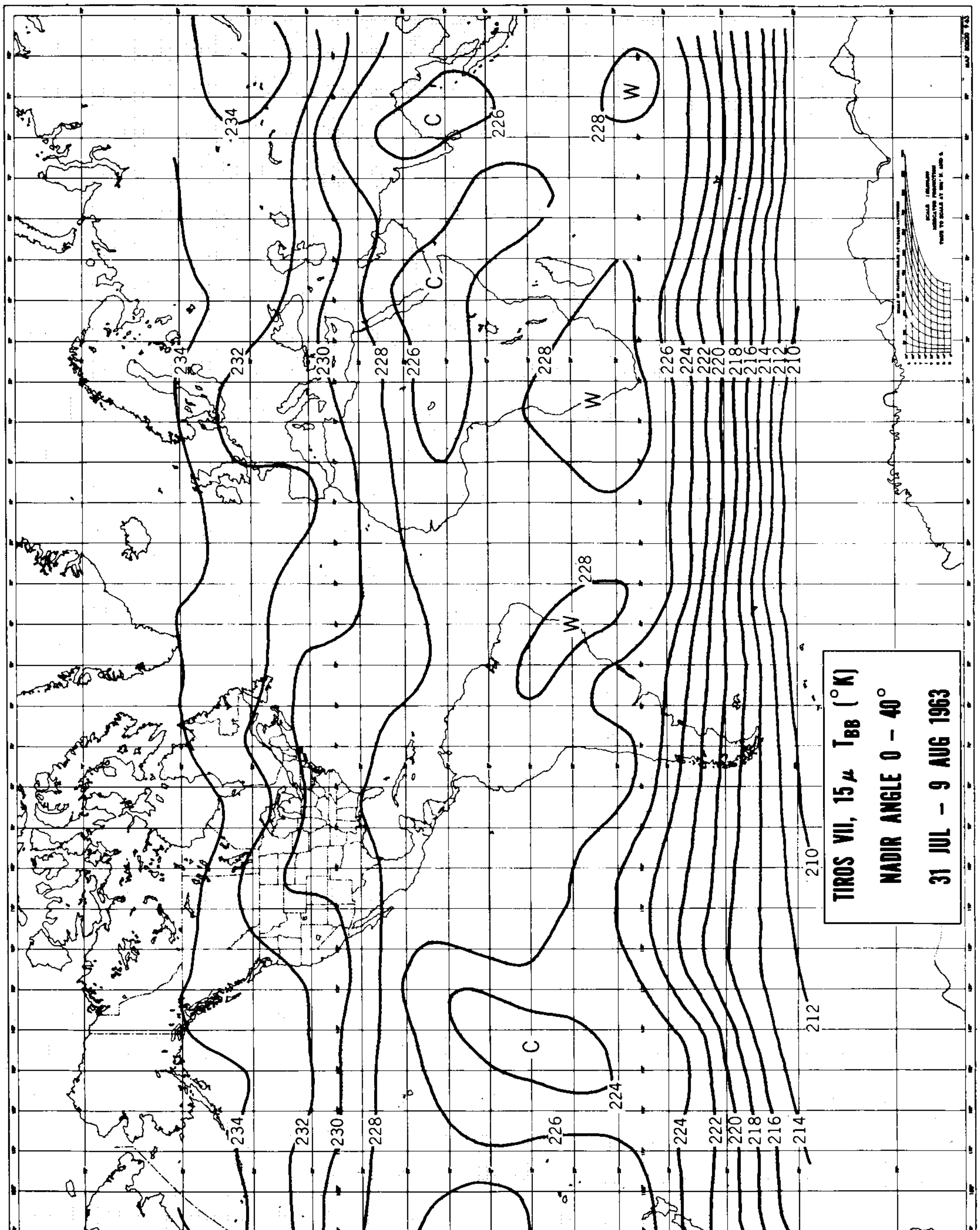
TIROS VII, 15 μ T_BB (°K)
NADIR ANGLE 0 – 40°
31 JUL – 9 AUG 1963

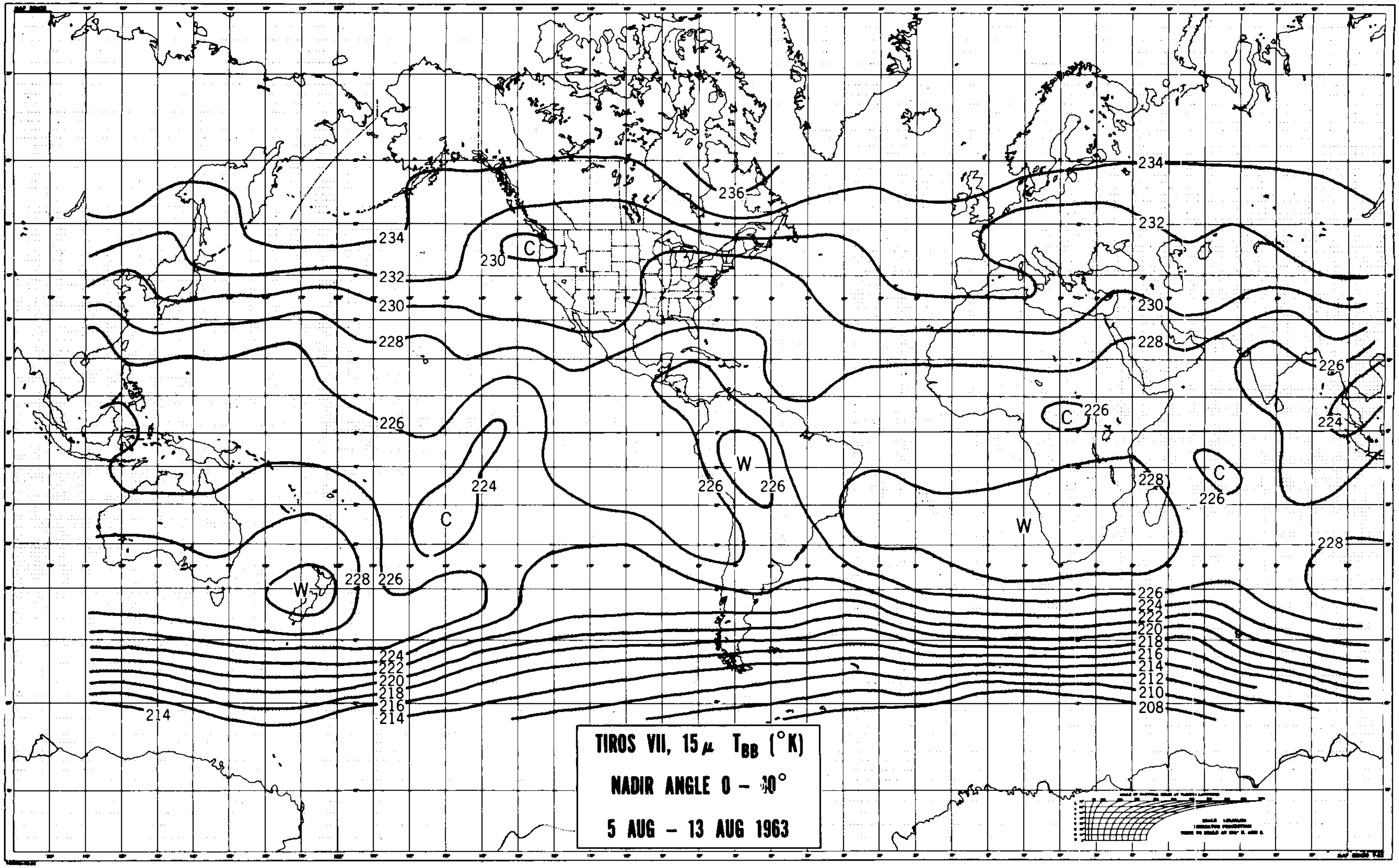
TIROS VII, 15μ T_BB (°K)
5 AUG – 13 AUG 1963

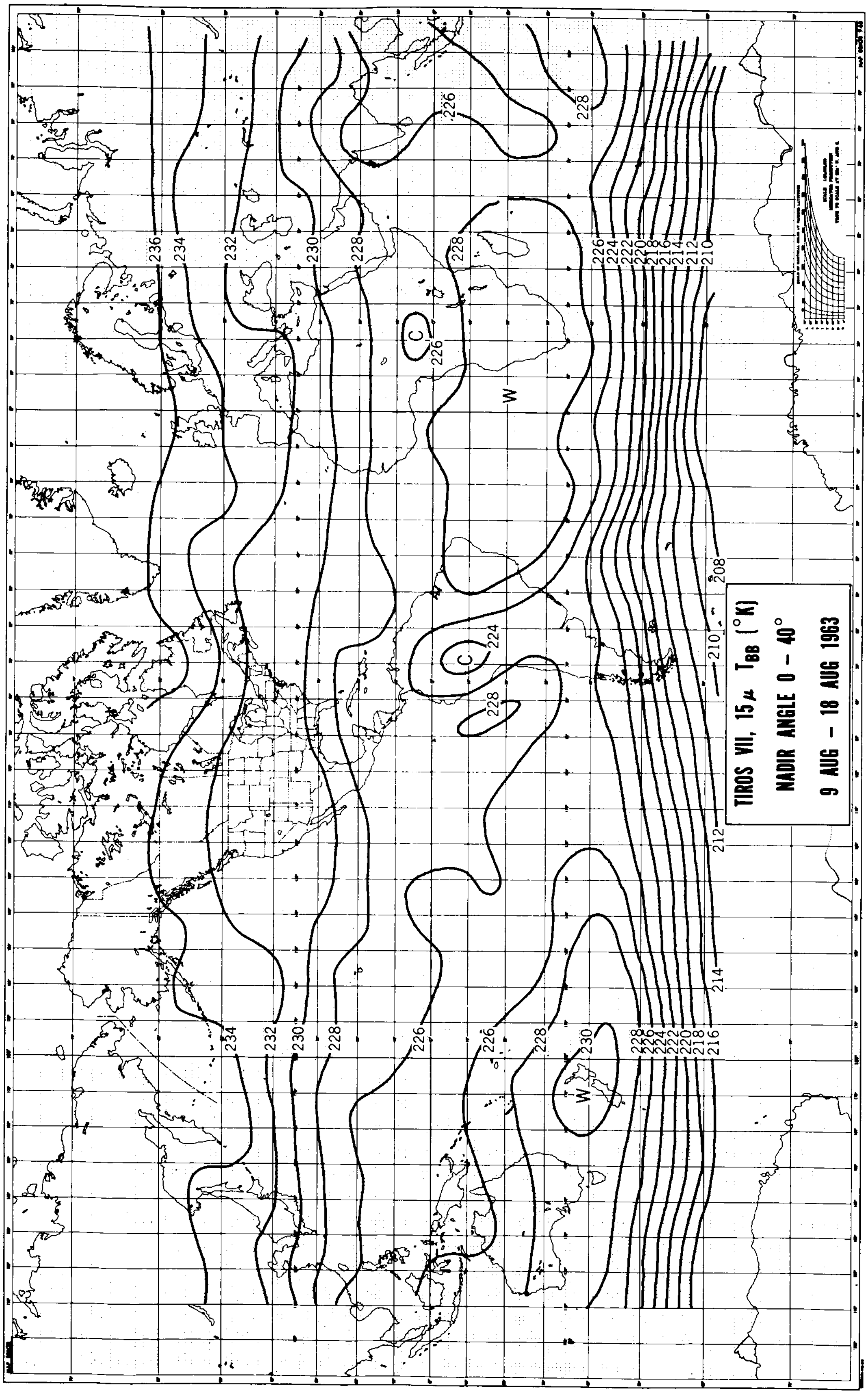
TIROS VII, 15 μ T_BB (°K)
NADIR ANGLE 0 - 40°
9 AUG - 18 AUG 1963

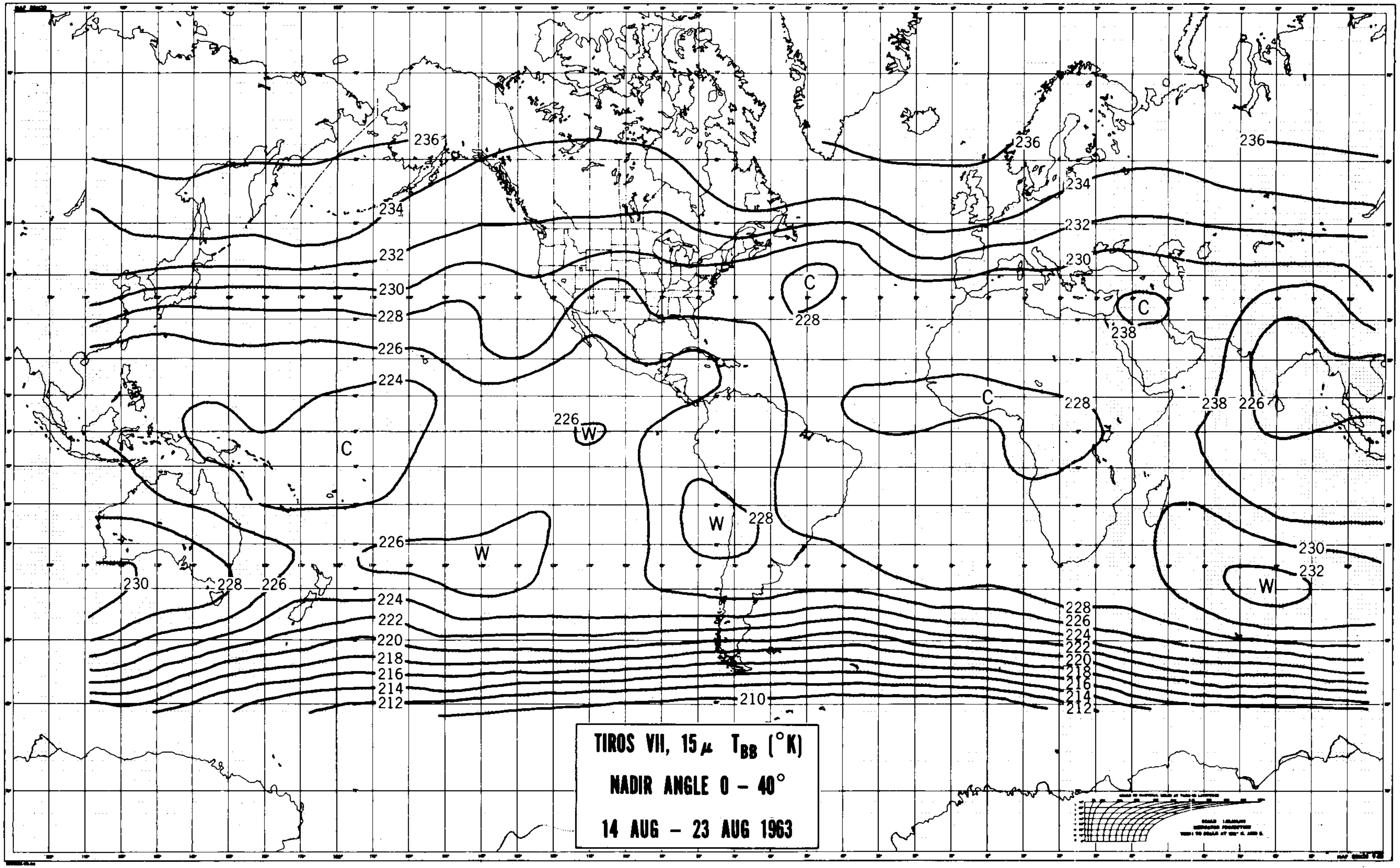
TIROS VII, 15 μ T_BB (°K)
NADIR ANGLE 0 – 40°
14 AUG – 23 AUG 1963
236
234
232
230
228
226
224
222
220
218
216
214
212
210
238
C
W

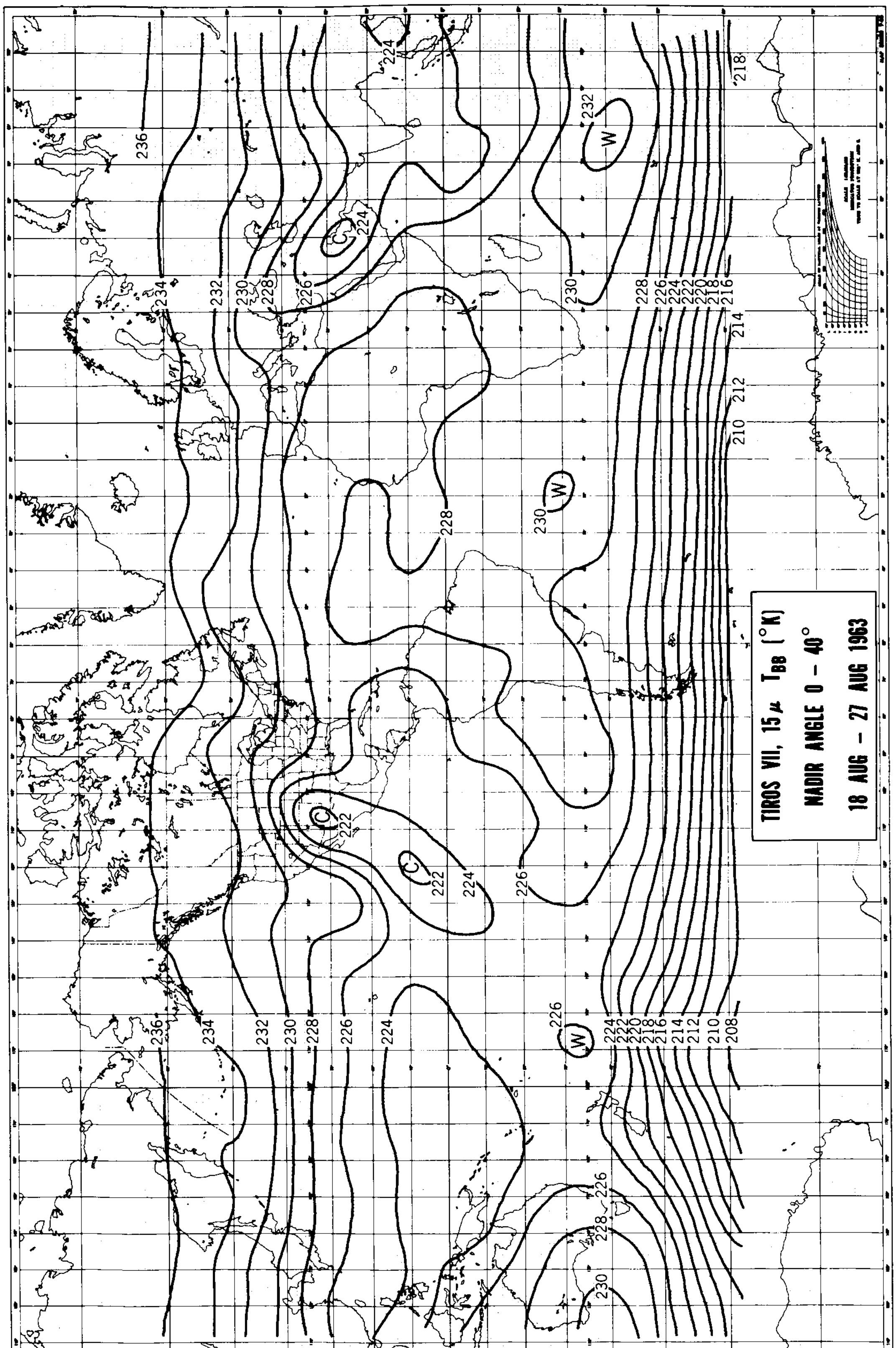
TIROS VII, 15 μ T_{BB} (°K)
NADIR ANGLE 0 – 40°
18 AUG – 27 AUG 1963

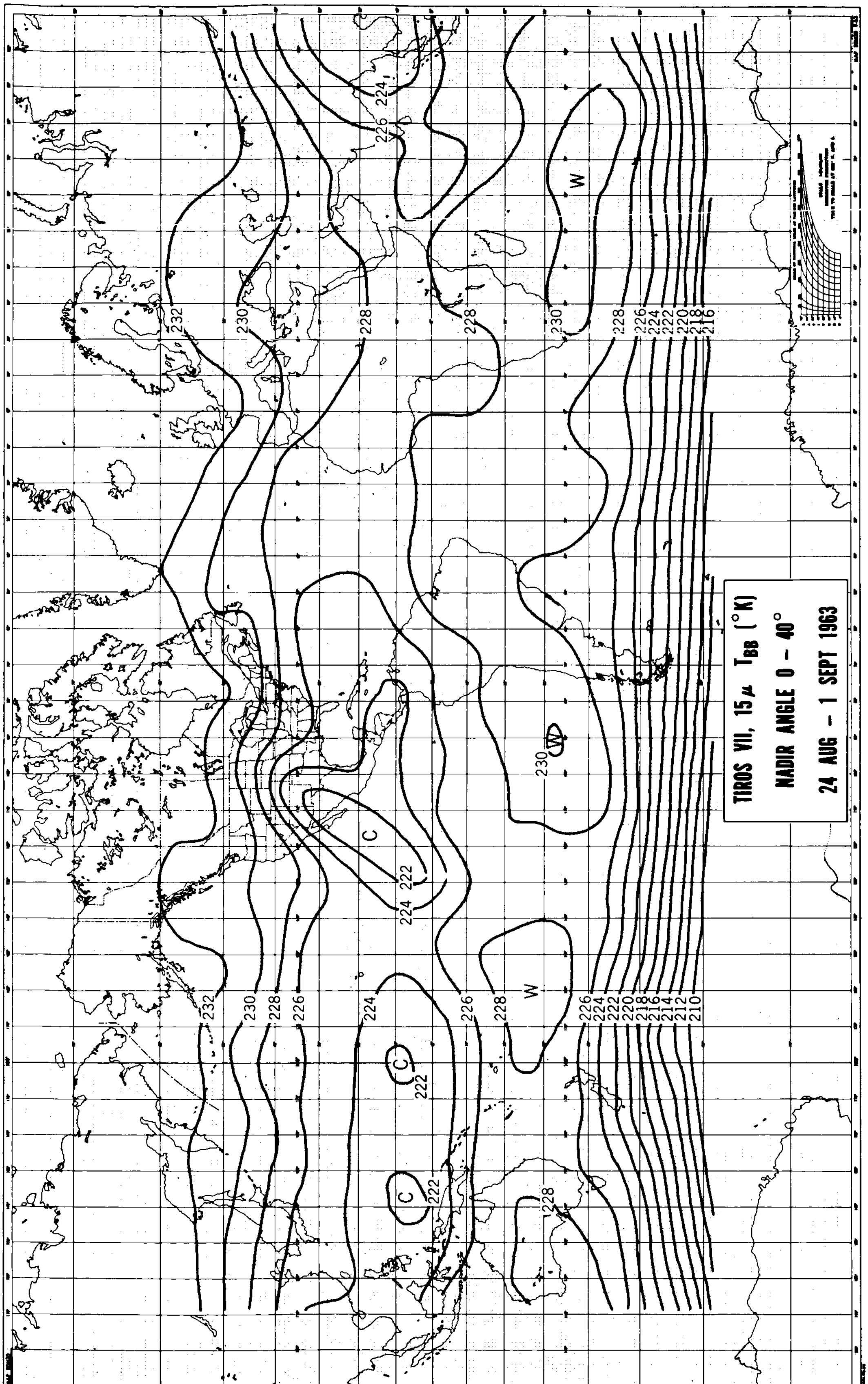
TIROS VII, 15 μ T_{BB} (°K)
NADIR ANGLE 0 – 40°
24 AUG – 1 SEPT 1963

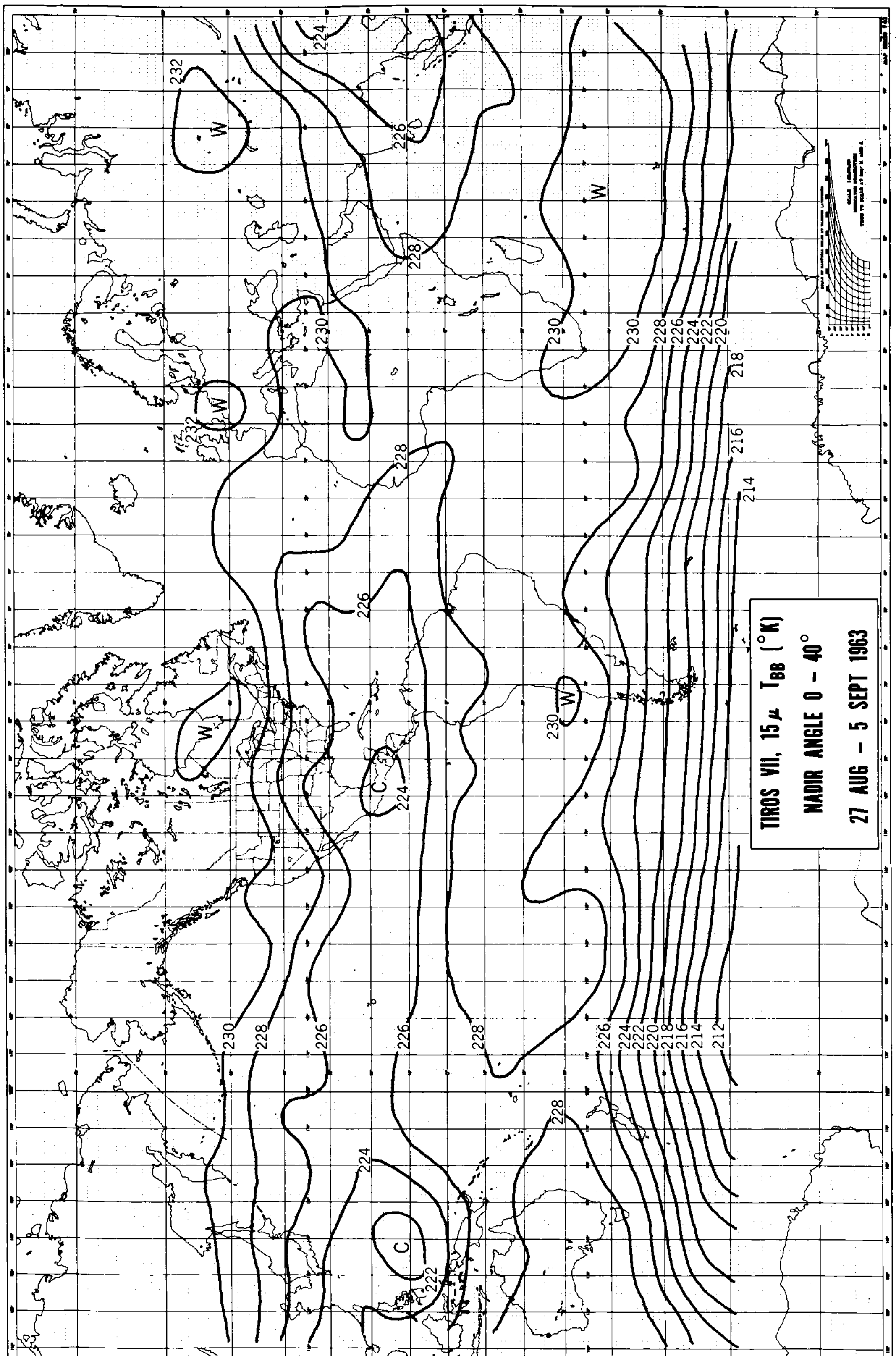
TIROS VII, 15 μ T_BB (°K)
NADIR ANGLE 0 - 40°
27 AUG - 5 SEPT 1963

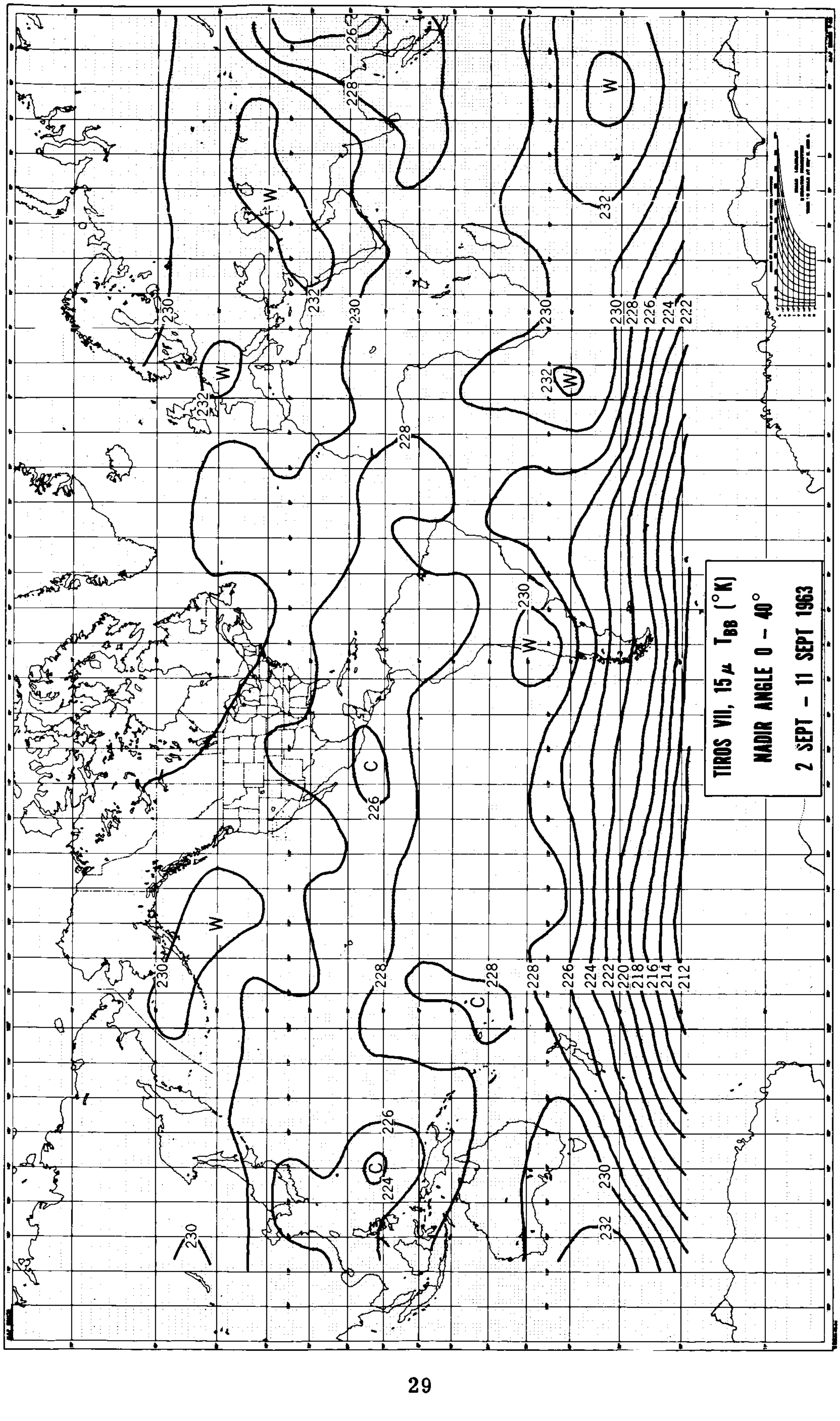

TIROS VII, 15μ T_{BB} (°K)
NADIR ANGLE 0 – 40°
2 SEPT – 11 SEPT 1963

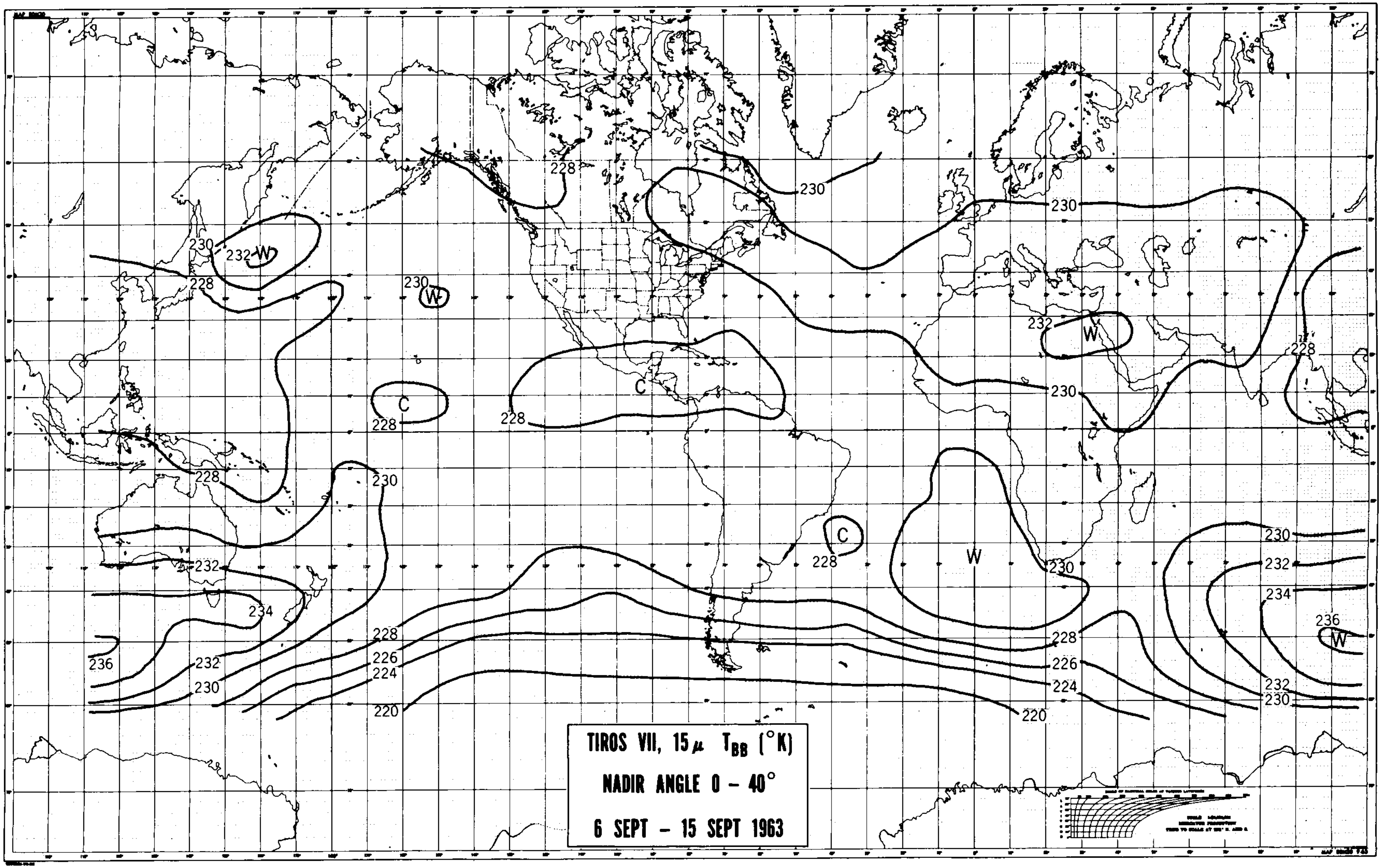

TIROS VII, 15μ T_{BB} (°K)

NADIR ANGLE 0 – 40°

6 SEPT – 15 SEPT 1963

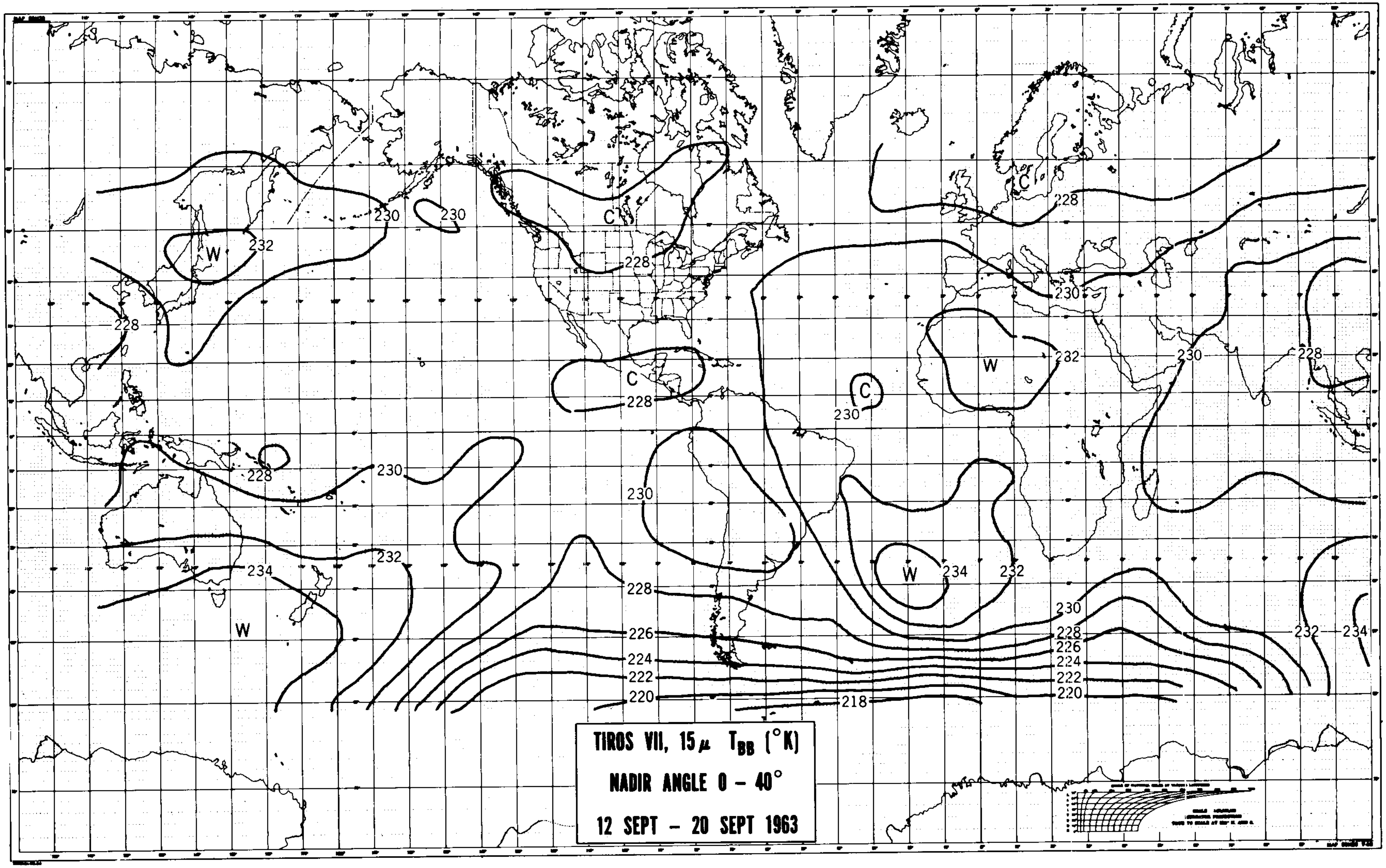
TIROS VII, 15μ T_{BB} (°K)
NADIR ANGLE 0 - 40°
12 SEPT - 20 SEPT 1963

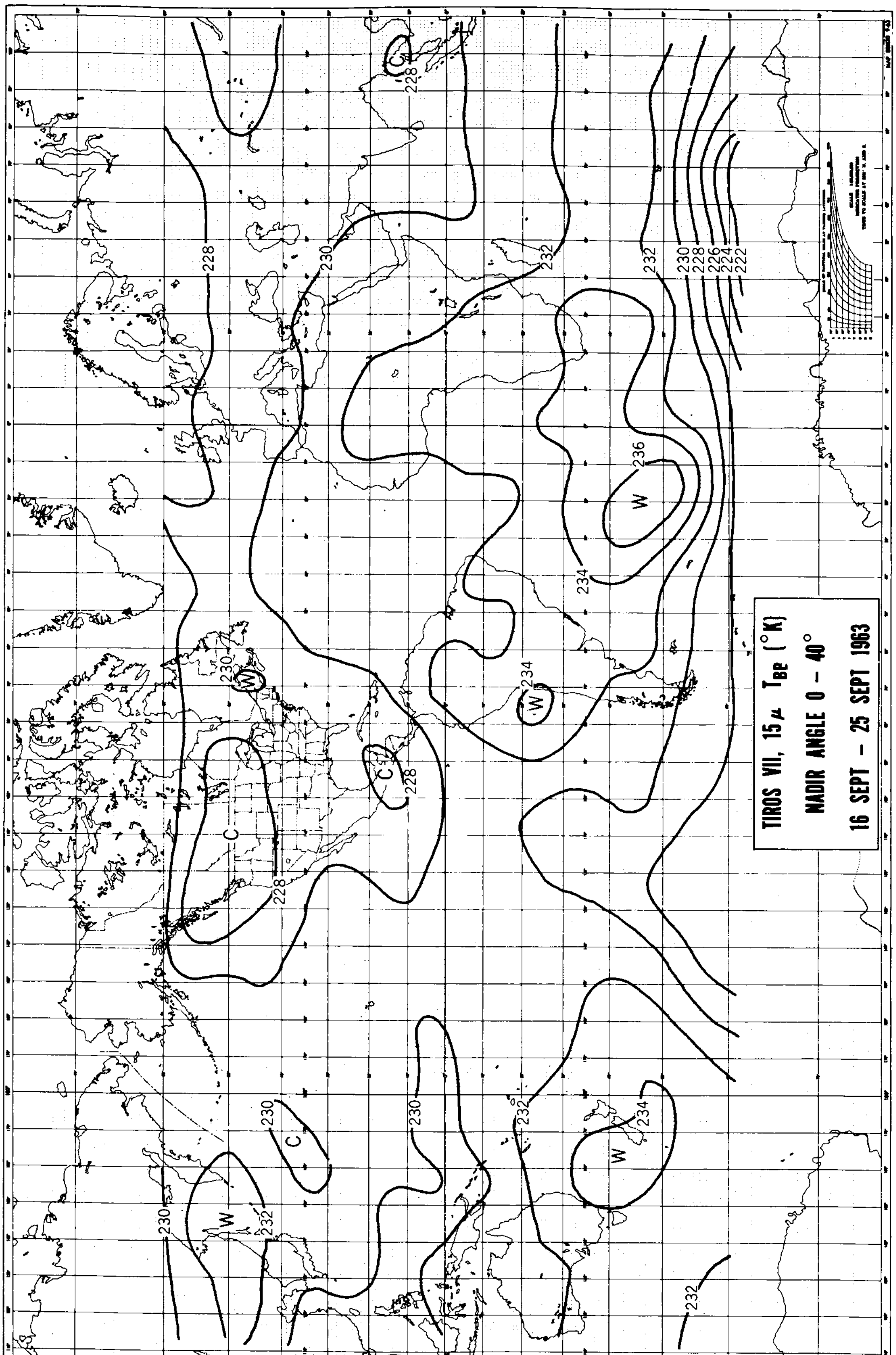

TIROS VII, 15 μ T_BB (°K)
NADIR ANGLE 0 – 40°
16 SEPT – 25 SEPT 1963
228
230
232
234
236
226
224
222
W
C

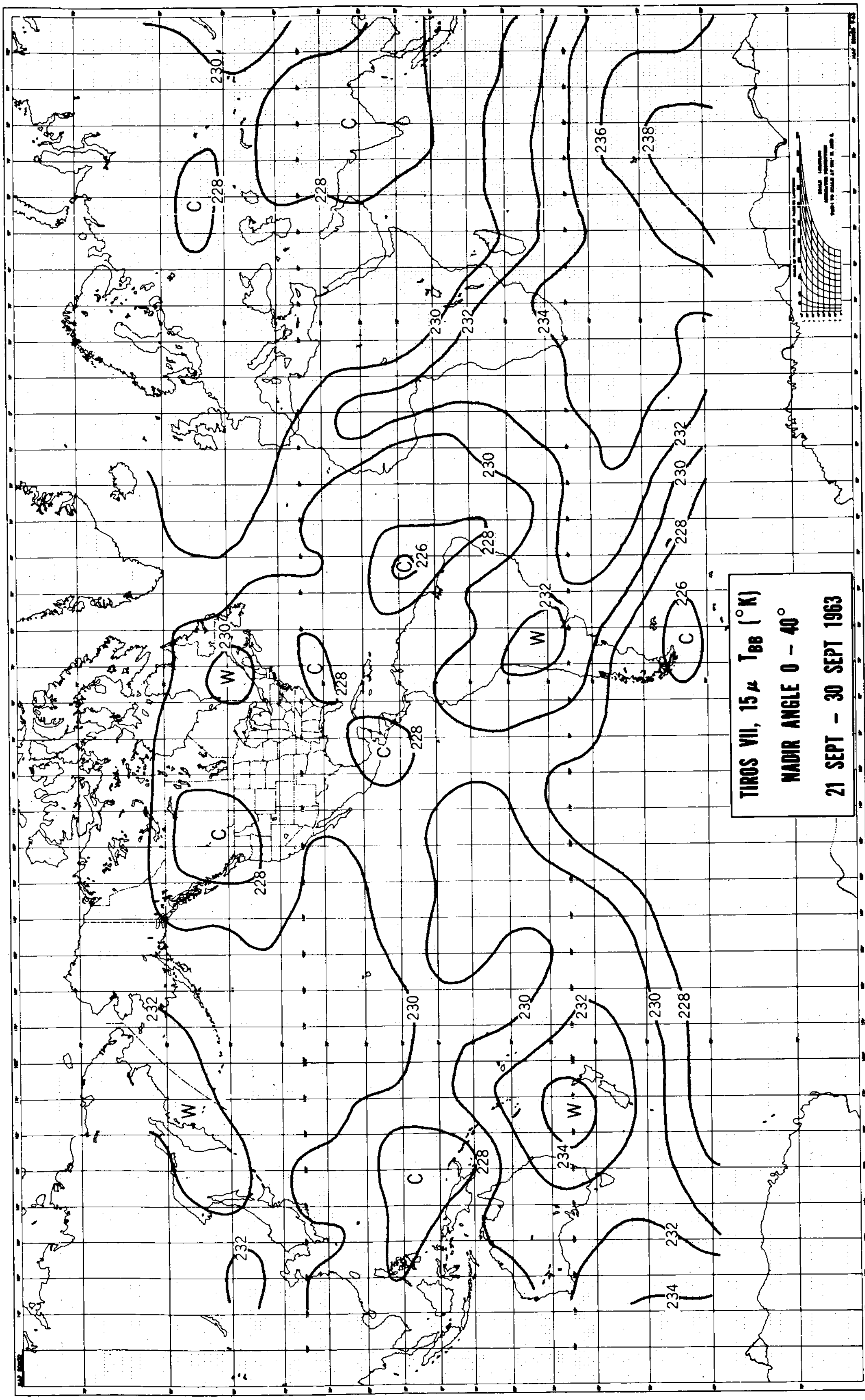
TIROS VII, 15 μ T_{BB} (°K)
NADIR ANGLE 0 – 40°
21 SEPT – 30 SEPT 1963

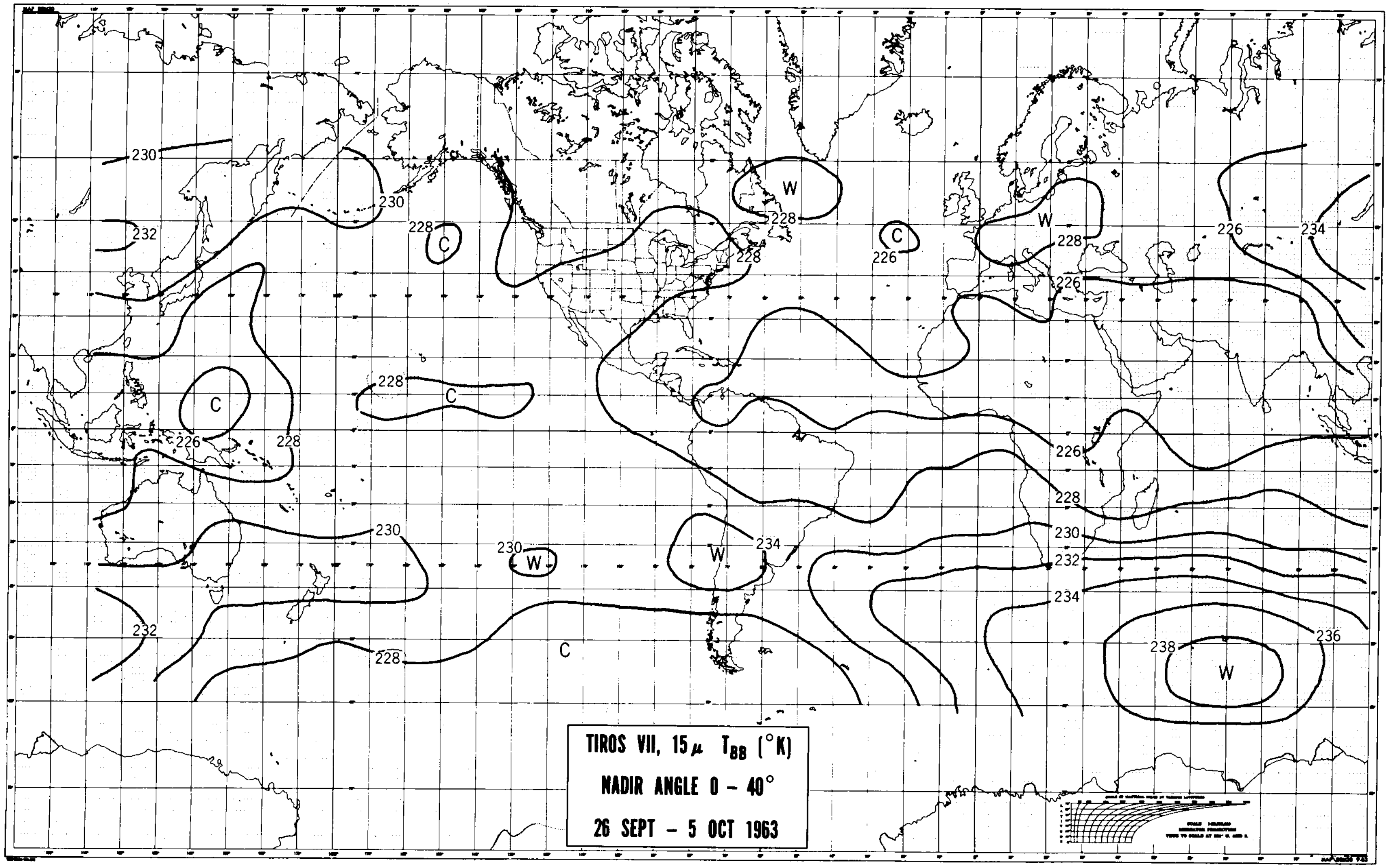
TIROS VII, 15 μ T_{BB} (°K)
NADIR ANGLE 0 - 40°
26 SEPT - 5 OCT 1963
230
232
226
228
C
W
234
236
238

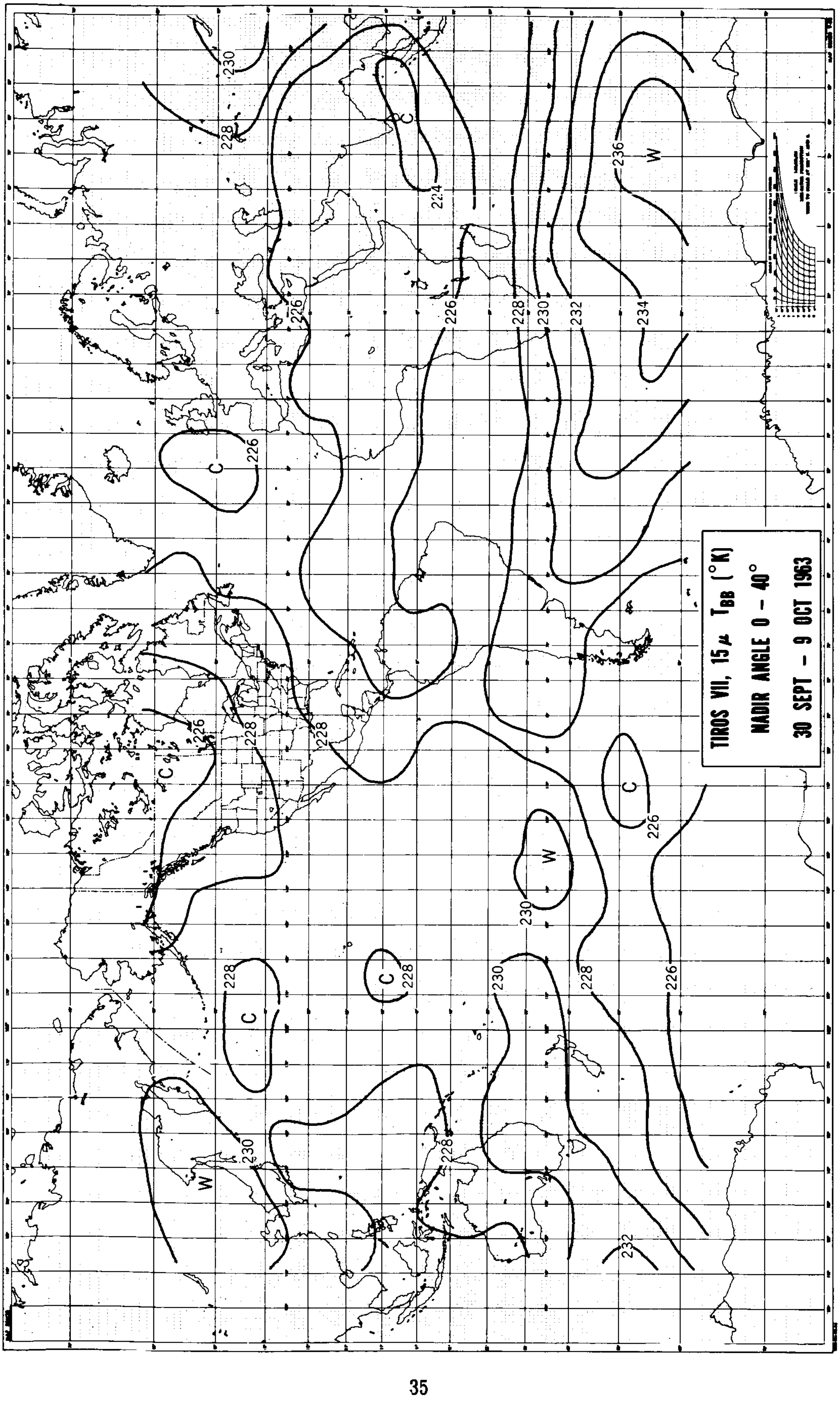

TIROS VII, 15 μ T$_{BB}$ (°K)
NADIR ANGLE 0 – 40°
30 SEPT – 9 OCT 1963
224
226
228
230
232
234
236
C
W

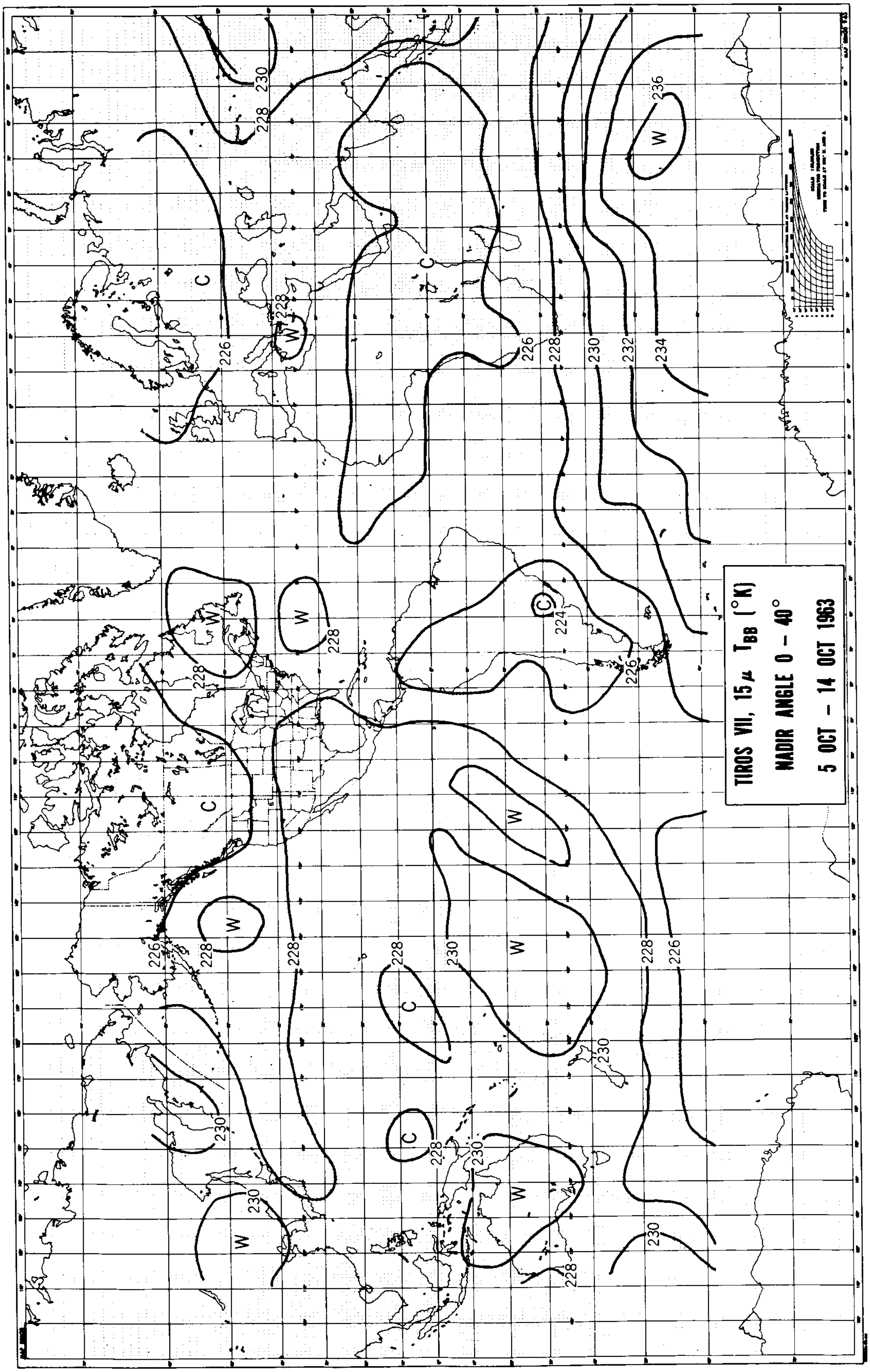
TIROS VII, 15 μ T_BB (°K)
NADIR ANGLE 0 – 40°
5 OCT – 14 OCT 1963

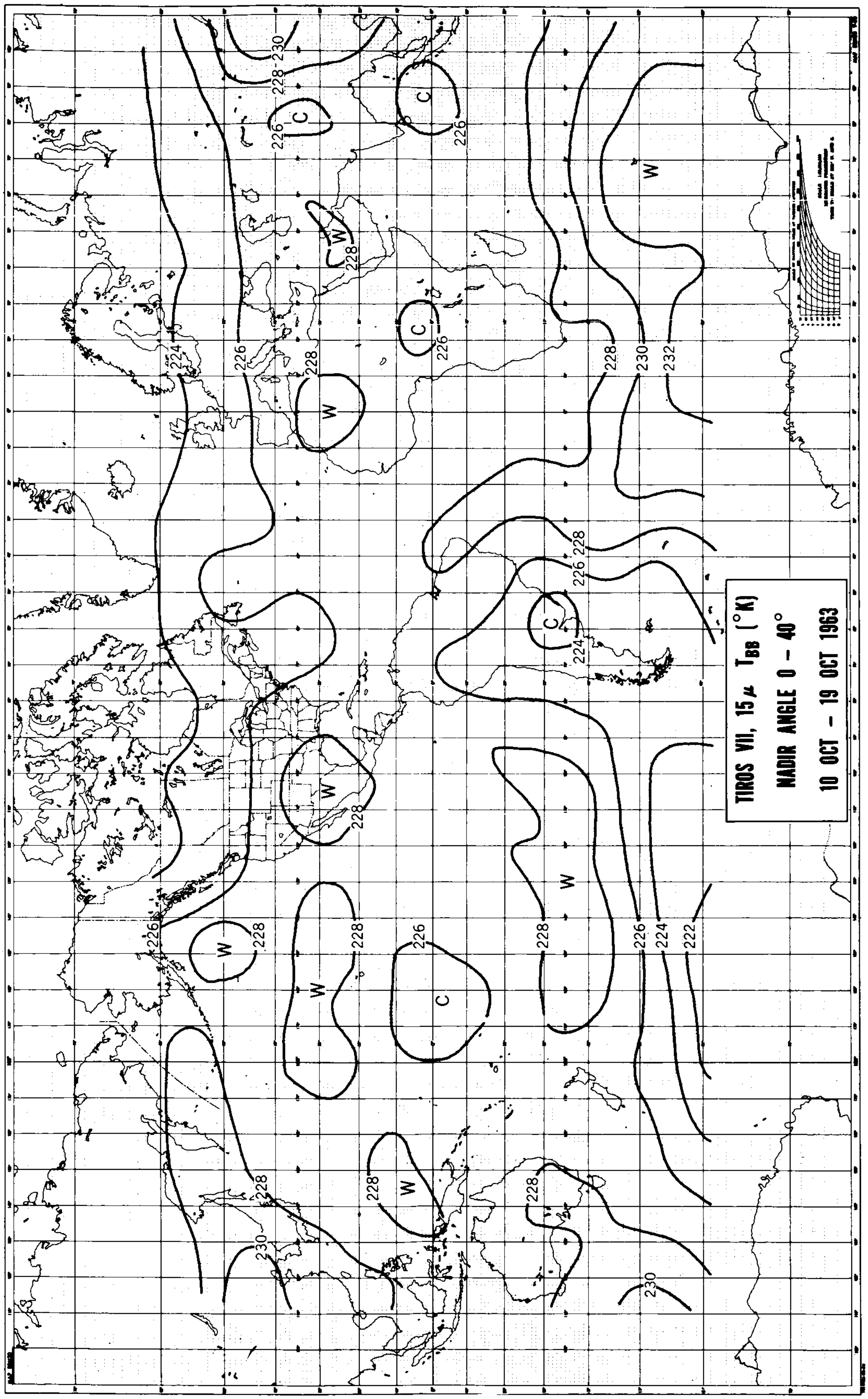
TIROS VII, 15 μ T_BB (°K)
NADIR ANGLE 0 – 40°
10 OCT – 19 OCT 1963

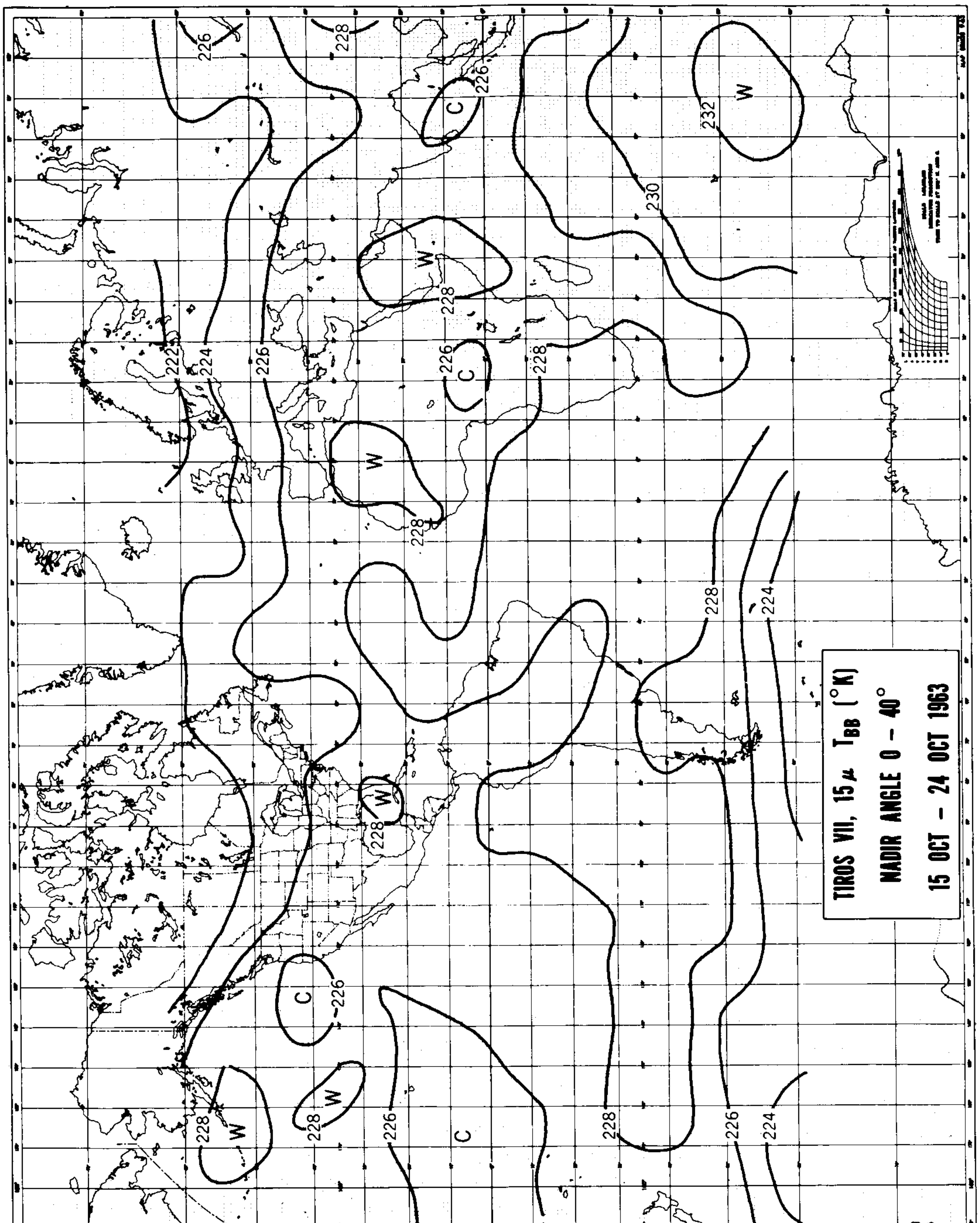
TIROS VII, 15 μ T_{BB} (°K)
NADIR ANGLE 0 – 40°
15 OCT – 24 OCT 1963

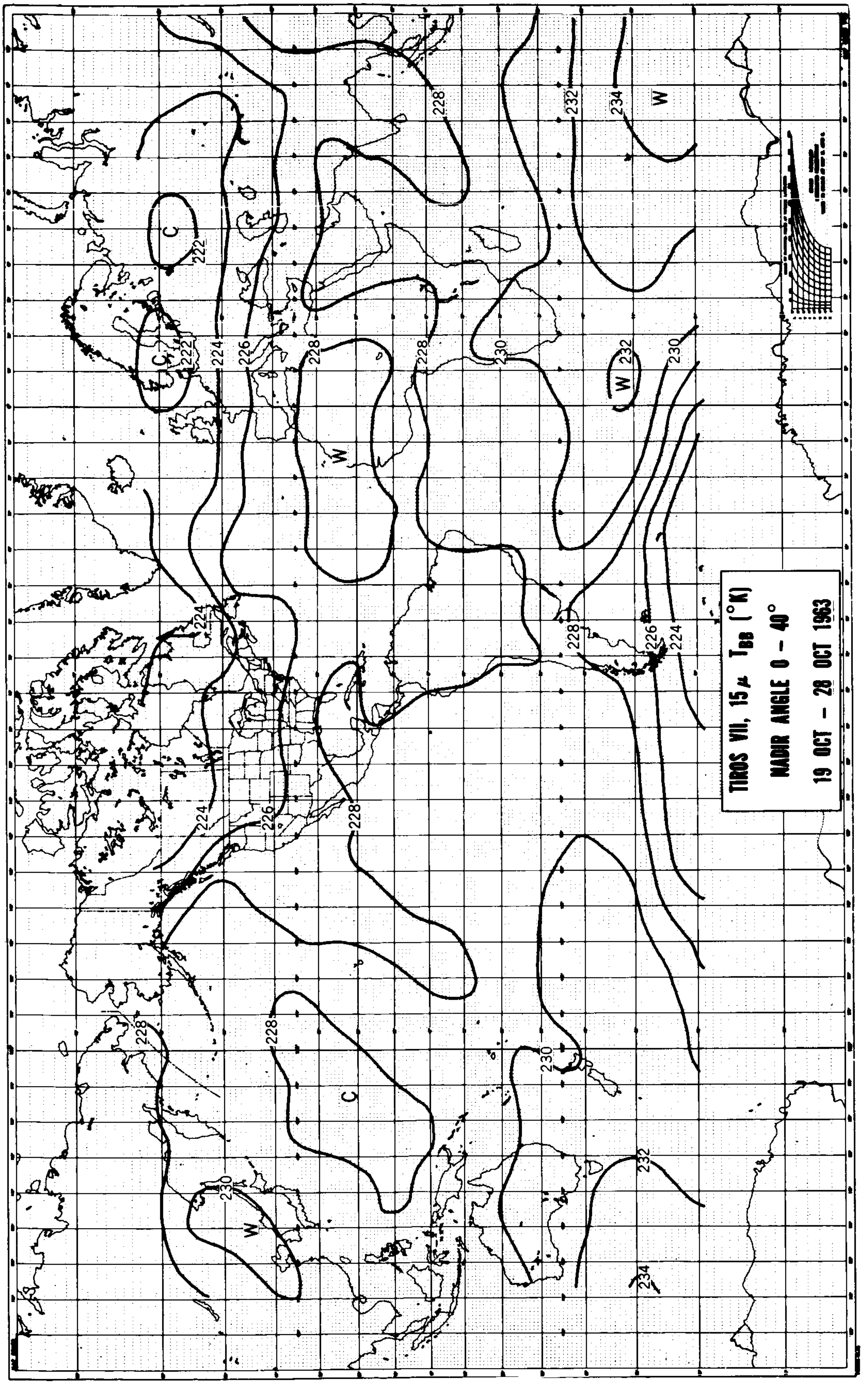
TIROS VII, 15μ T$_{BB}$ (°K)
NADIR ANGLE 0 – 40°
19 OCT – 28 OCT 1963

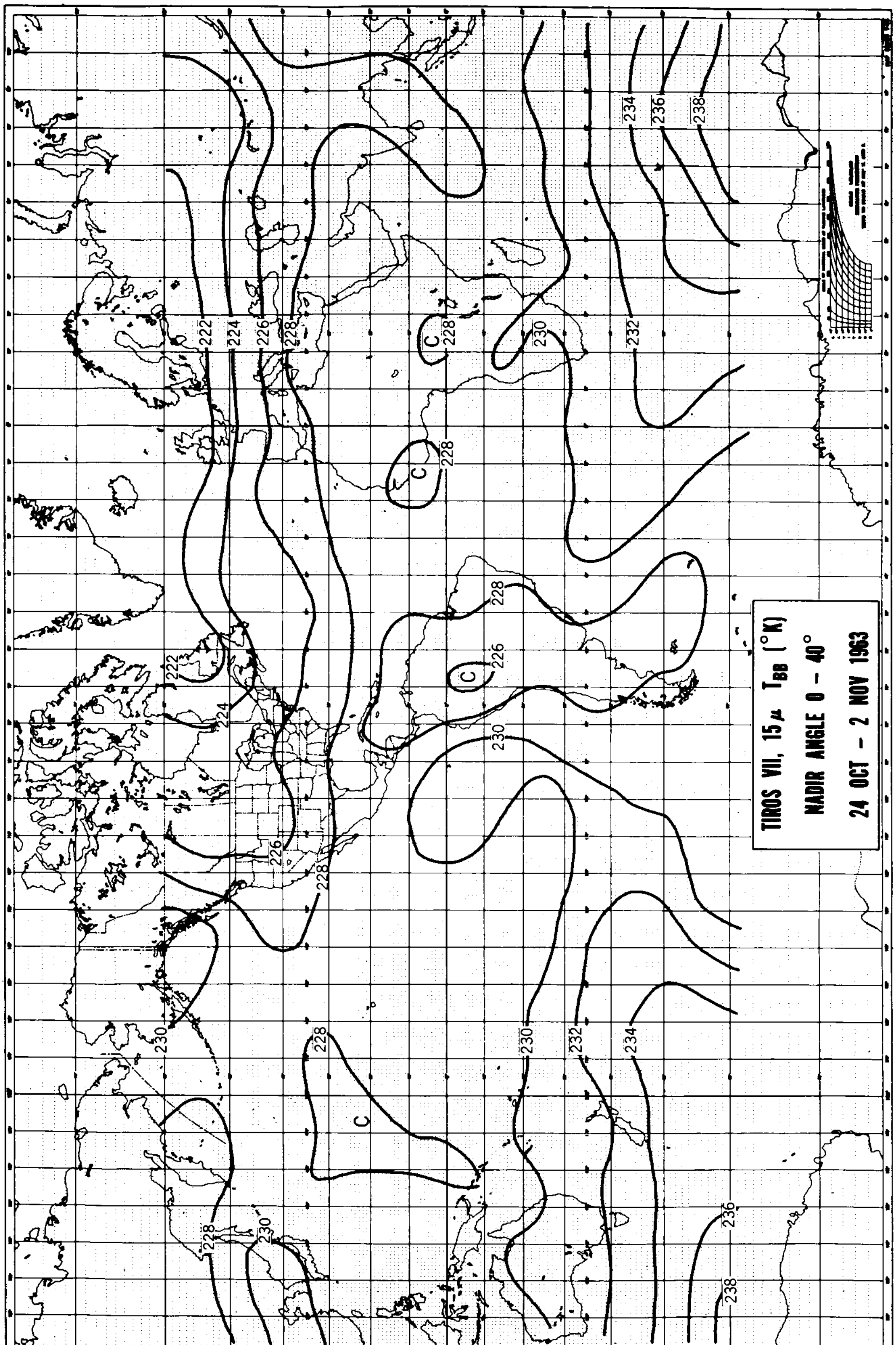
TIROS VII, 15 μ T$_{BB}$ (°K)
NADIR ANGLE 0 – 40°
24 OCT – 2 NOV 1963

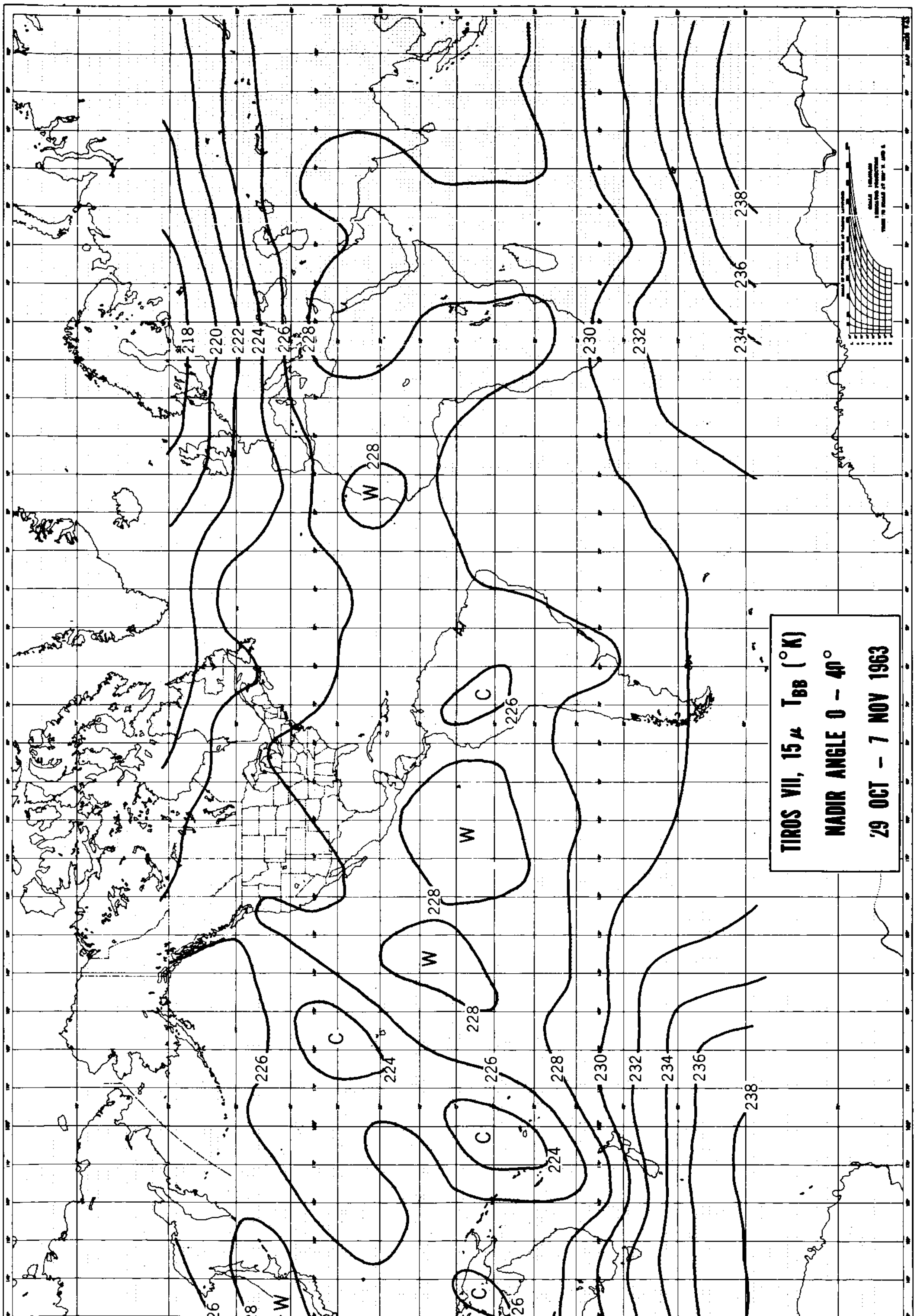
TIROS VII, 15 μ T_{BB} (°K)
NADIR ANGLE 0 – 40°
29 OCT – 7 NOV 1963

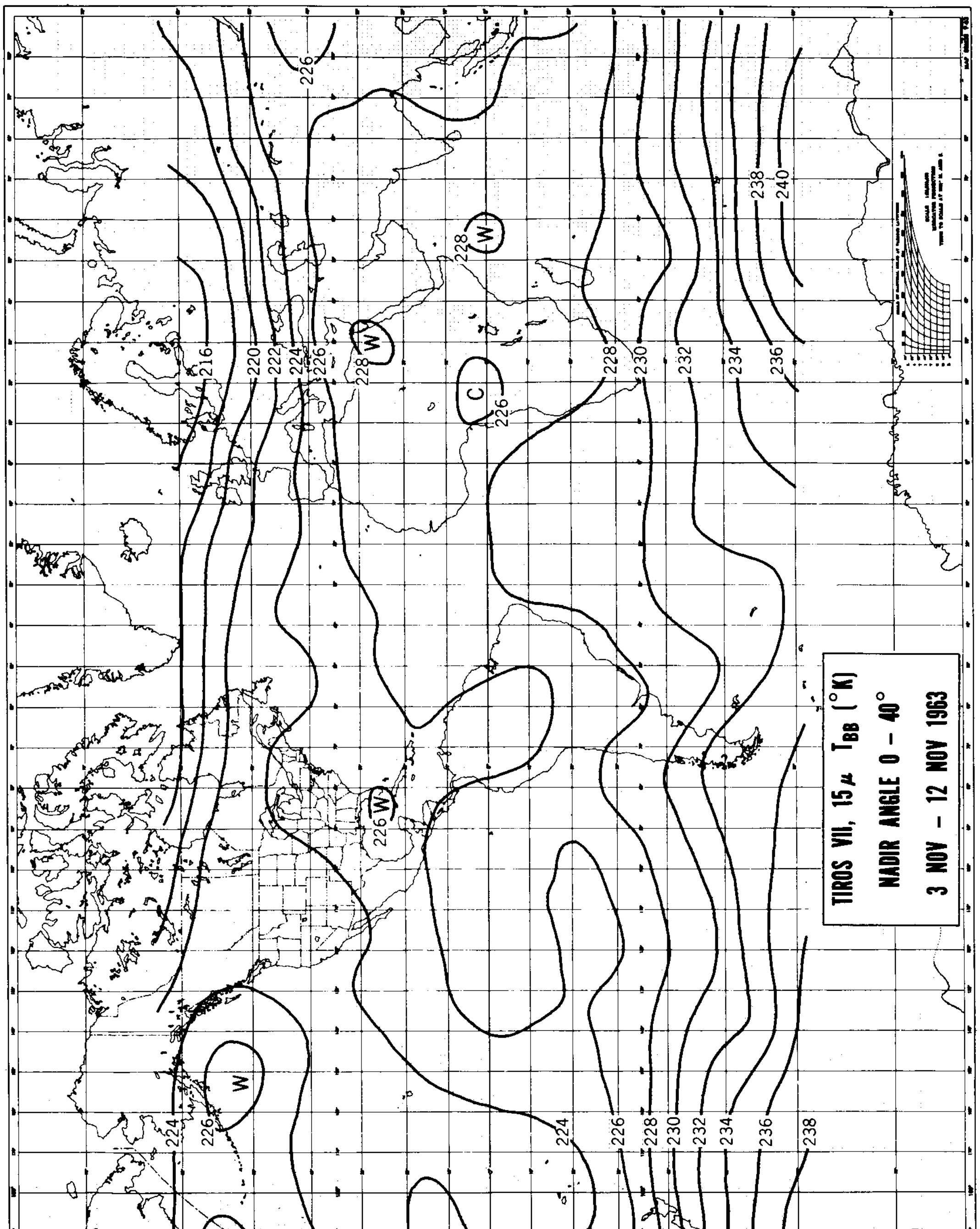
TIROS VII, 15μ T_{BB} (°K)
NADIR ANGLE 0 – 40°
3 NOV – 12 NOV 1963

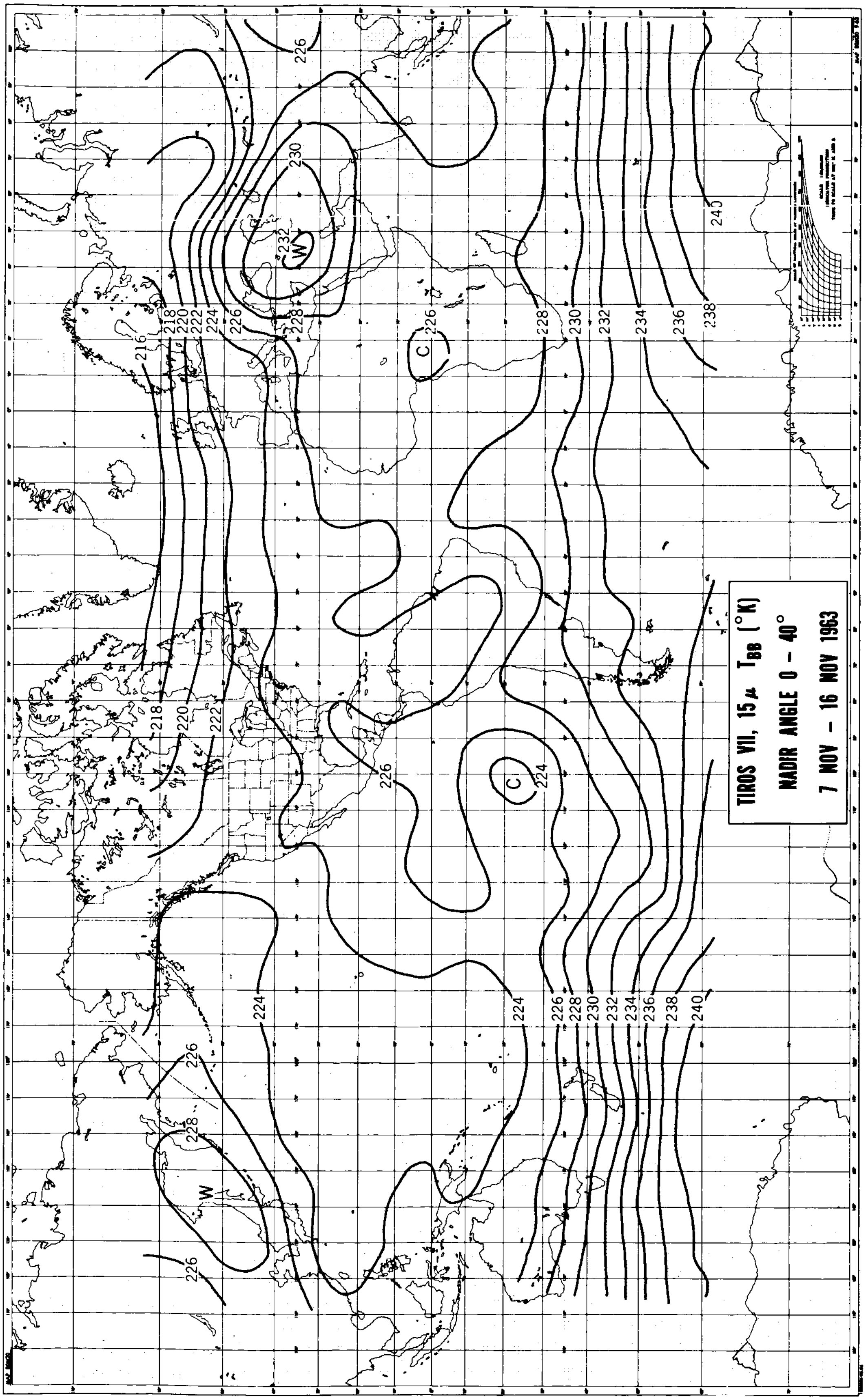
TIROS VII, 15 μ T_{BB} (°K)
NADIR ANGLE 0 – 40°
7 NOV – 16 NOV 1963

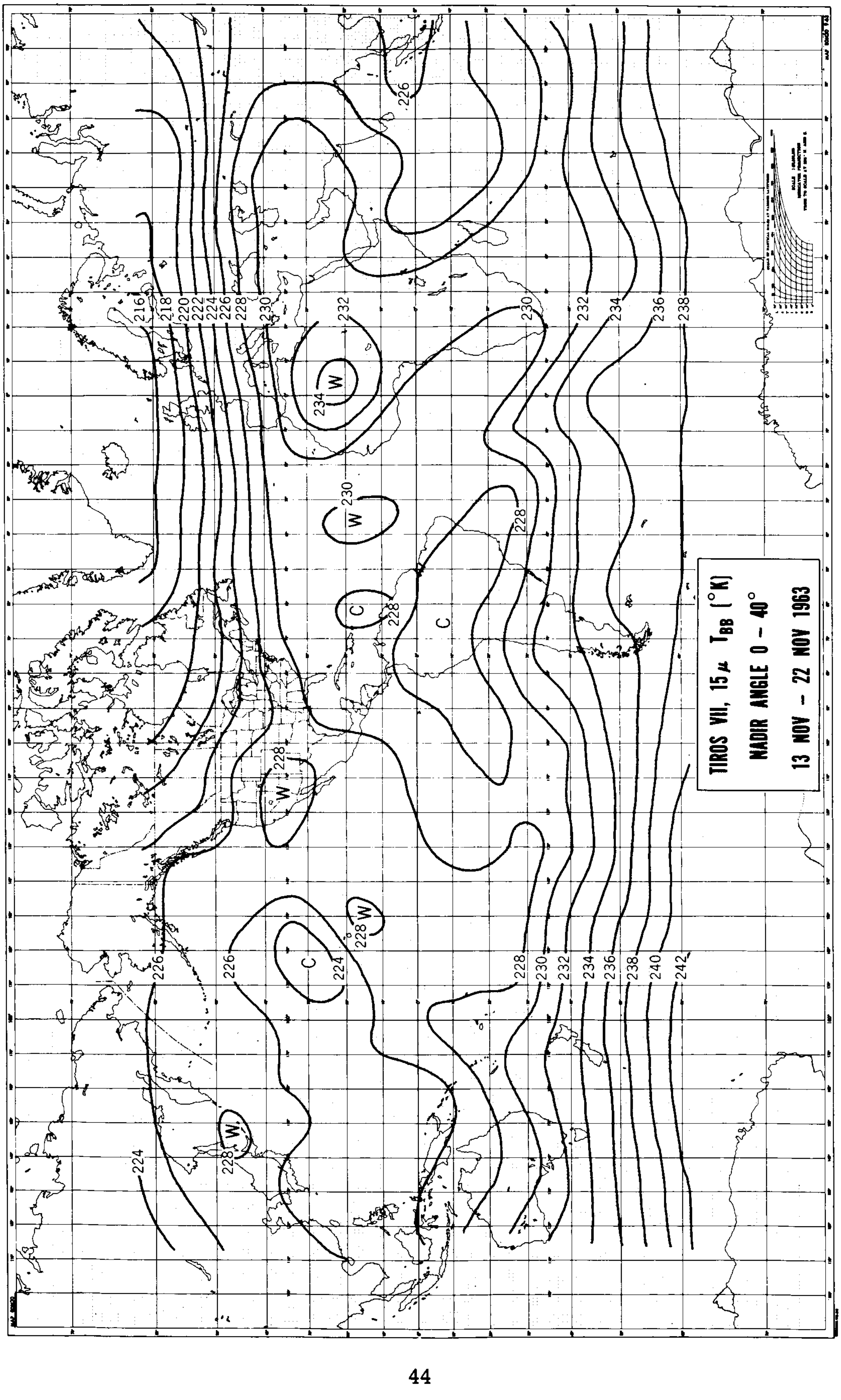
TIROS VII, 15 μ T_{BB} (°K)
NADIR ANGLE 0 – 40°
13 NOV – 22 NOV 1963

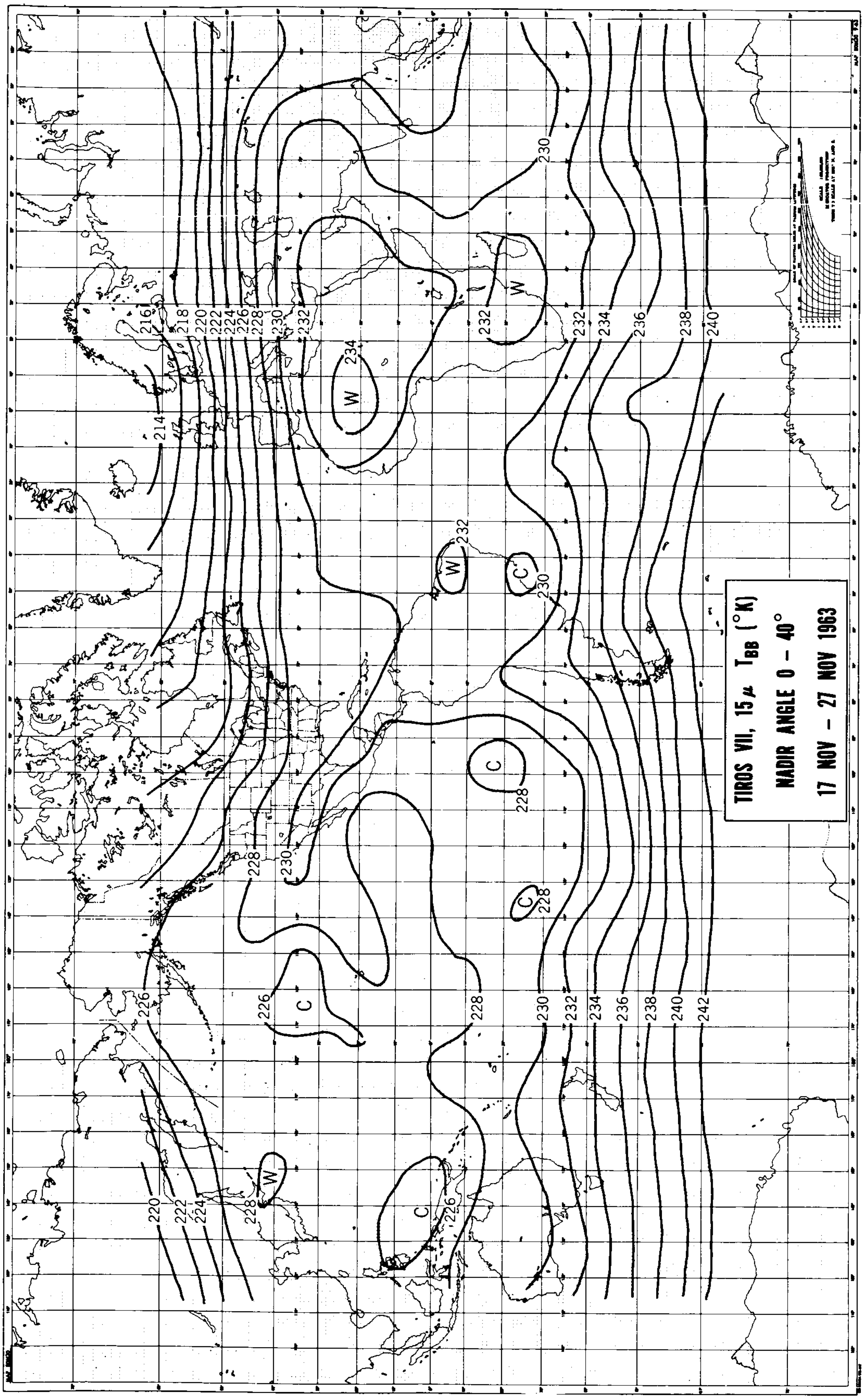
TIROS VII, 15μ T_BB (°K)
NADIR ANGLE 0 - 40°
17 NOV - 27 NOV 1963

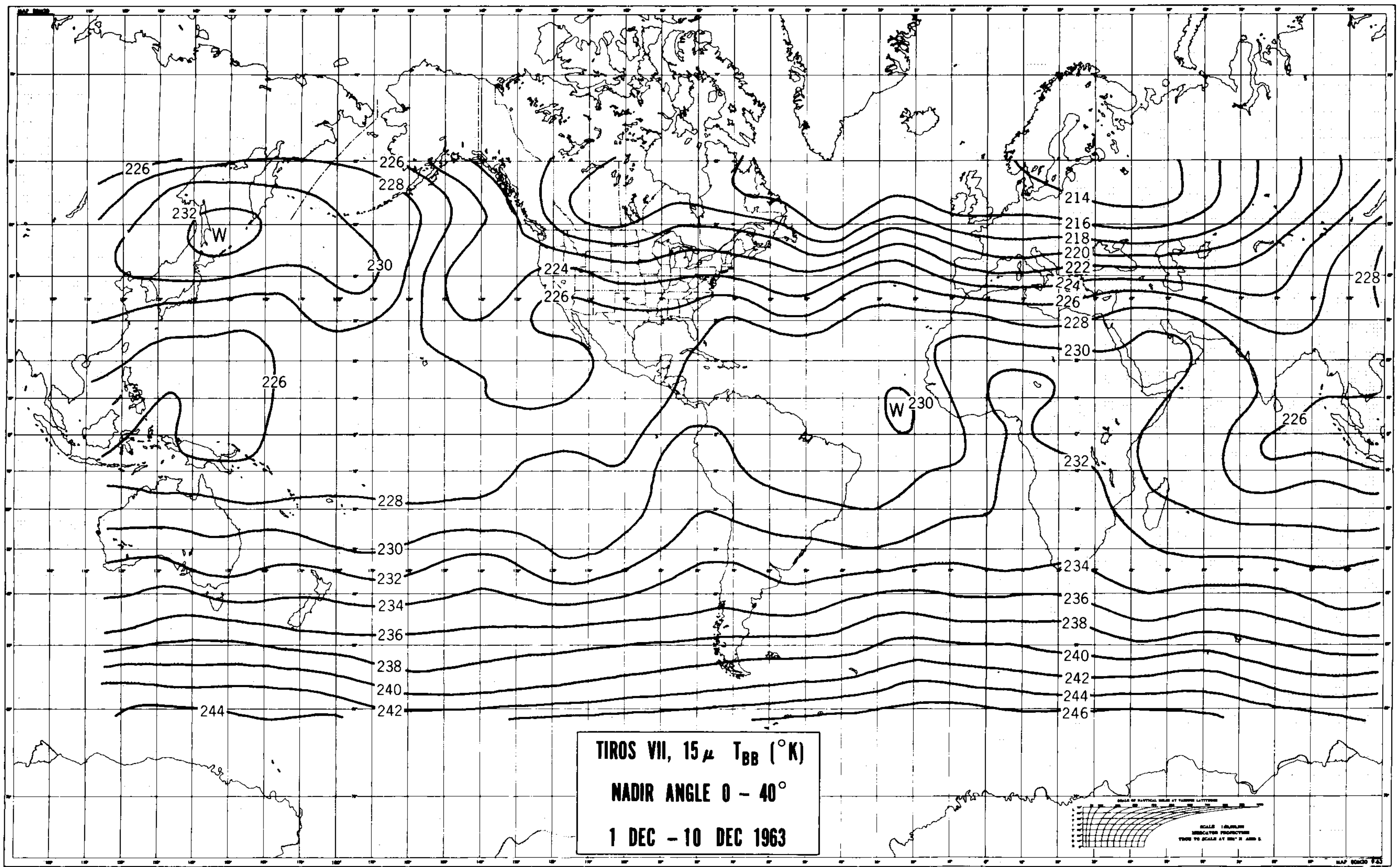

TIROS VII, 15 μ T_{BB} (°K)
NADIR ANGLE 0 – 40°
1 DEC – 10 DEC 1963

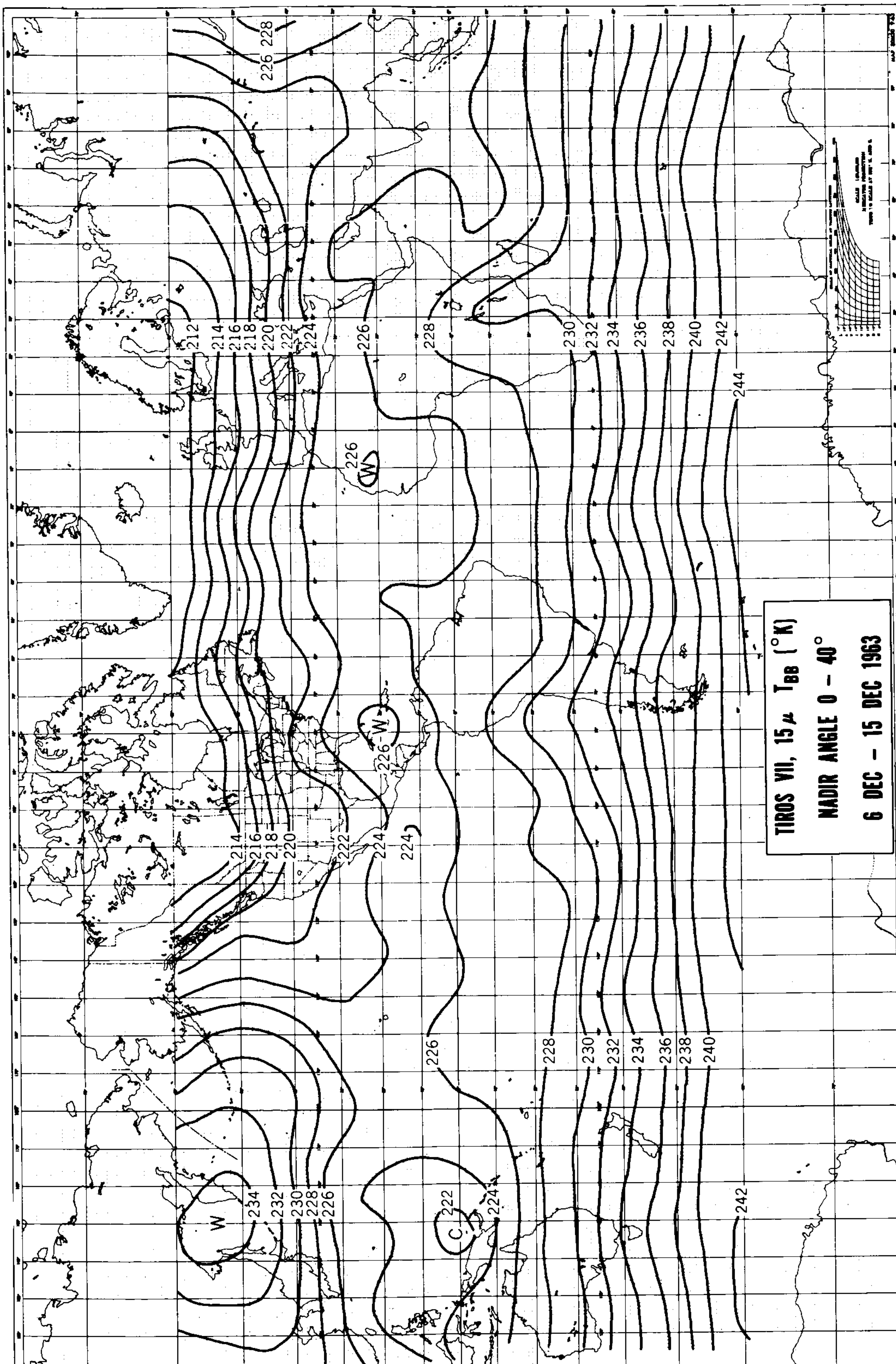
TIROS VII, 15μ T_{BB} (°K)
NADIR ANGLE 0 – 40°
6 DEC – 15 DEC 1963

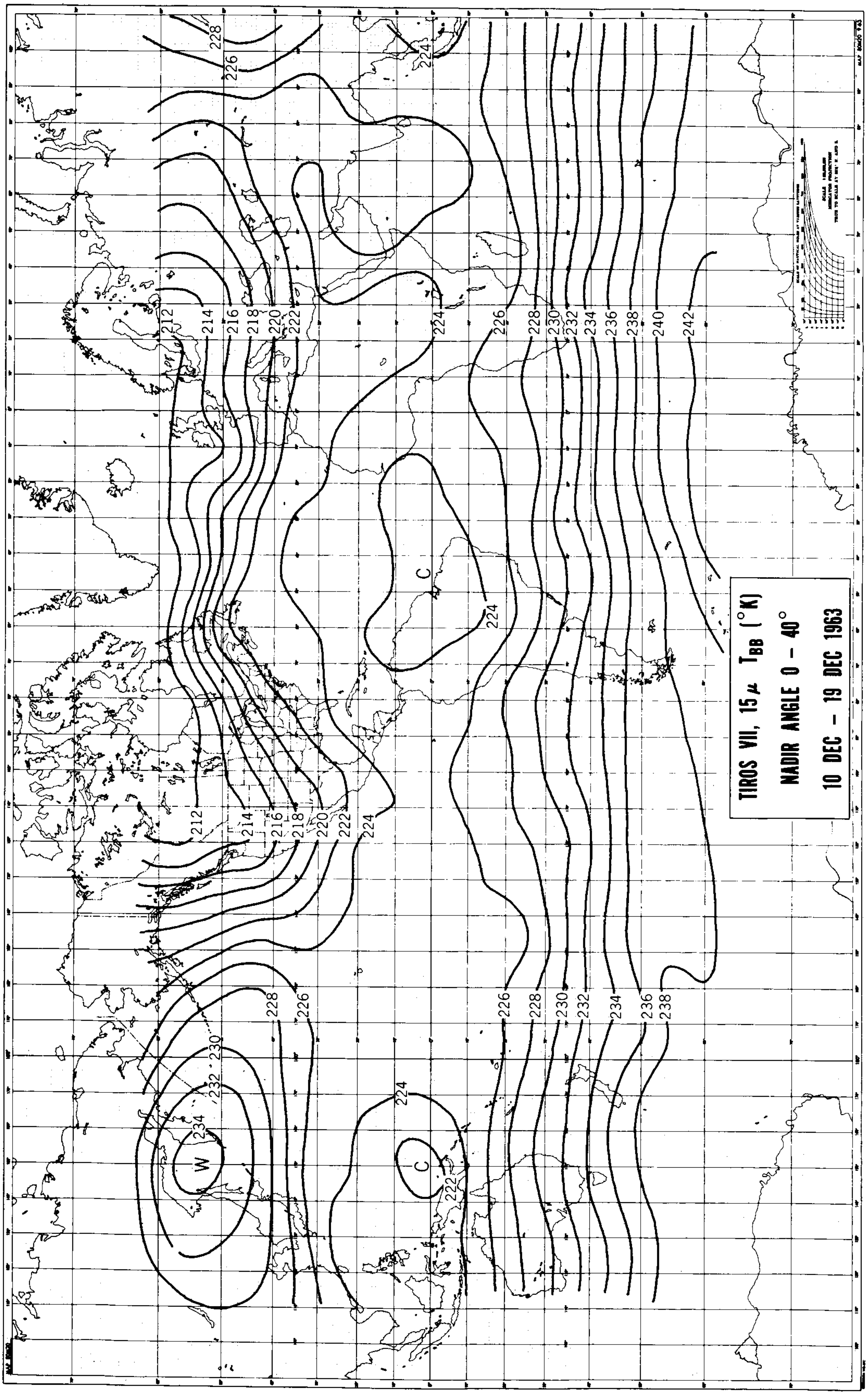
TIROS VII, 15 μ T_BB (°K)
NADIR ANGLE 0 – 40°
10 DEC – 19 DEC 1963

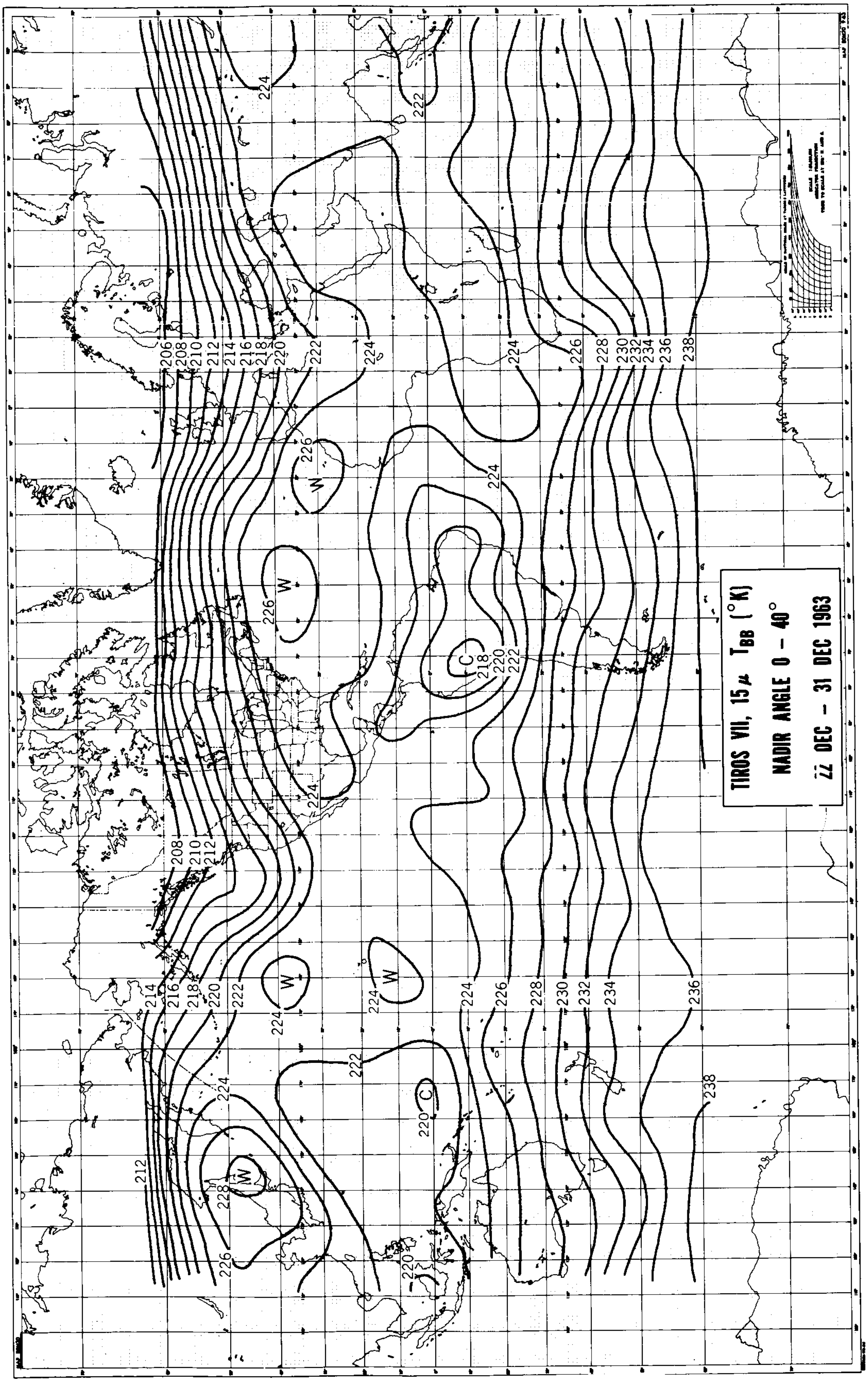
TIROS VII, 15 μ T_BB (°K)
NADIR ANGLE 0 – 40°
22 DEC – 31 DEC 1963

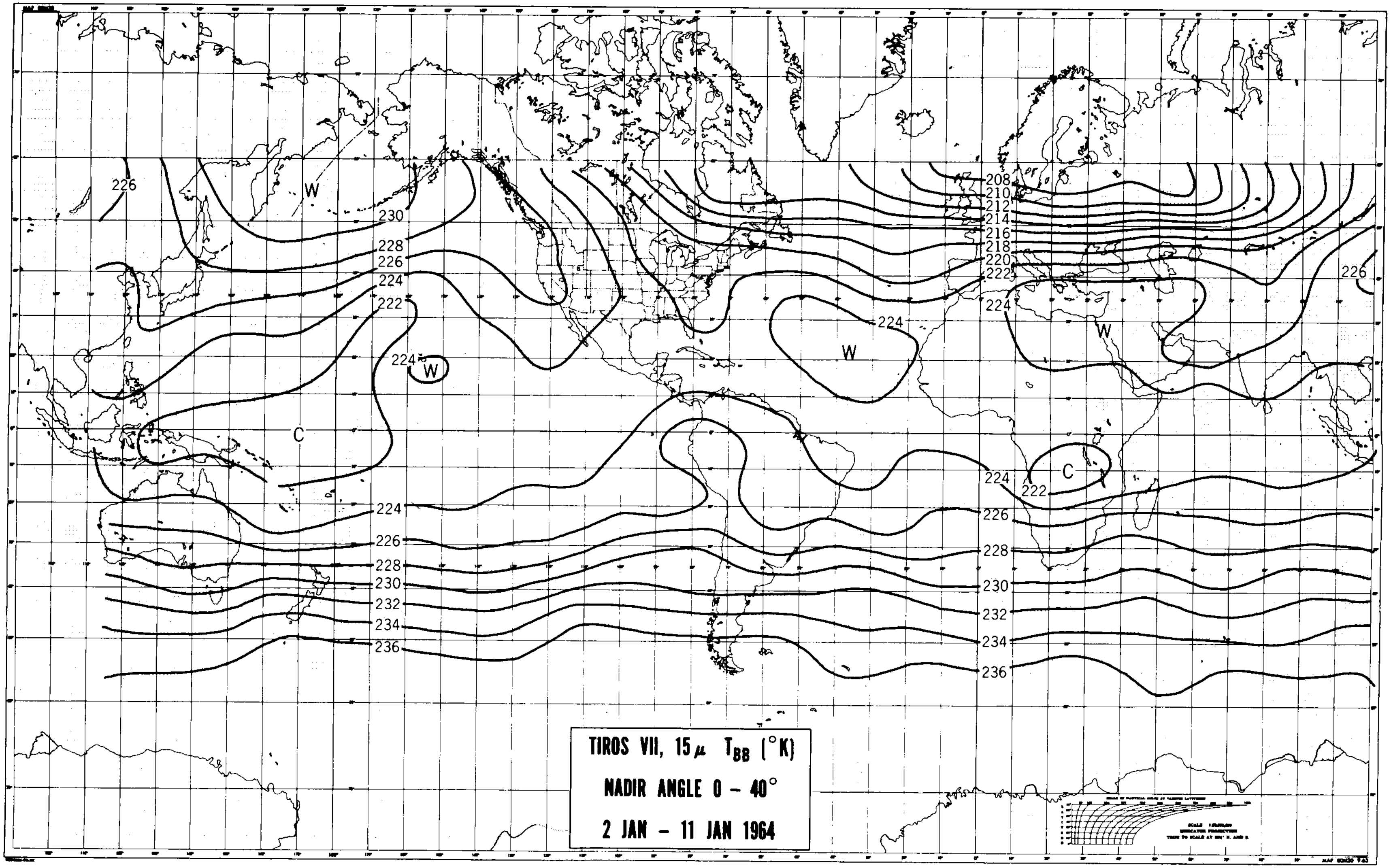
TIROS VII, 15μ T_BB (°K)
NADIR ANGLE 0 – 40°
2 JAN – 11 JAN 1964
208
210
212
214
216
218
220
222
224
226
228
230
232
234
236
W
C

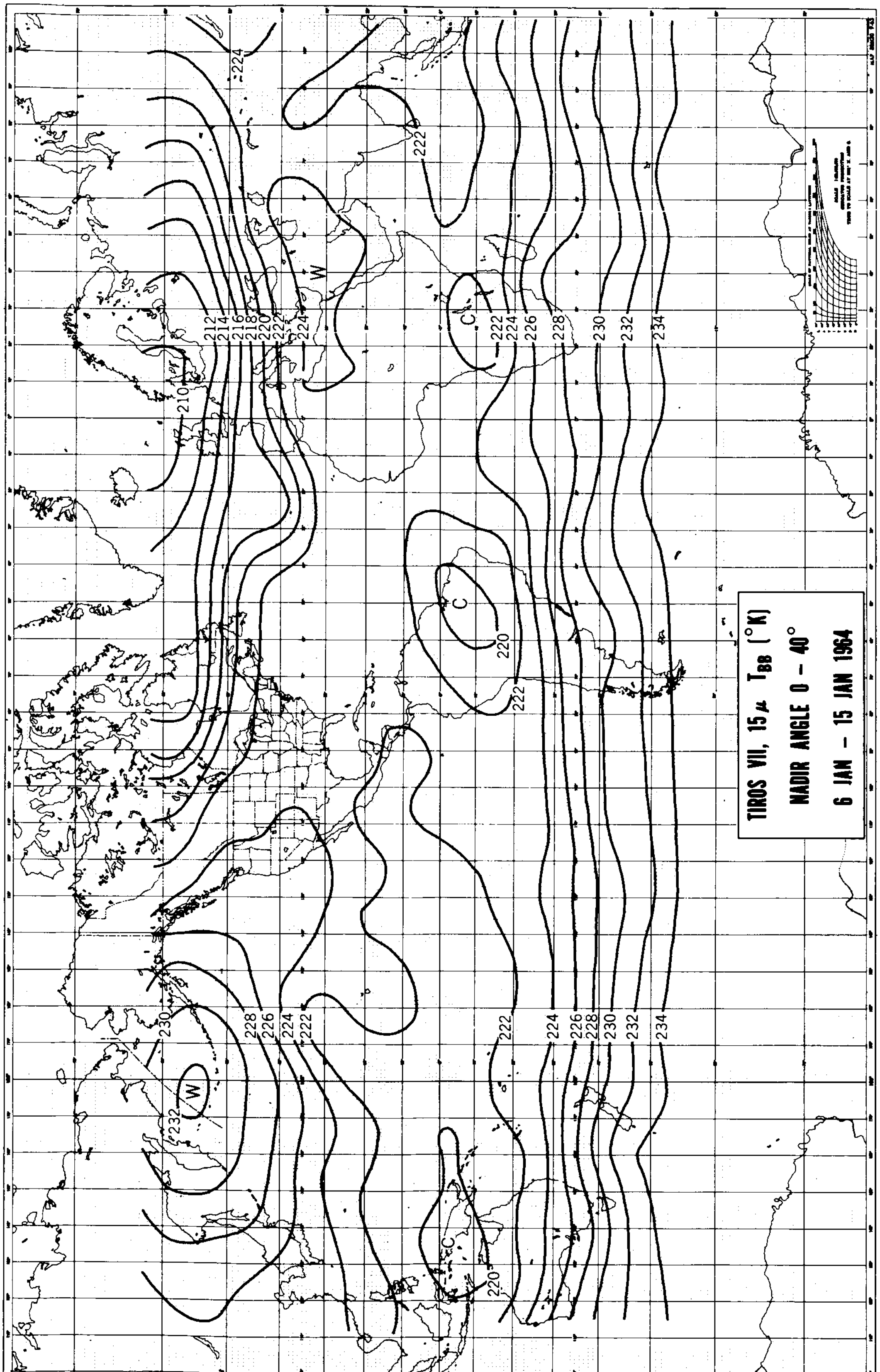
TIROS VII, 15 μ T_{BB} (°K)
NADIR ANGLE 0 – 40°
6 JAN – 15 JAN 1964

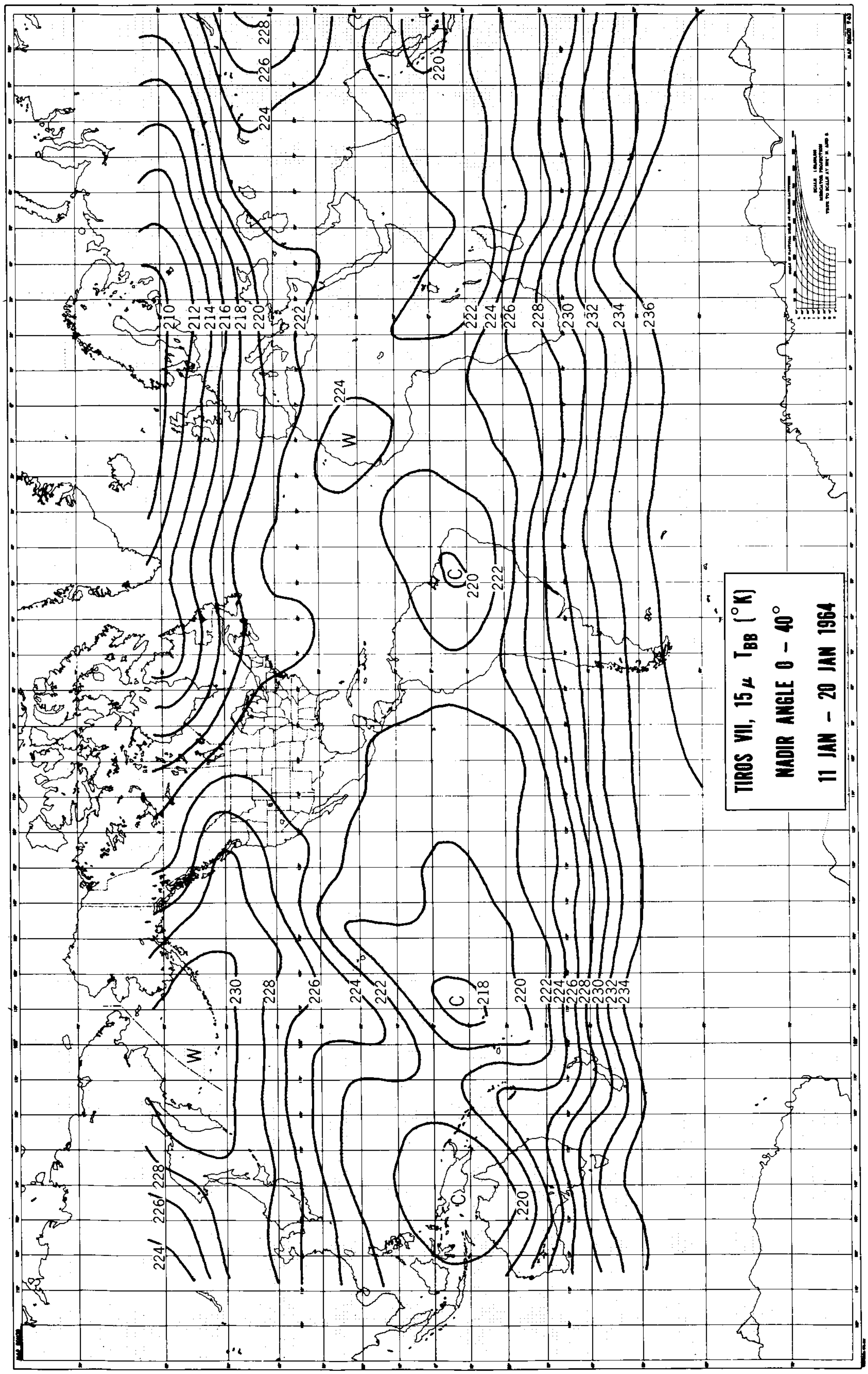
TIROS VII, 15 μ T_{BB} (°K)
NADIR ANGLE 0 – 40°
11 JAN – 20 JAN 1964

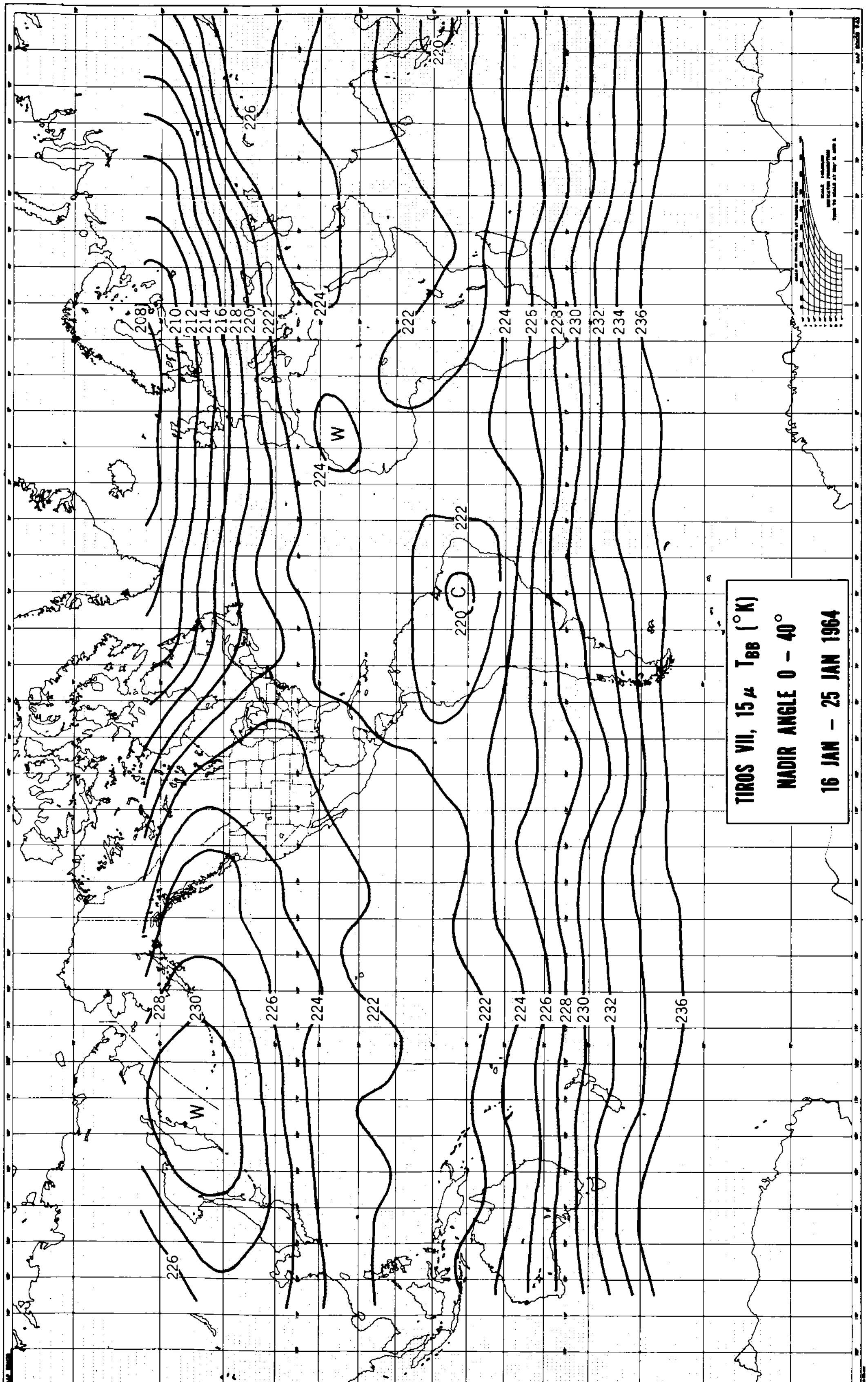
TIROS VII, 15μ T_{BB} (°K)
NADIR ANGLE 0 – 40°
16 JAN – 25 JAN 1964
208
210
212
214
216
218
220
222
224
225
228
230
232
234
236
226
W
C

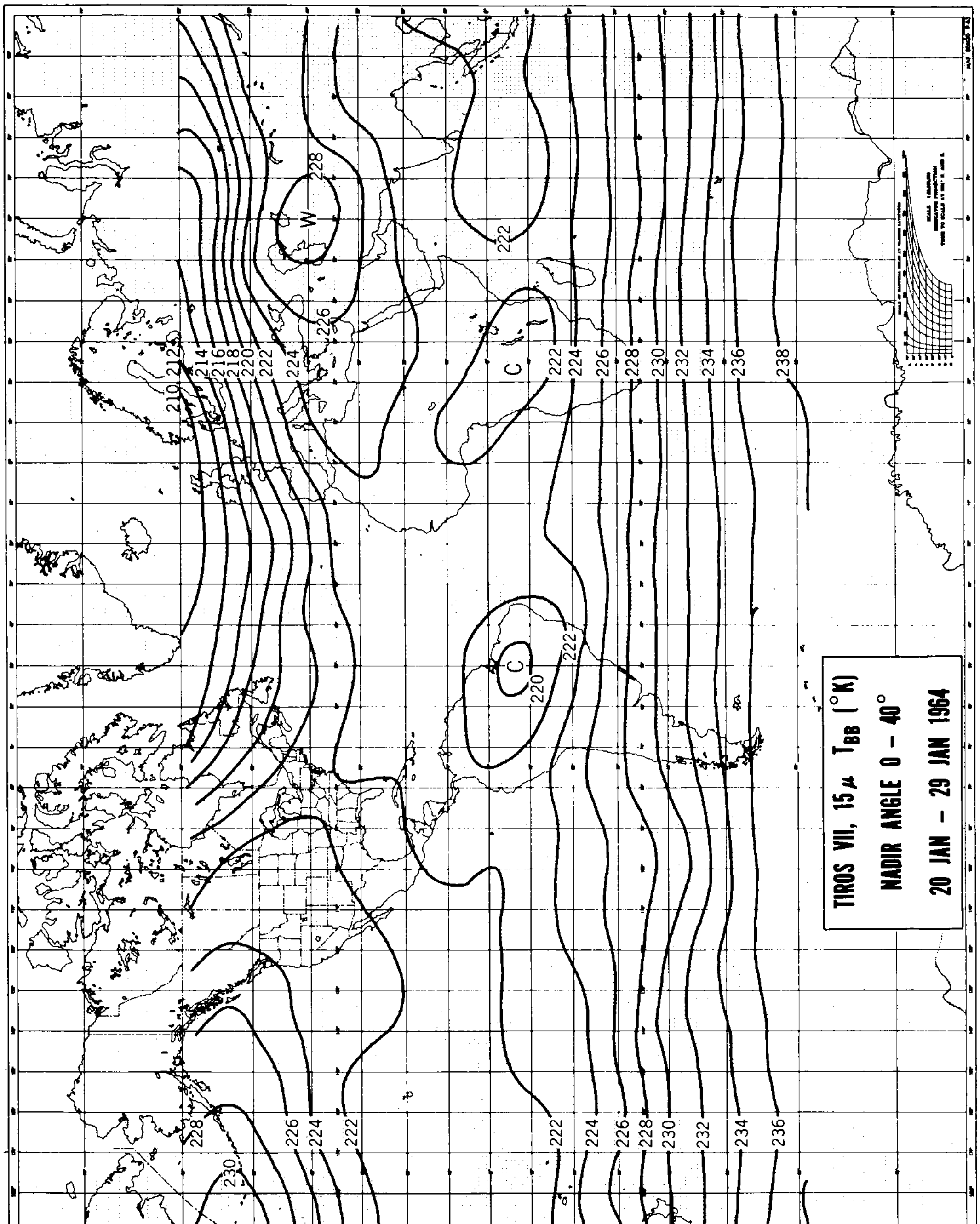
TIROS VII, 15 μ T_{BB} (°K)
NADIR ANGLE 0 – 40°
20 JAN – 29 JAN 1964

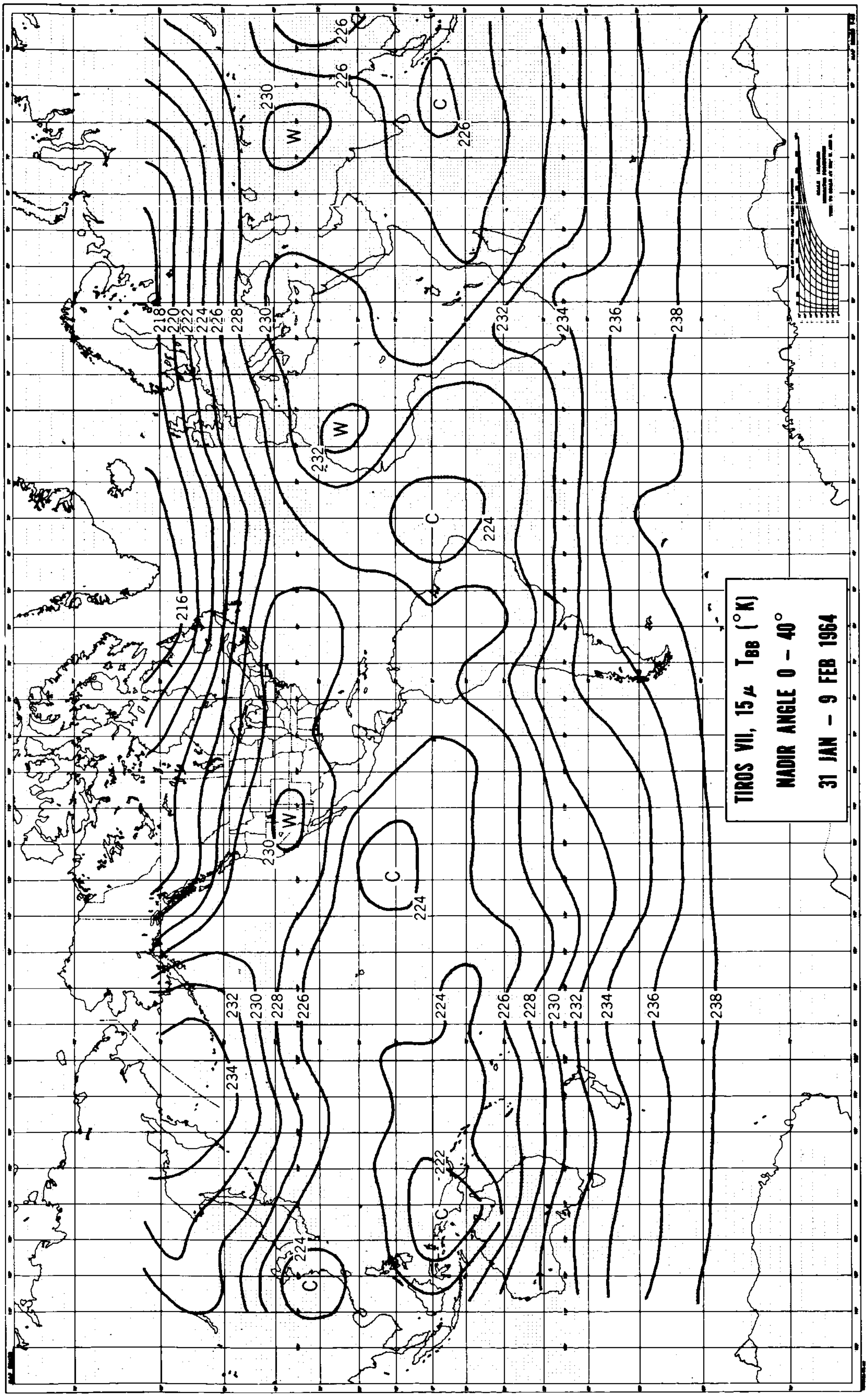
TIROS VII, 15μ T_BB (°K)
NADIR ANGLE 0 – 40°
31 JAN – 9 FEB 1964

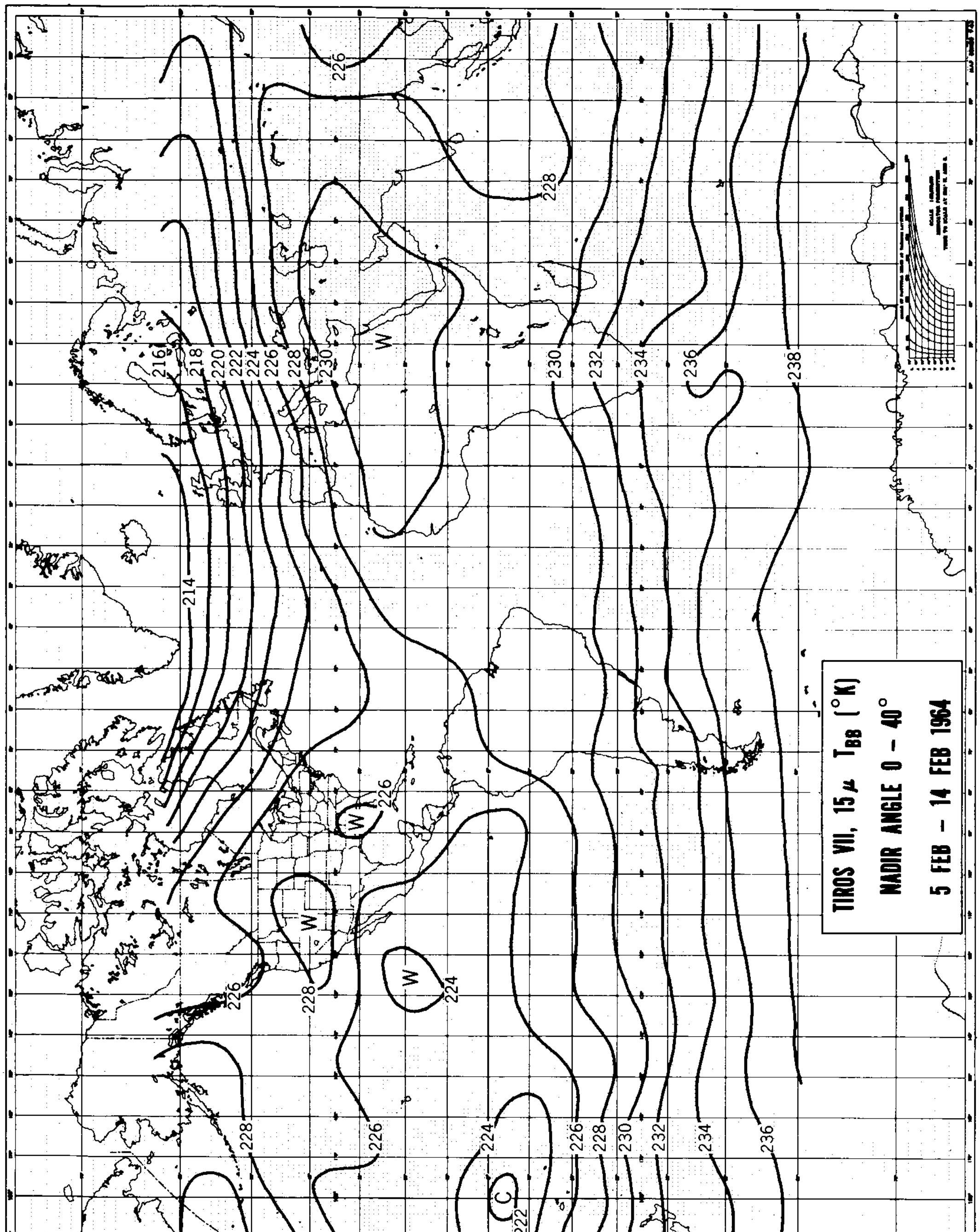

TIROS VII, 15μ T_BB (°K)
NADIR ANGLE 0 – 40°
5 FEB – 14 FEB 1964

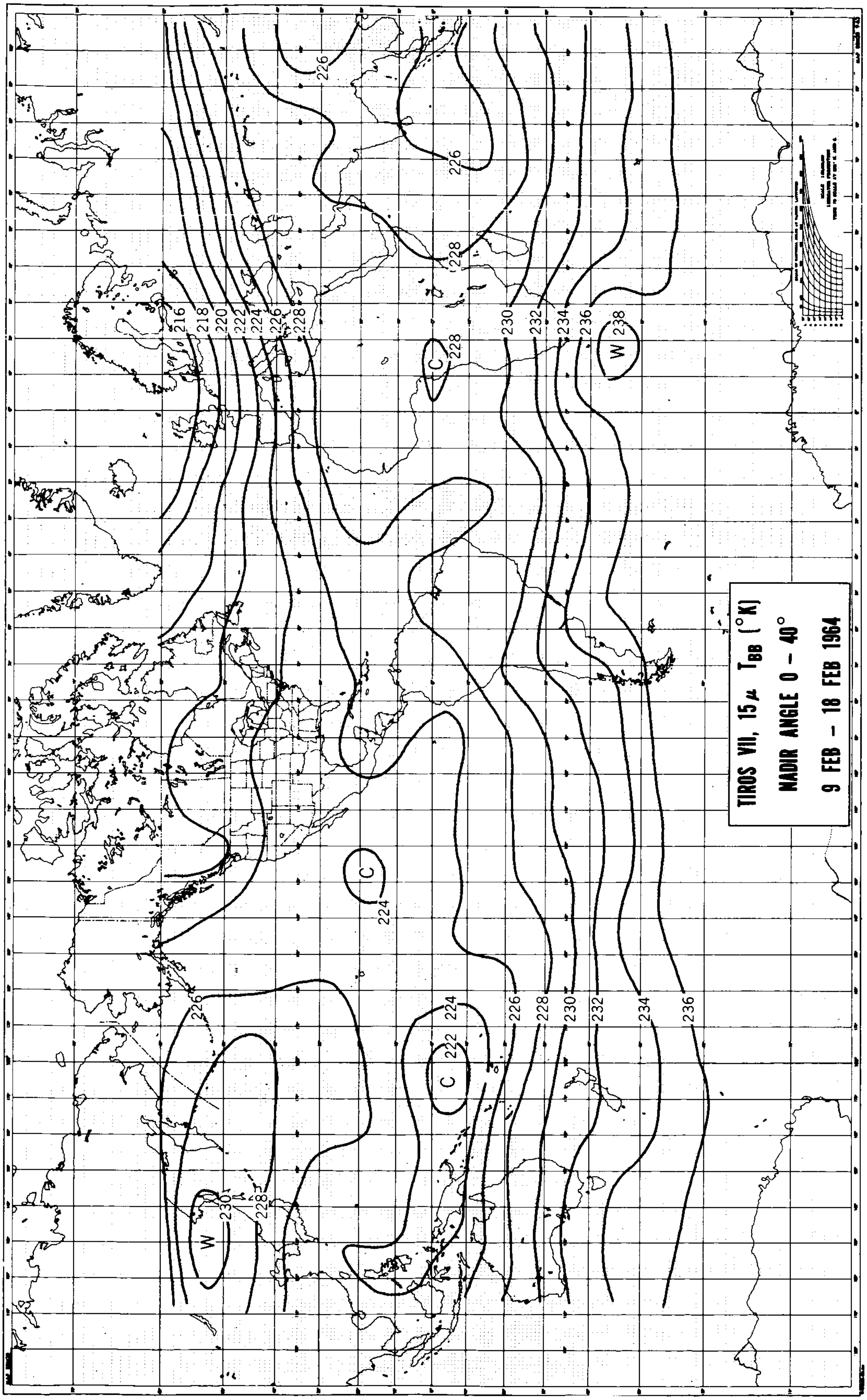
TIROS VII, 15μ T_{BB} (°K)
NADIR ANGLE 0 – 40°
9 FEB – 18 FEB 1964

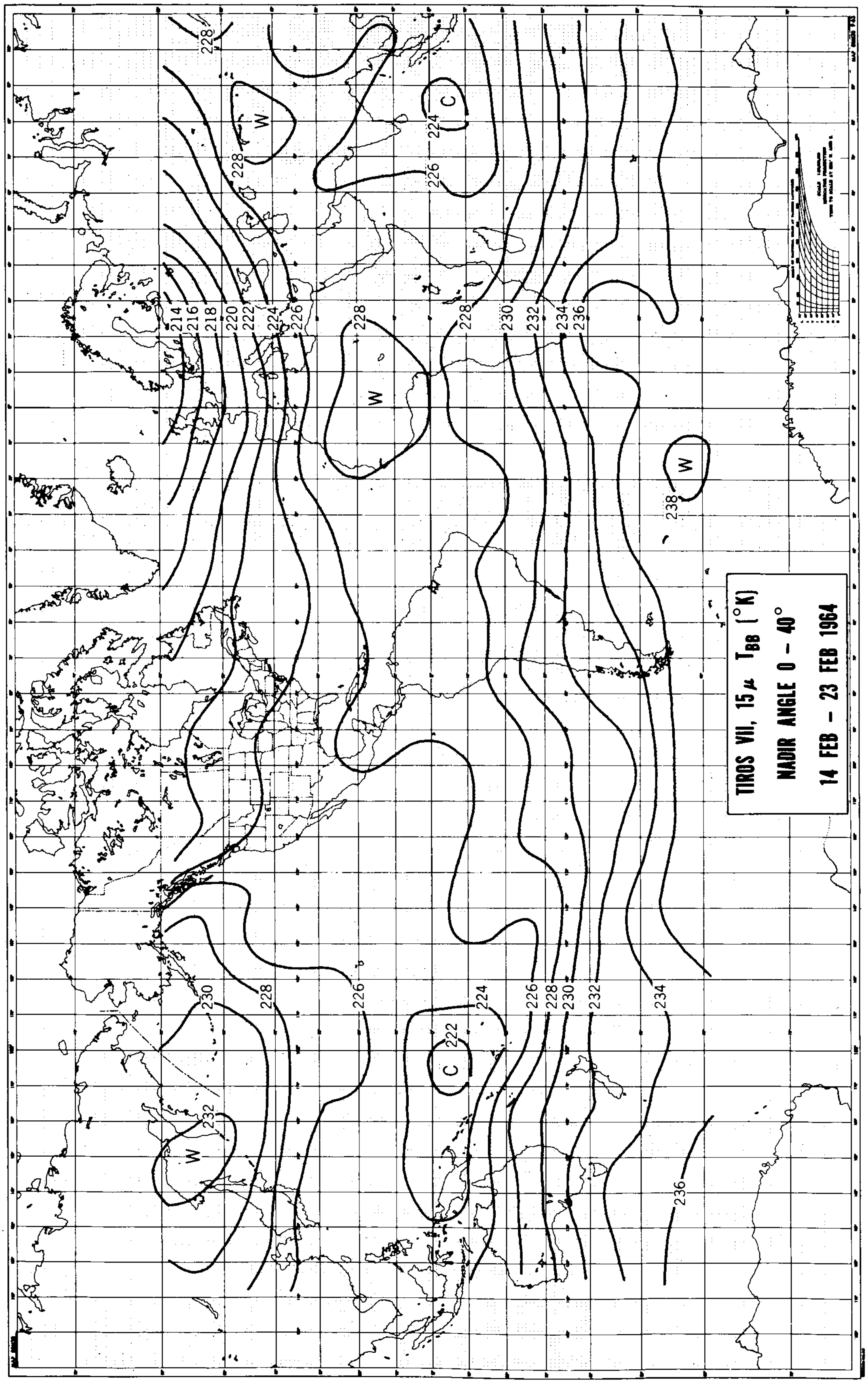
TIROS VII, 15μ T_{BB} (°K)
NADIR ANGLE 0 - 40°
14 FEB - 23 FEB 1964

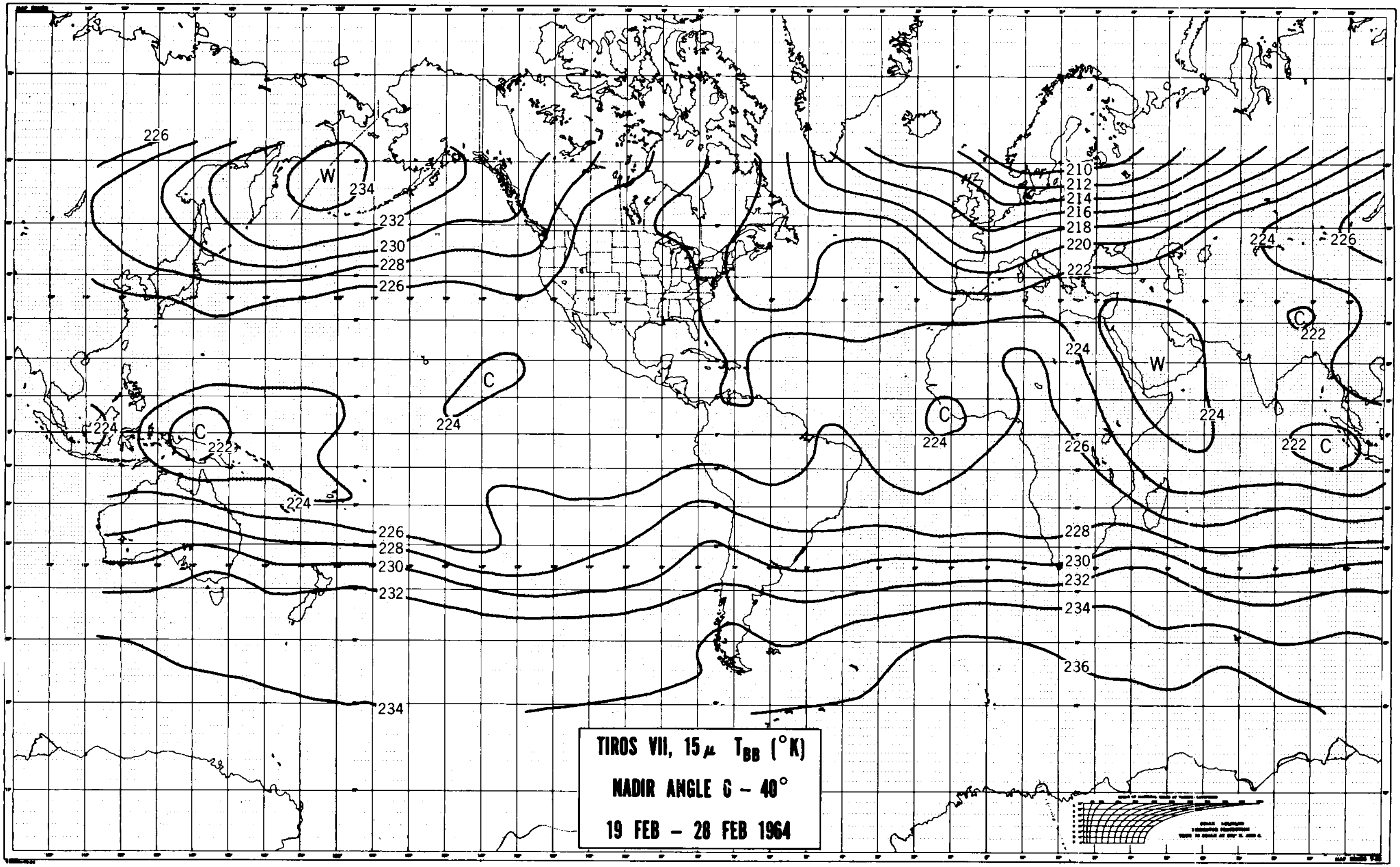
TIROS VII, 15 μ T_BB (°K)
NADIR ANGLE 0 - 40°
19 FEB - 28 FEB 1964

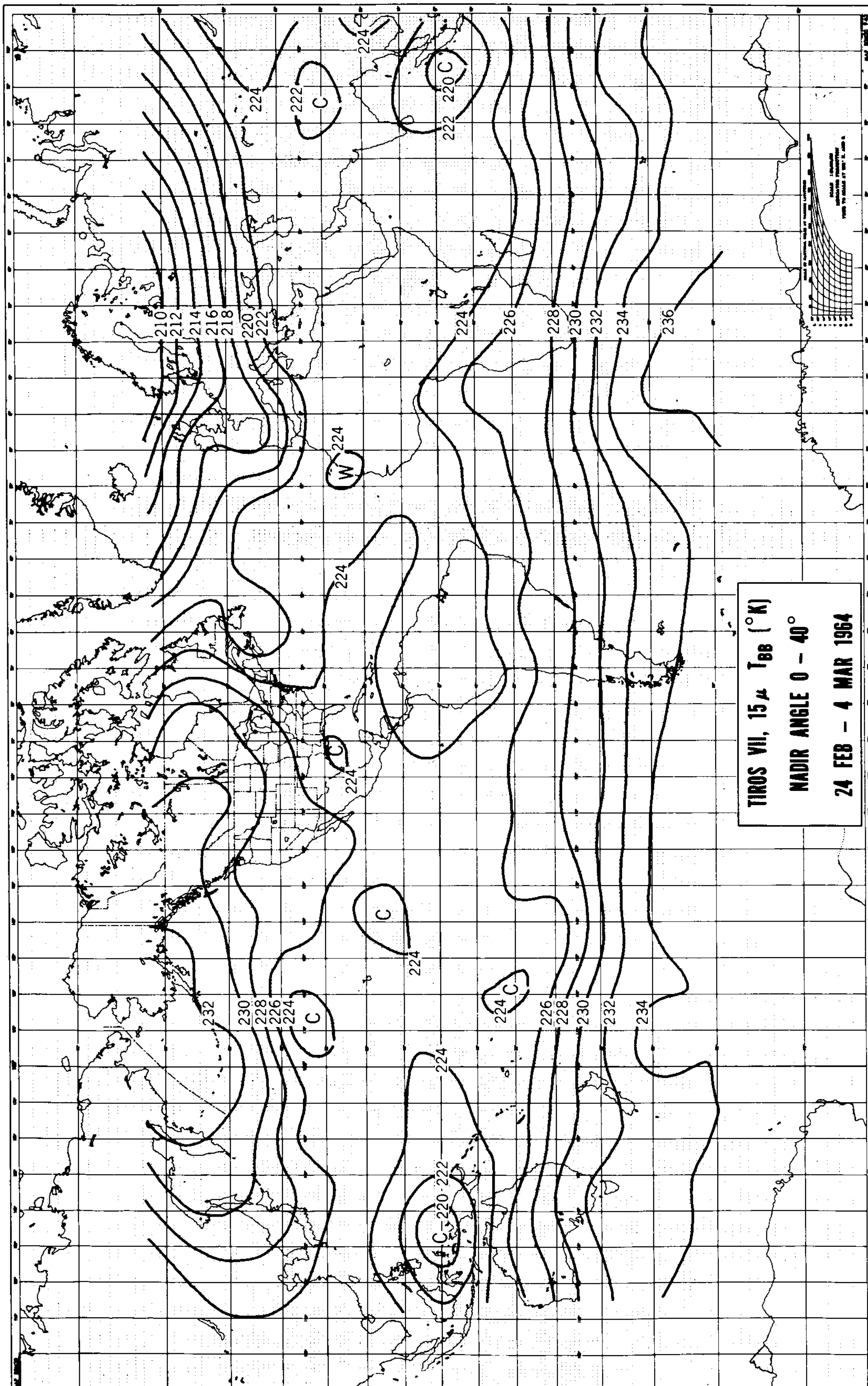
TIROS VII, 15μ T_{BB} (°K)
NADIR ANGLE 0 - 40°
24 FEB - 4 MAR 1964

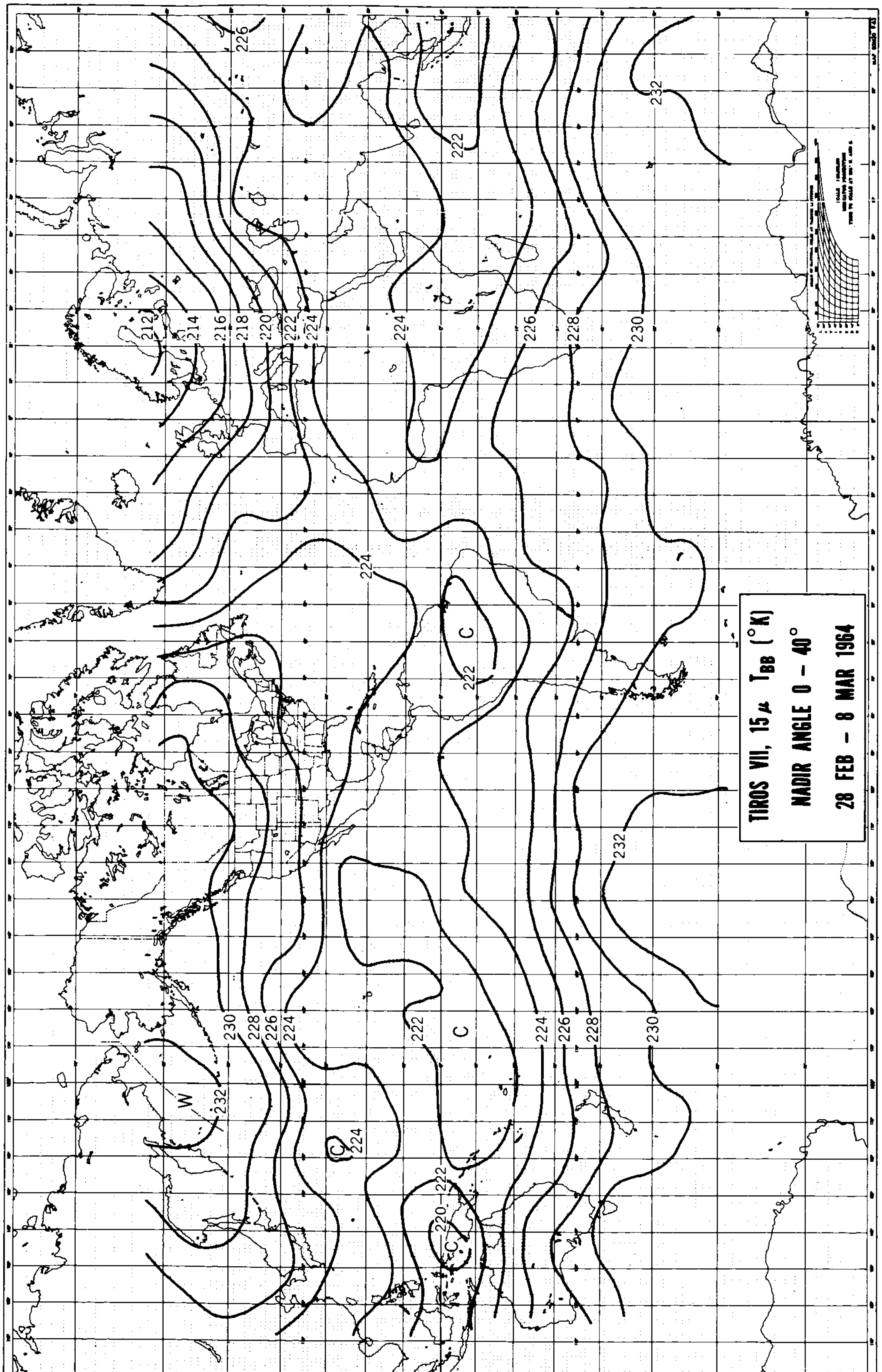
TIROS VII, 15 μ T_{BB} (°K)
NADIR ANGLE 0 – 40°
28 FEB – 8 MAR 1964

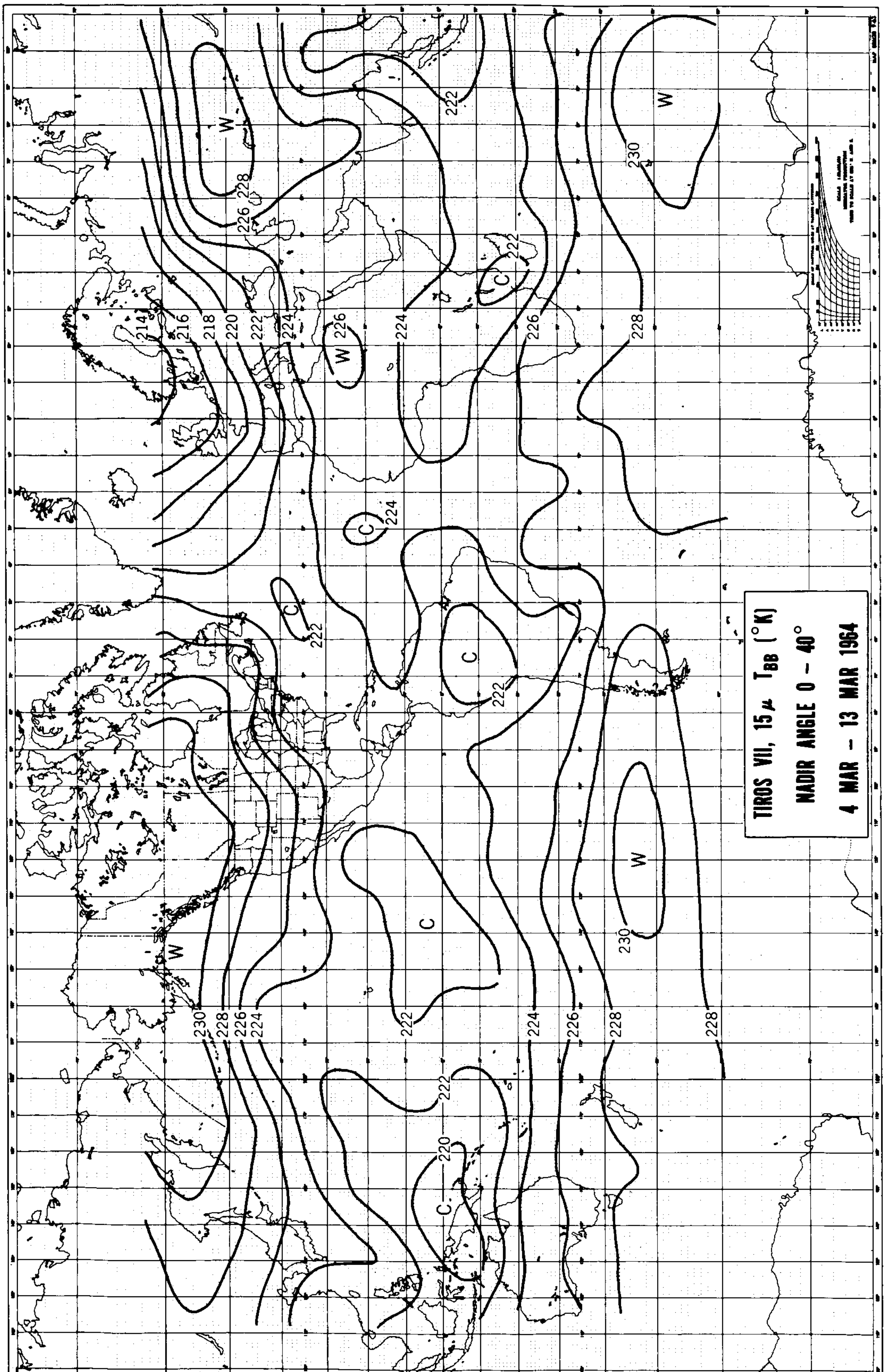
TIROS VII, 15 μ T_{BB} (°K)
NADIR ANGLE 0 – 40°
4 MAR – 13 MAR 1964

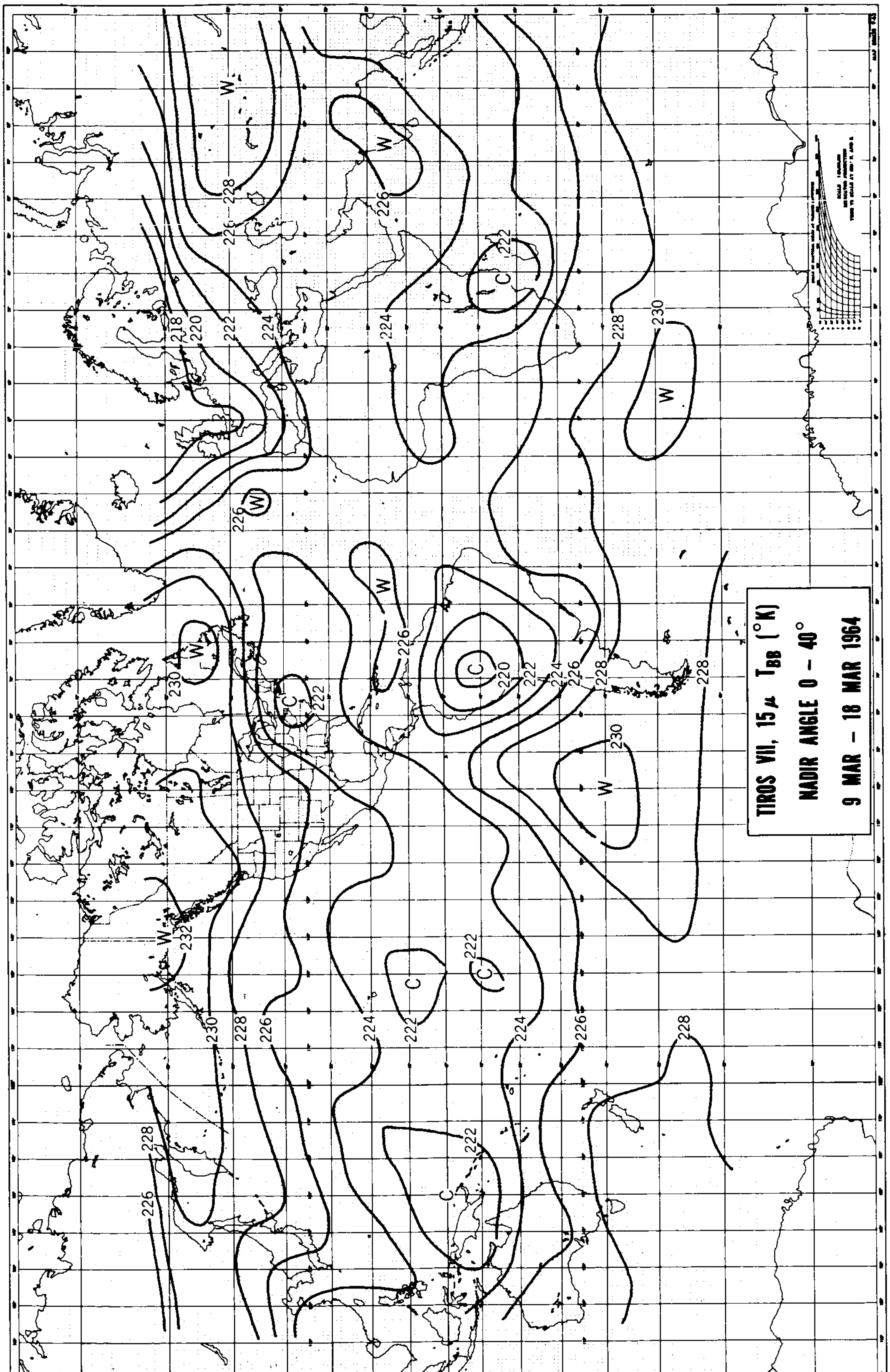
TIROS VII, 15 μ T_{BB} (°K)
NADIR ANGLE 0 – 40°
9 MAR – 18 MAR 1964

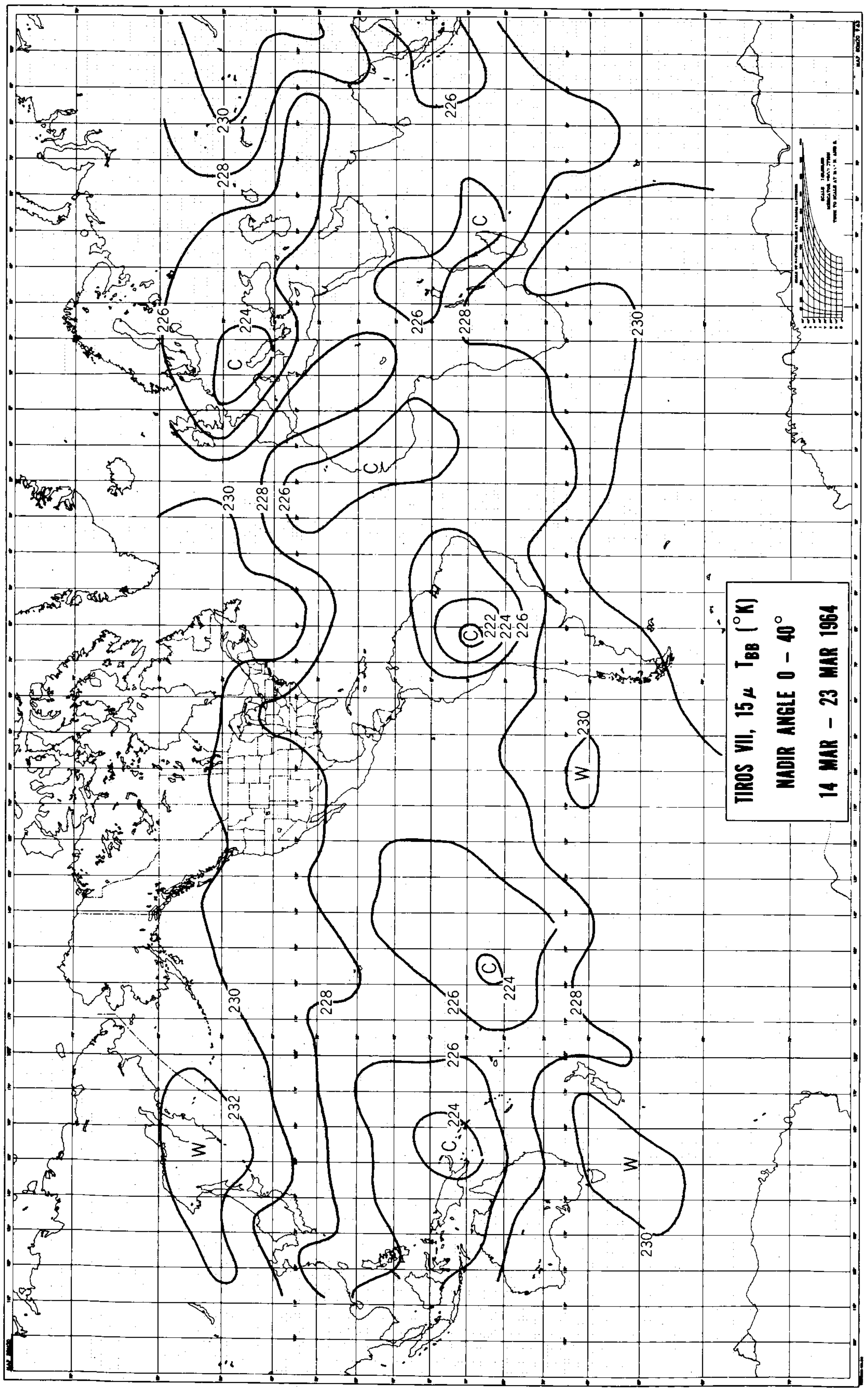
TIROS VII, 15 μ T_{BB} (°K)
NADIR ANGLE 0 – 40°
14 MAR – 23 MAR 1964
222
224
226
228
230
232
C
W

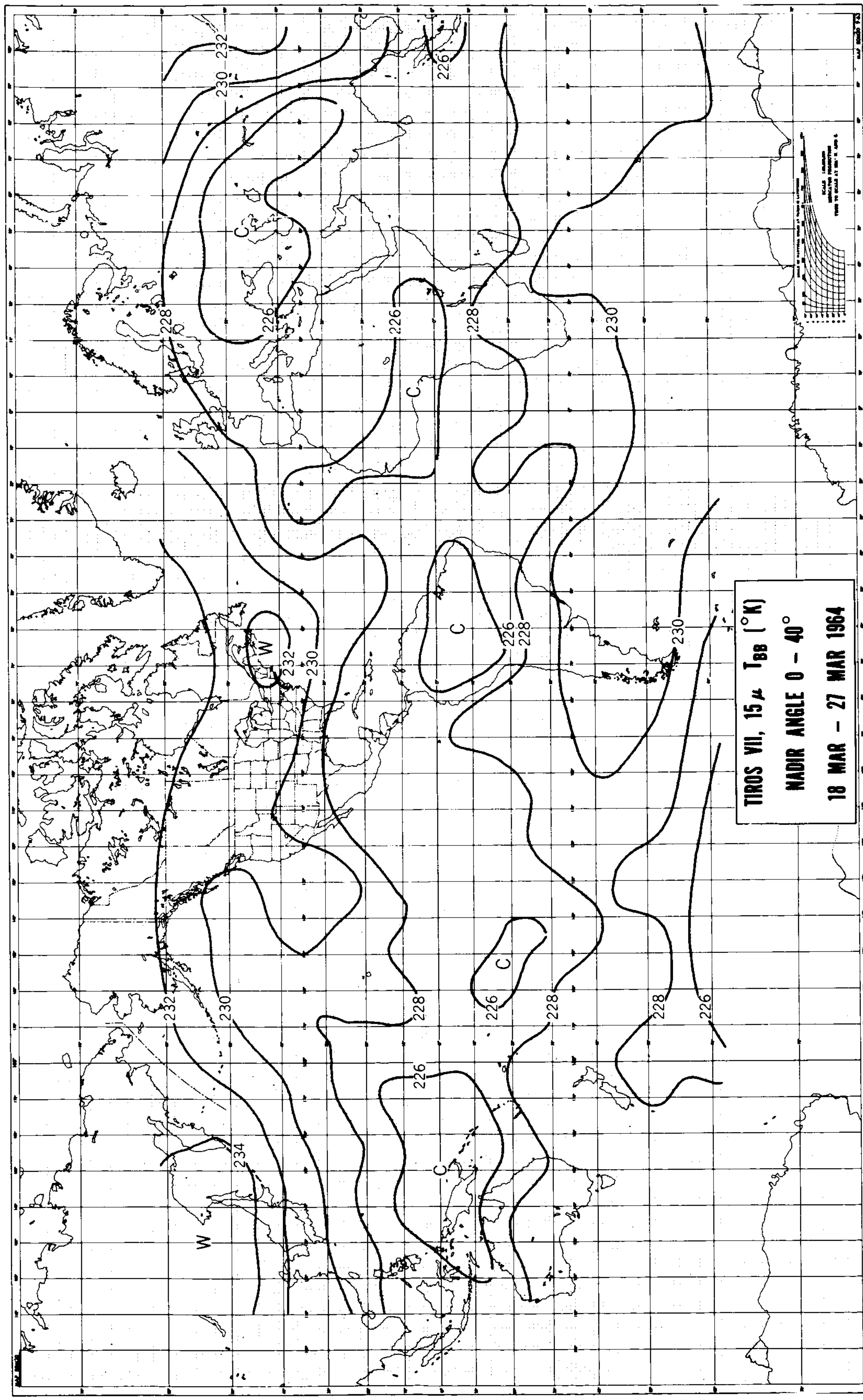
TIROS VII, 15μ T_{BB} (°K)
NADIR ANGLE 0 – 40°
18 MAR – 27 MAR 1964

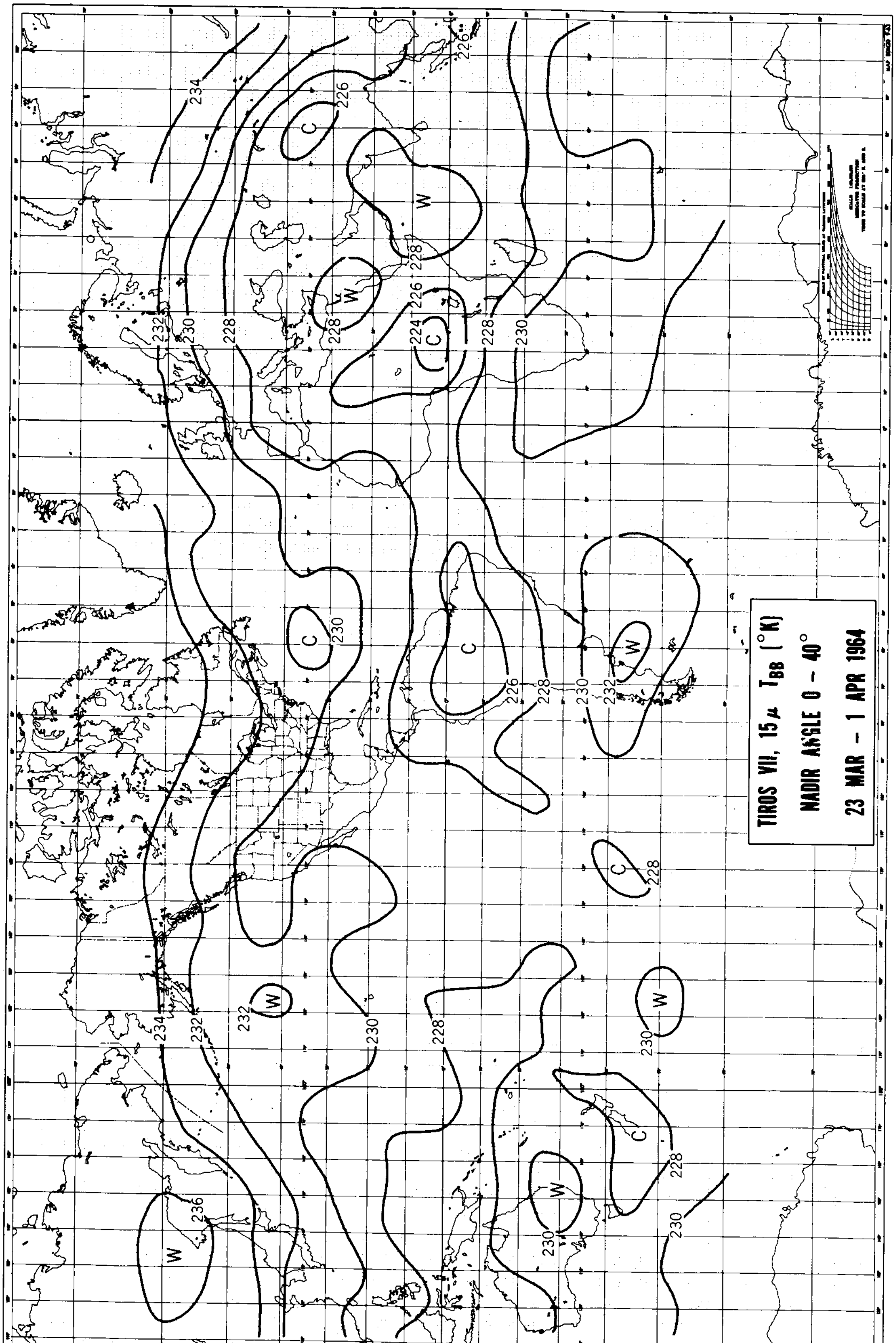
TIROS VII, 15 μ T_BB (°K)
NADIR ANGLE 0 – 40°
23 MAR – 1 APR 1964

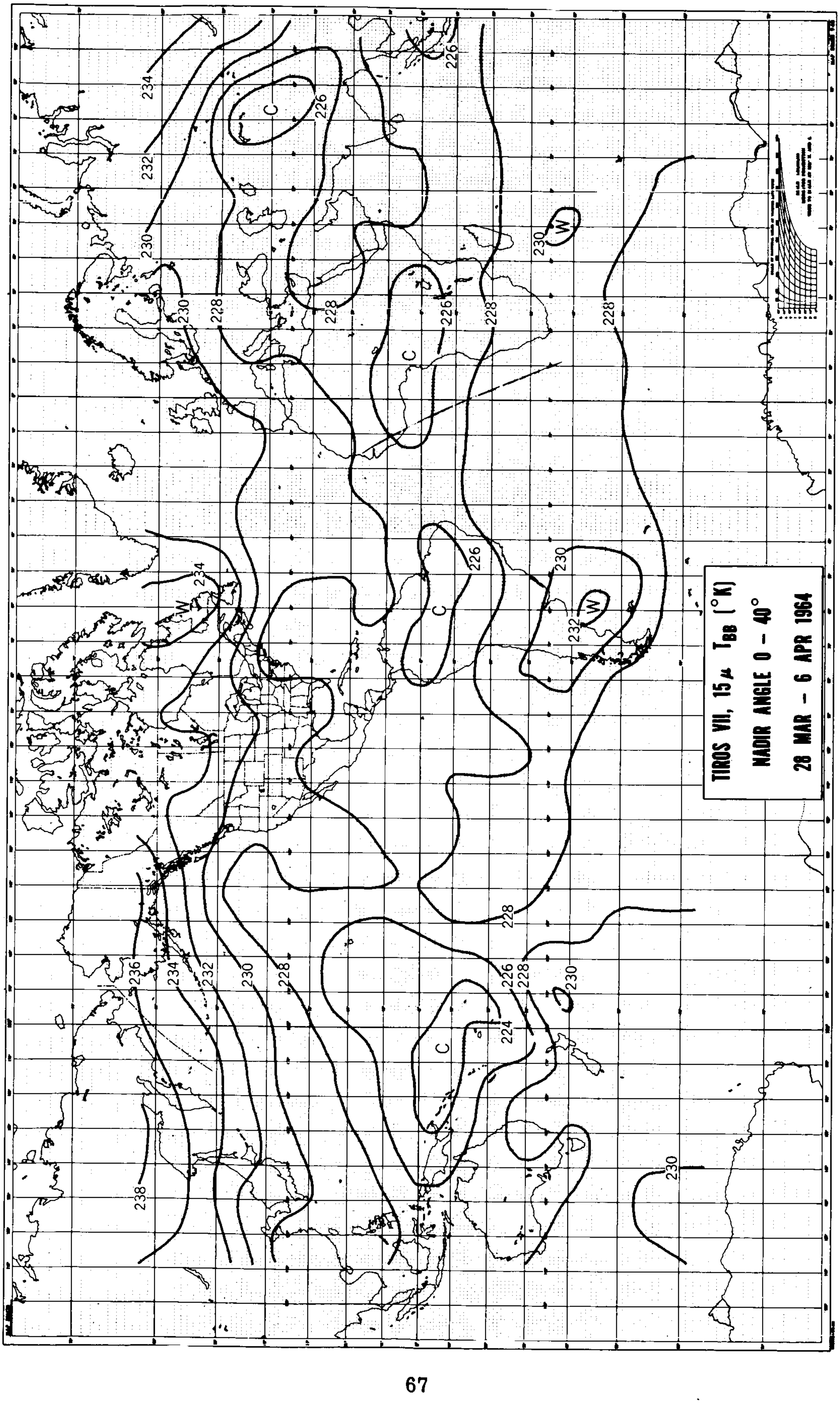
TIROS VII, 15μ T_{BB} (°K)
NADIR ANGLE 0 – 40°
28 MAR – 6 APR 1964

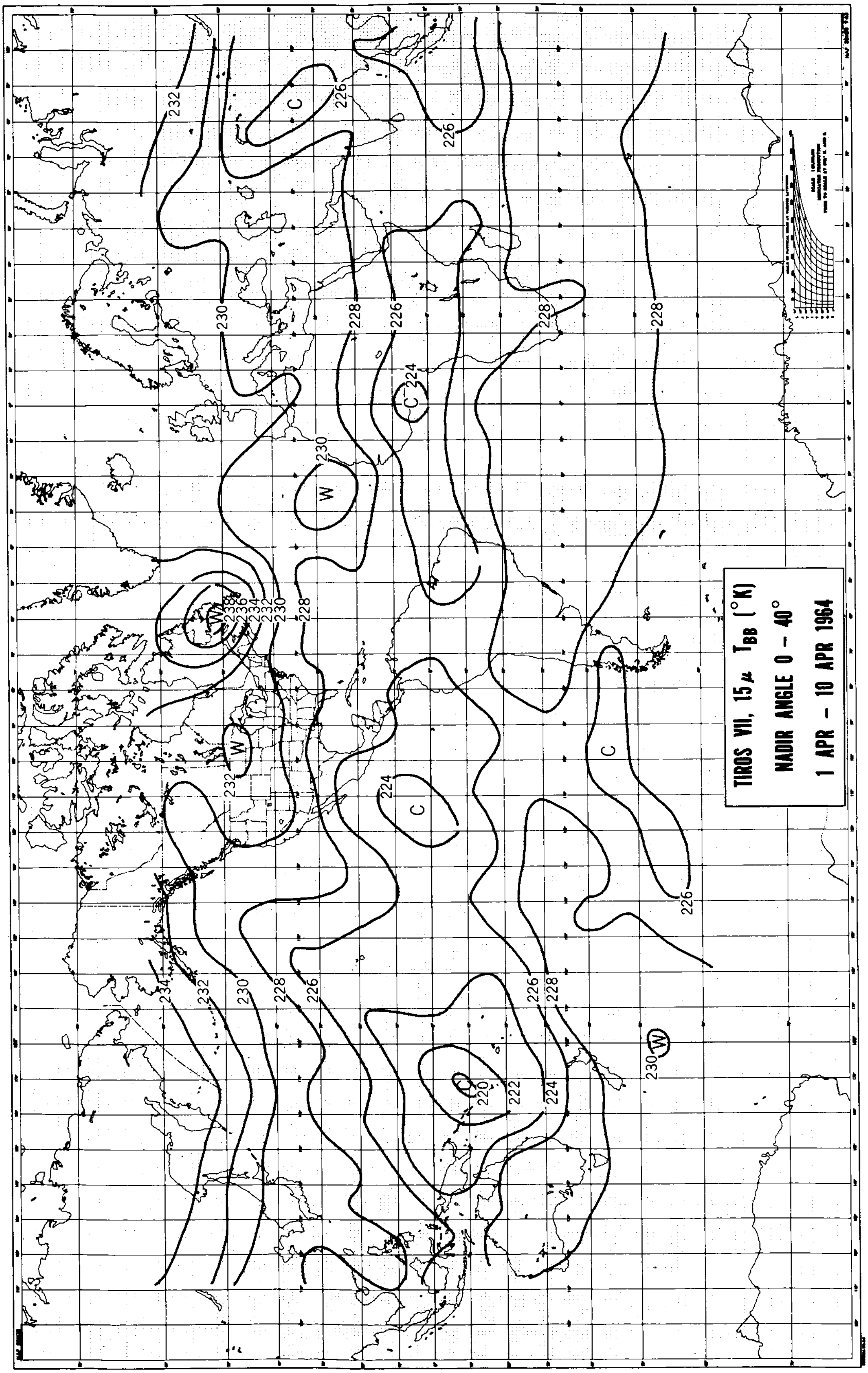
TIROS VII, 15μ T_BB (°K)
NADIR ANGLE 0 – 40°
1 APR – 10 APR 1964

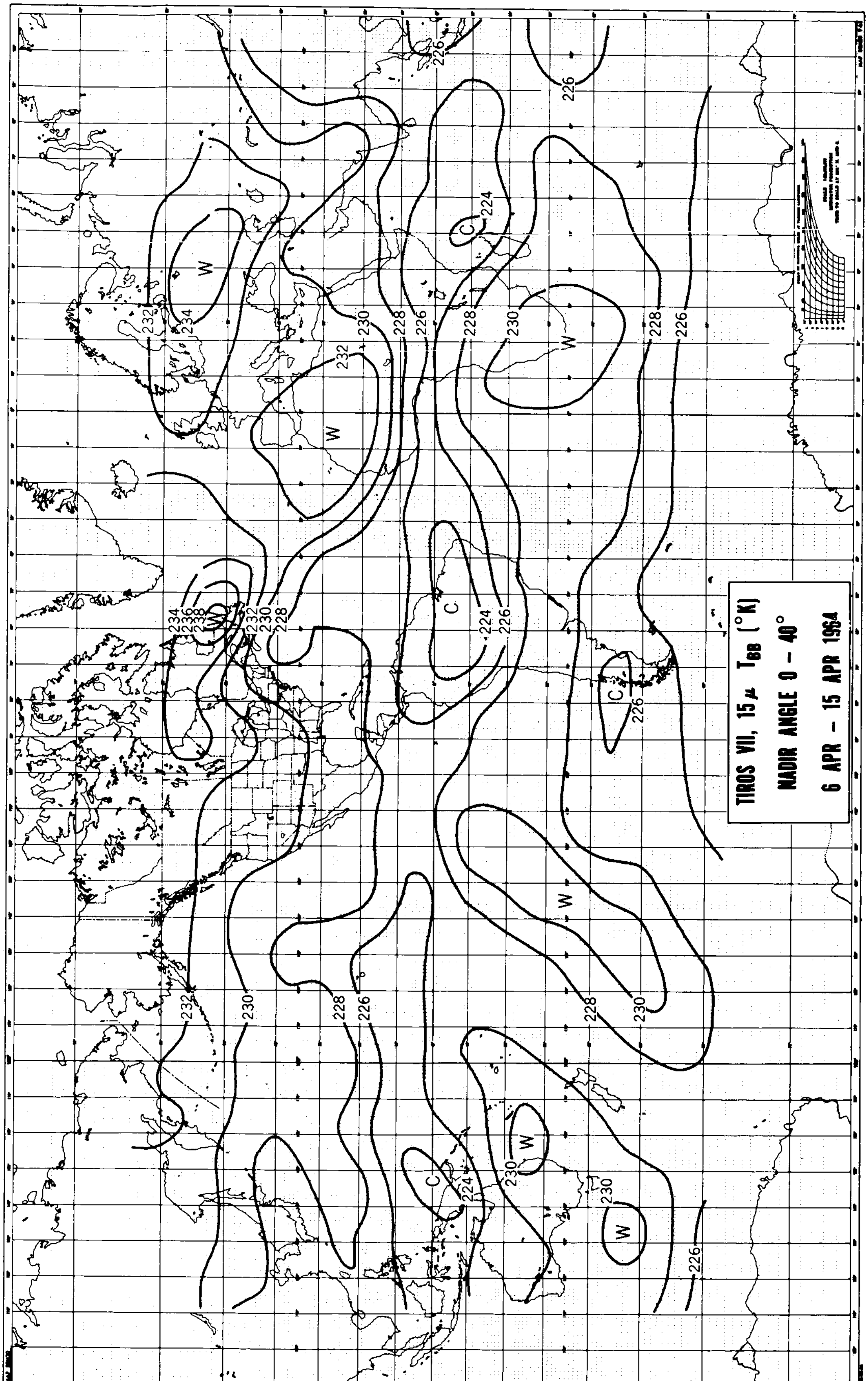

TIROS VII, 15μ T_{BB} (°K)
NADIR ANGLE 0 – 40°
6 APR – 15 APR 1964

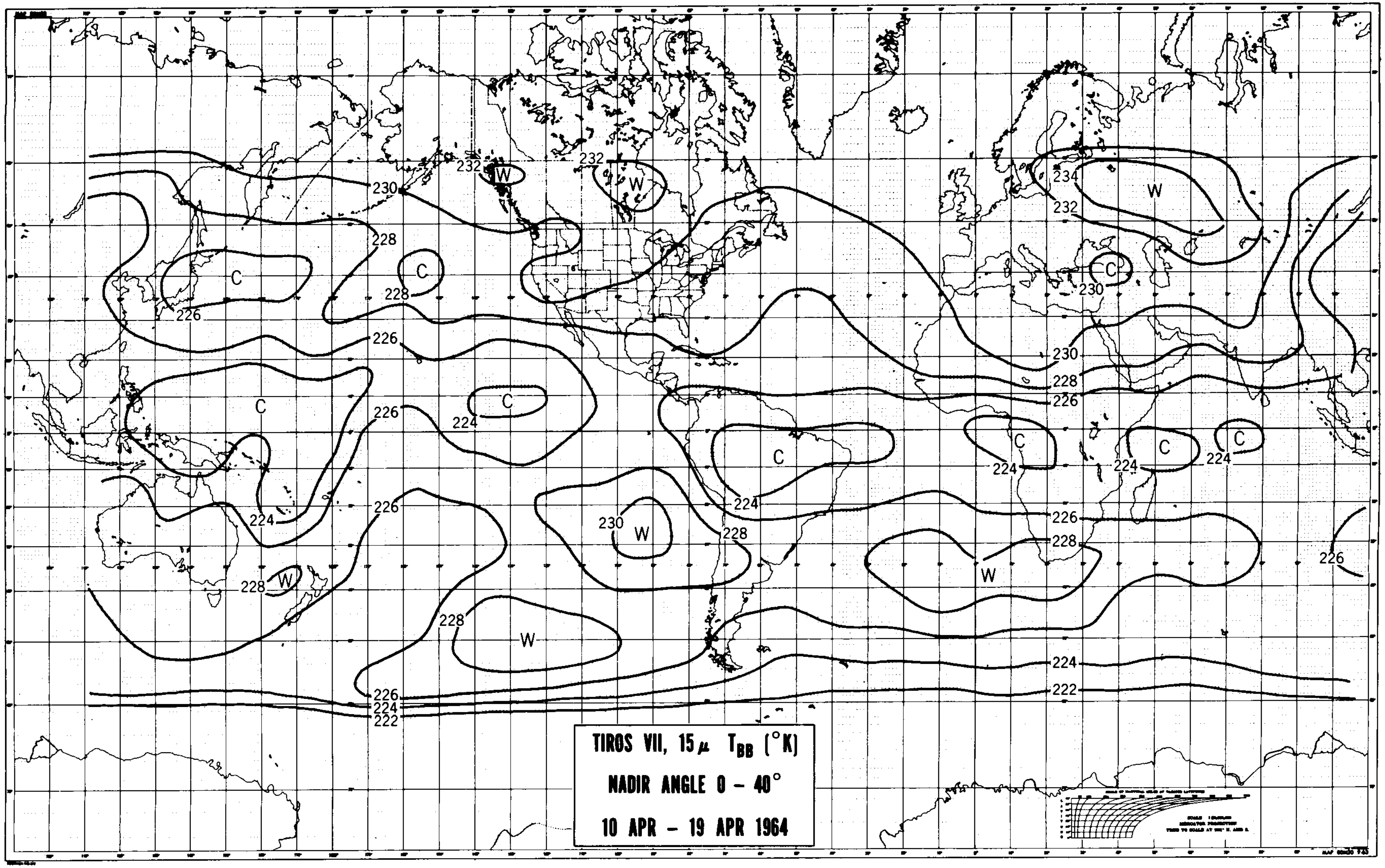
TIROS VII, 15 μ T_{BB} (°K)
NADIR ANGLE 0 – 40°
10 APR – 19 APR 1964

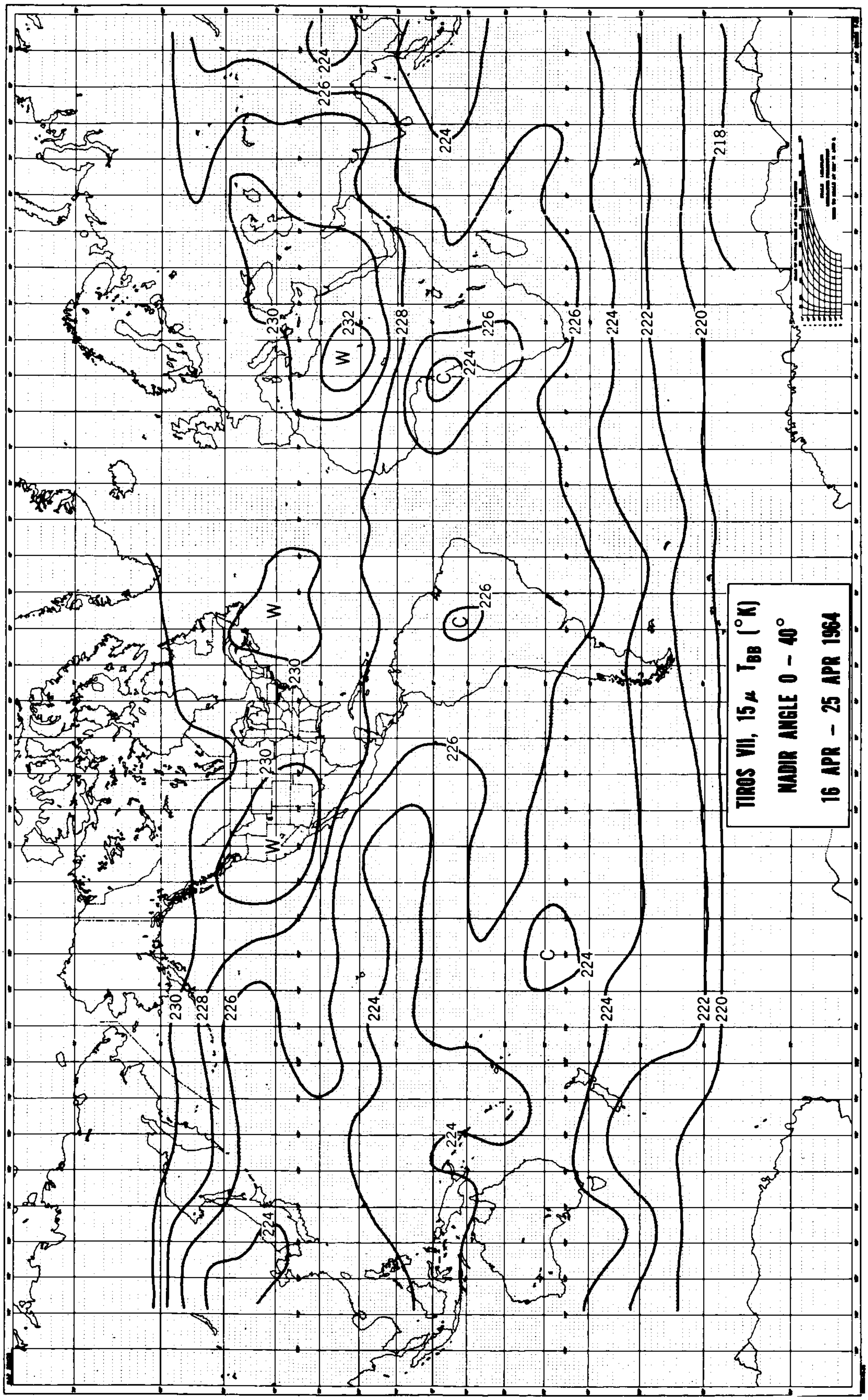

TIROS VII, 15μ T_{BB} (°K)
NADIR ANGLE 0 – 40°
16 APR – 25 APR 1964

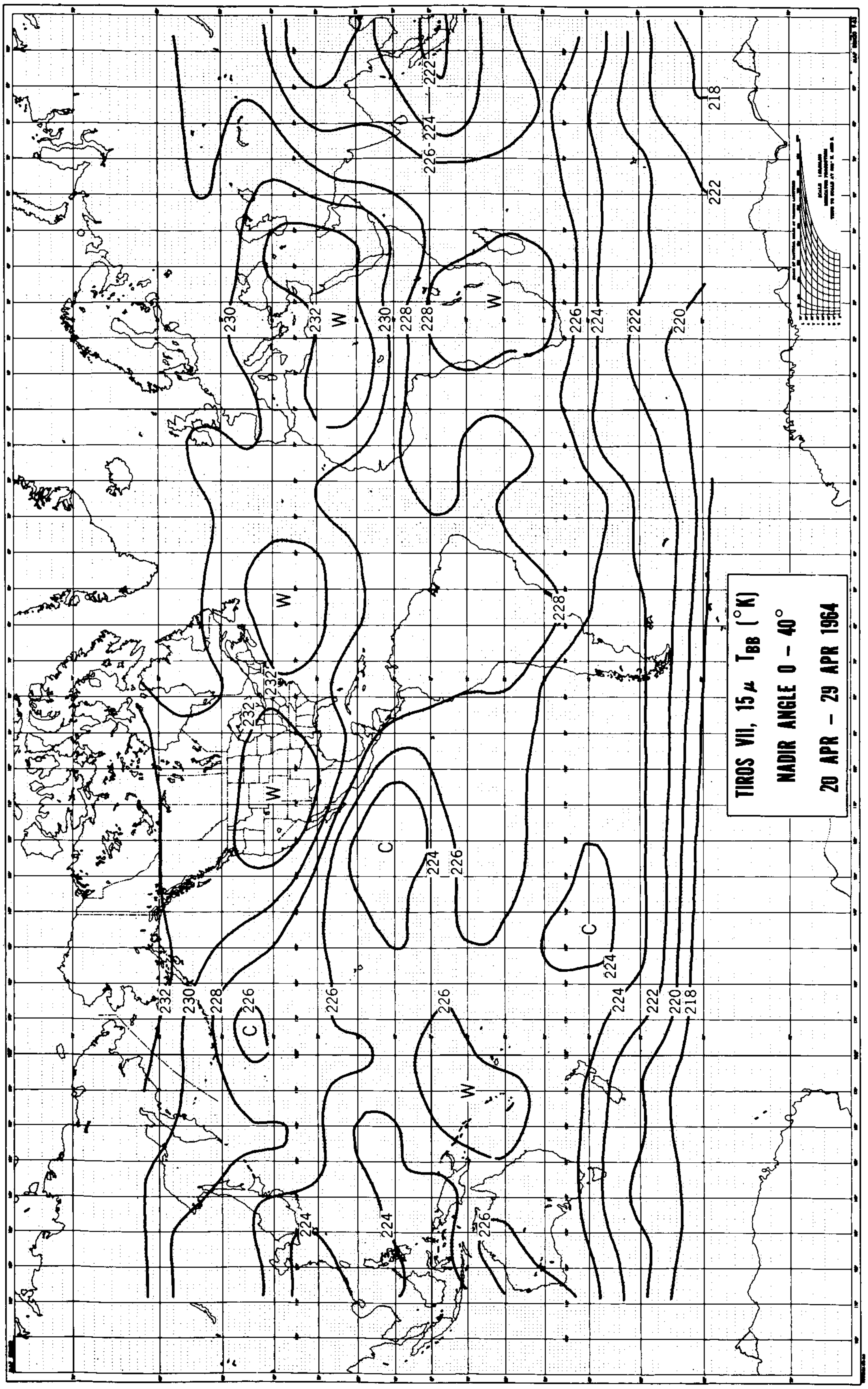
TIROS VII, 15 μ T_BB (°K)
NADIR ANGLE 0 - 40°
20 APR - 29 APR 1964

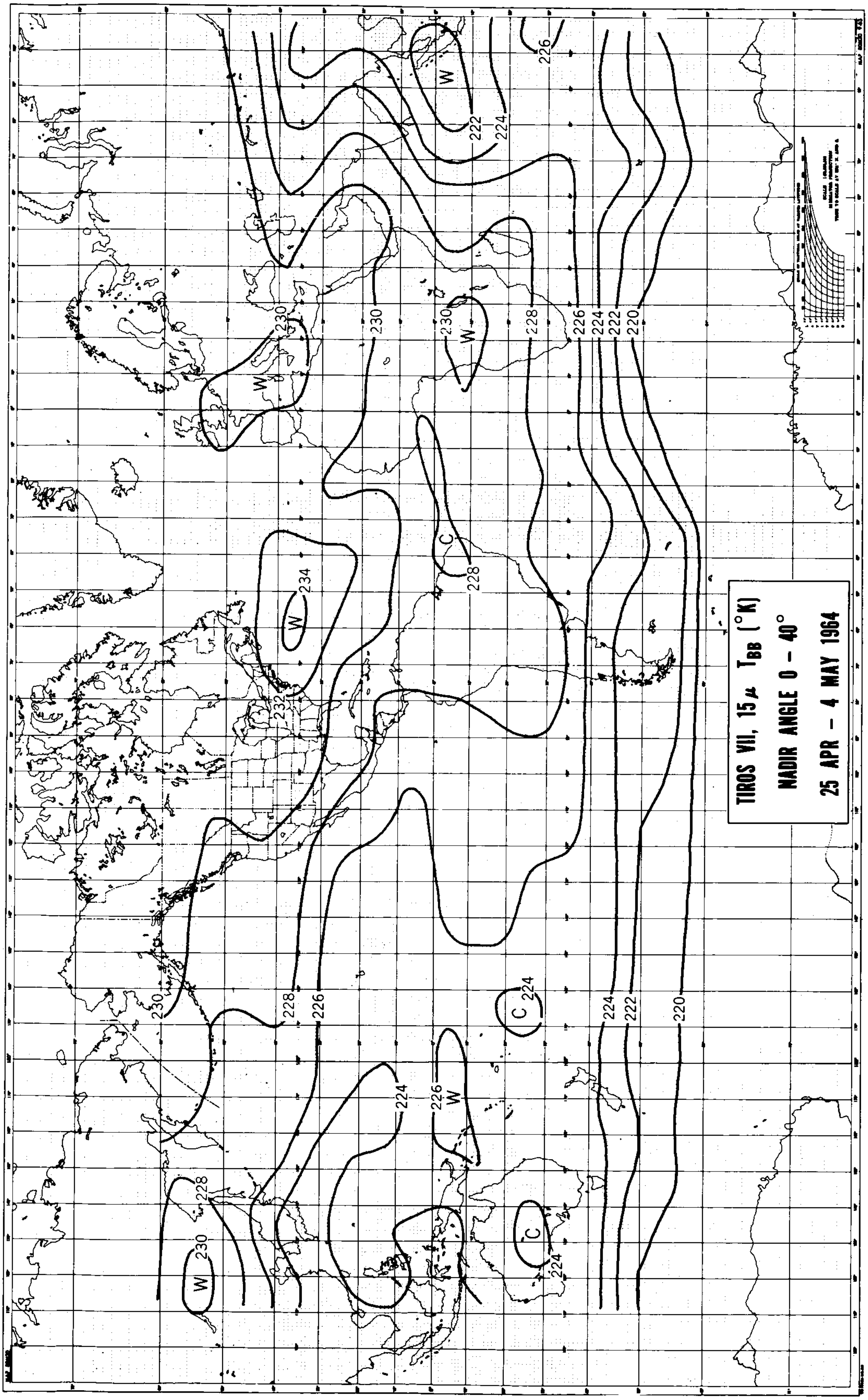

TIROS VII, 15μ T_{BB} (°K)
NADIR ANGLE 0 - 40°
25 APR - 4 MAY 1964

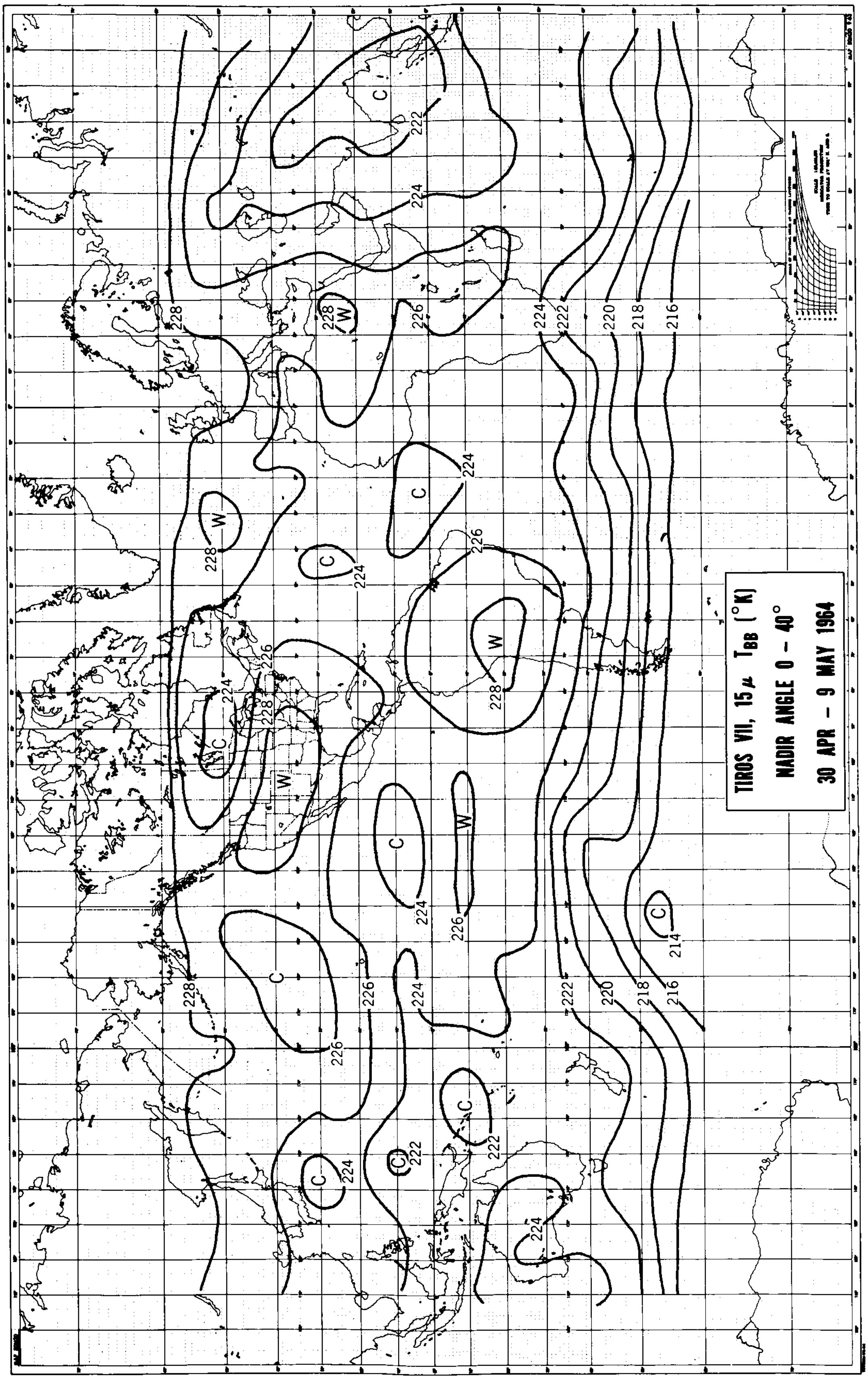
TIROS VII, 15 μ T_{BB} (°K)
NADIR ANGLE 0 – 40°
30 APR – 9 MAY 1964

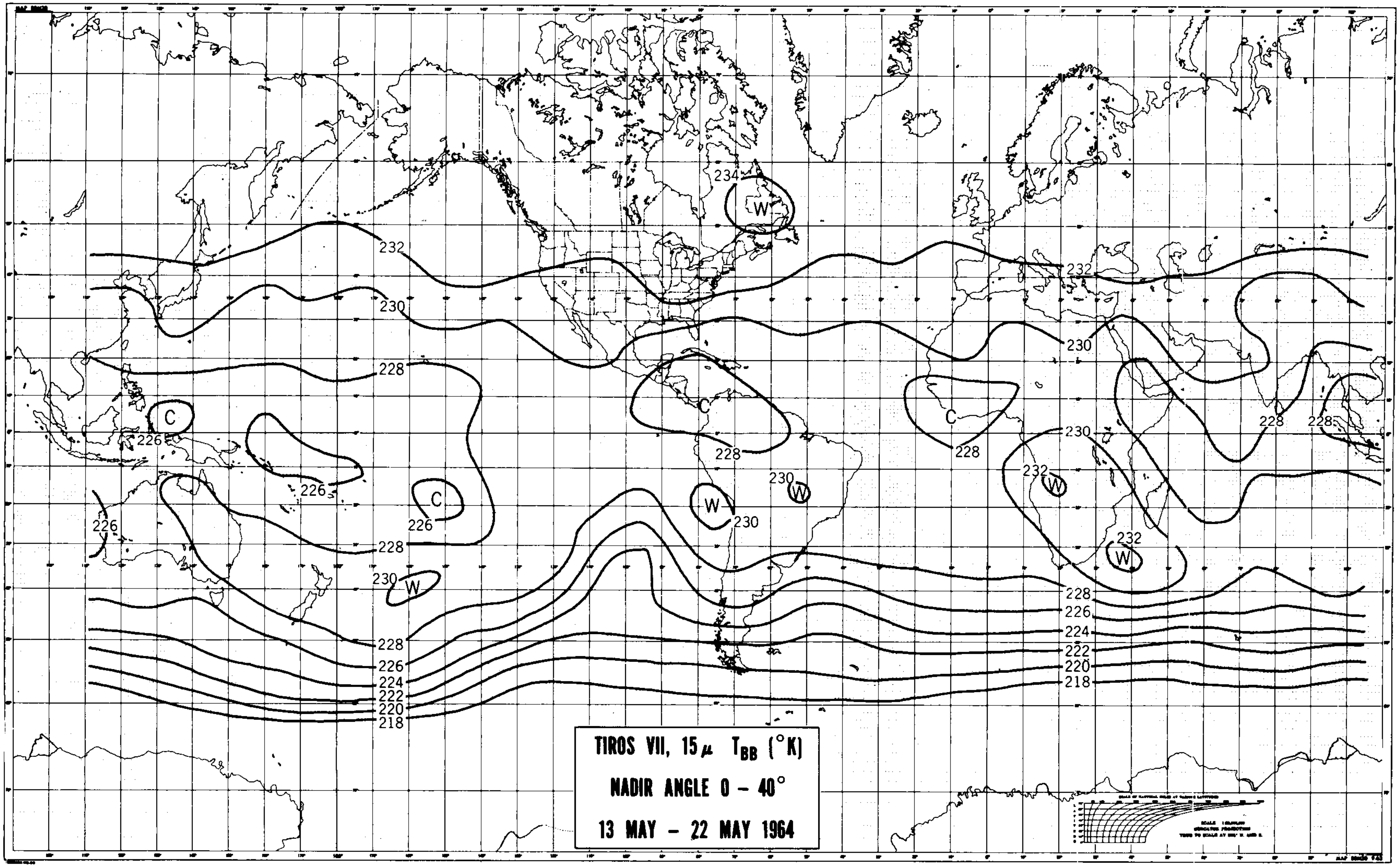
TIROS VII, 15 μ T_BB (°K)
NADIR ANGLE 0 – 40°
13 MAY – 22 MAY 1964
232
230
228
226
224
222
220
218
234
W
C

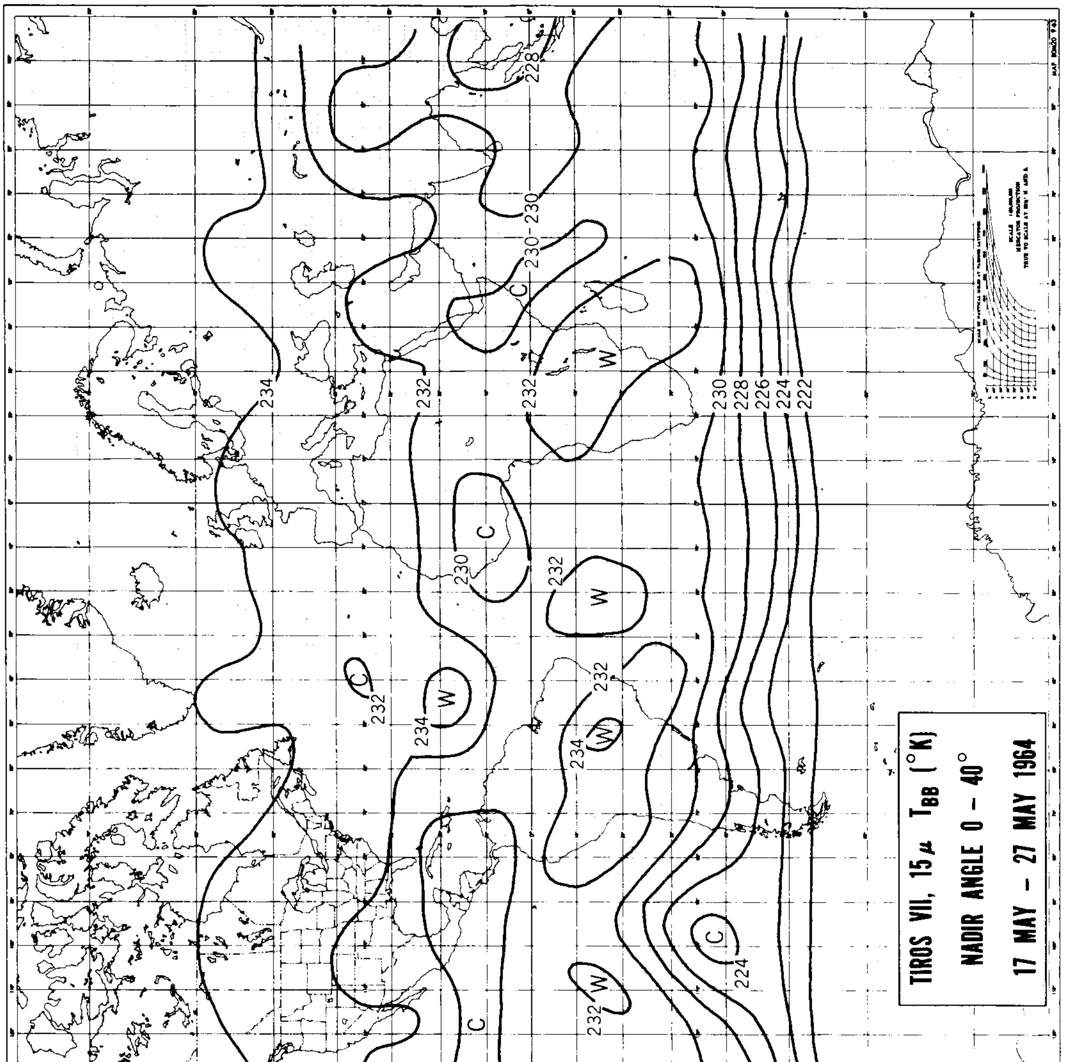
TIROS VII, 15 μ T_BB (°K)
NADIR ANGLE 0 – 40°
17 MAY – 27 MAY 1964

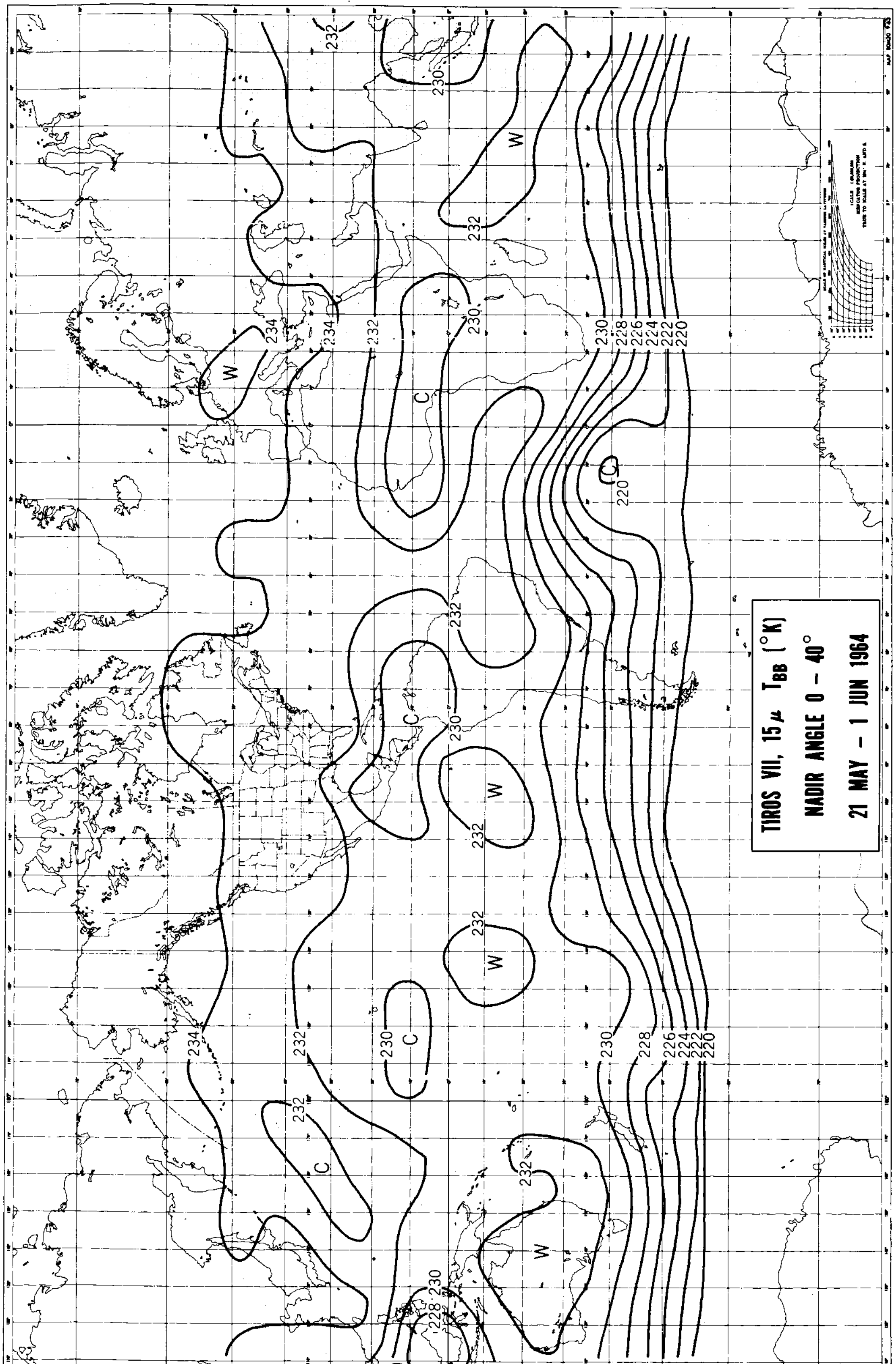
TIROS VII, 15 μ T_{BB} (°K)
NADIR ANGLE 0 – 40°
21 MAY – 1 JUN 1964

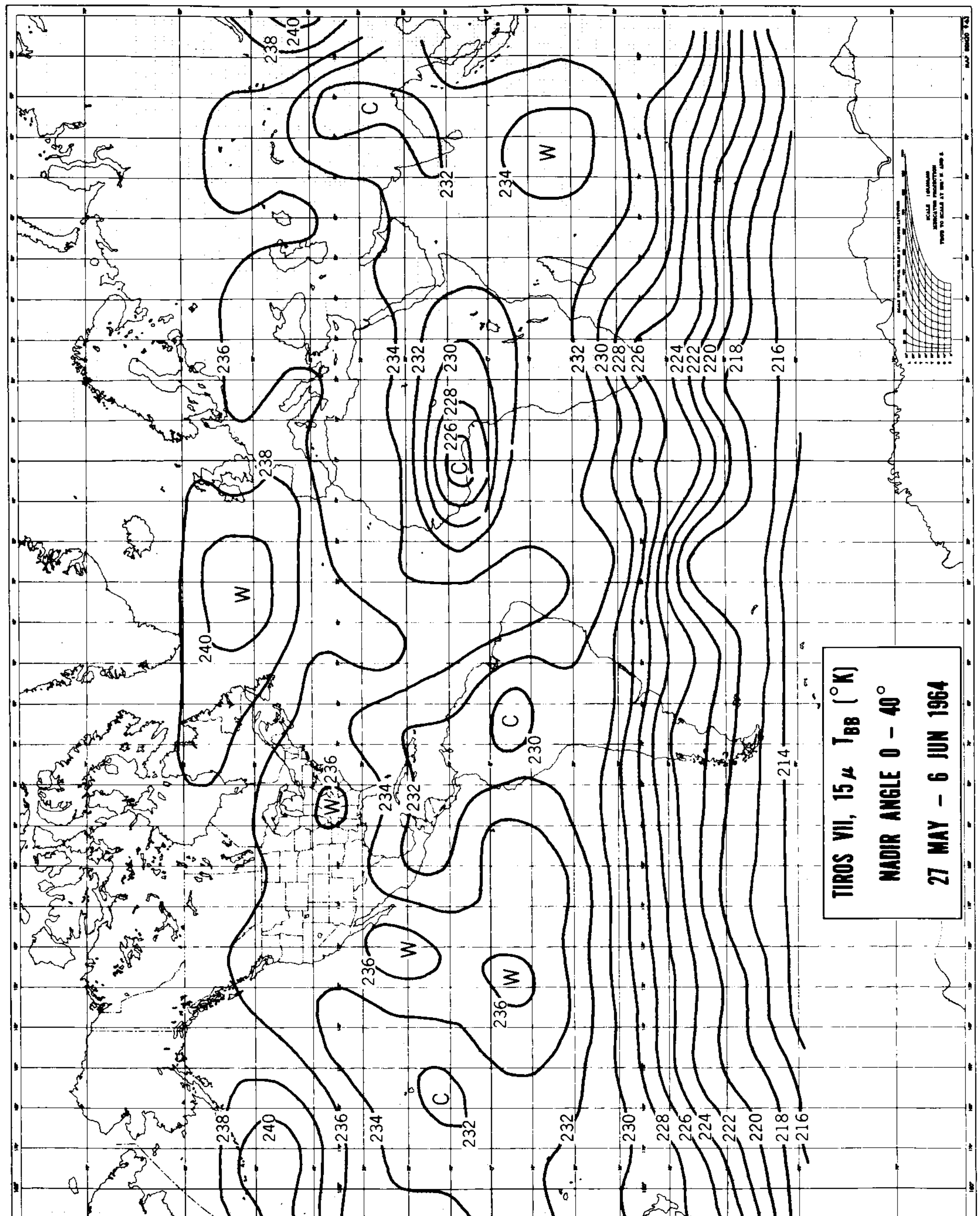
TIROS VII, 15μ T_BB (°K)
NADIR ANGLE 0 – 40°
27 MAY – 6 JUN 1964

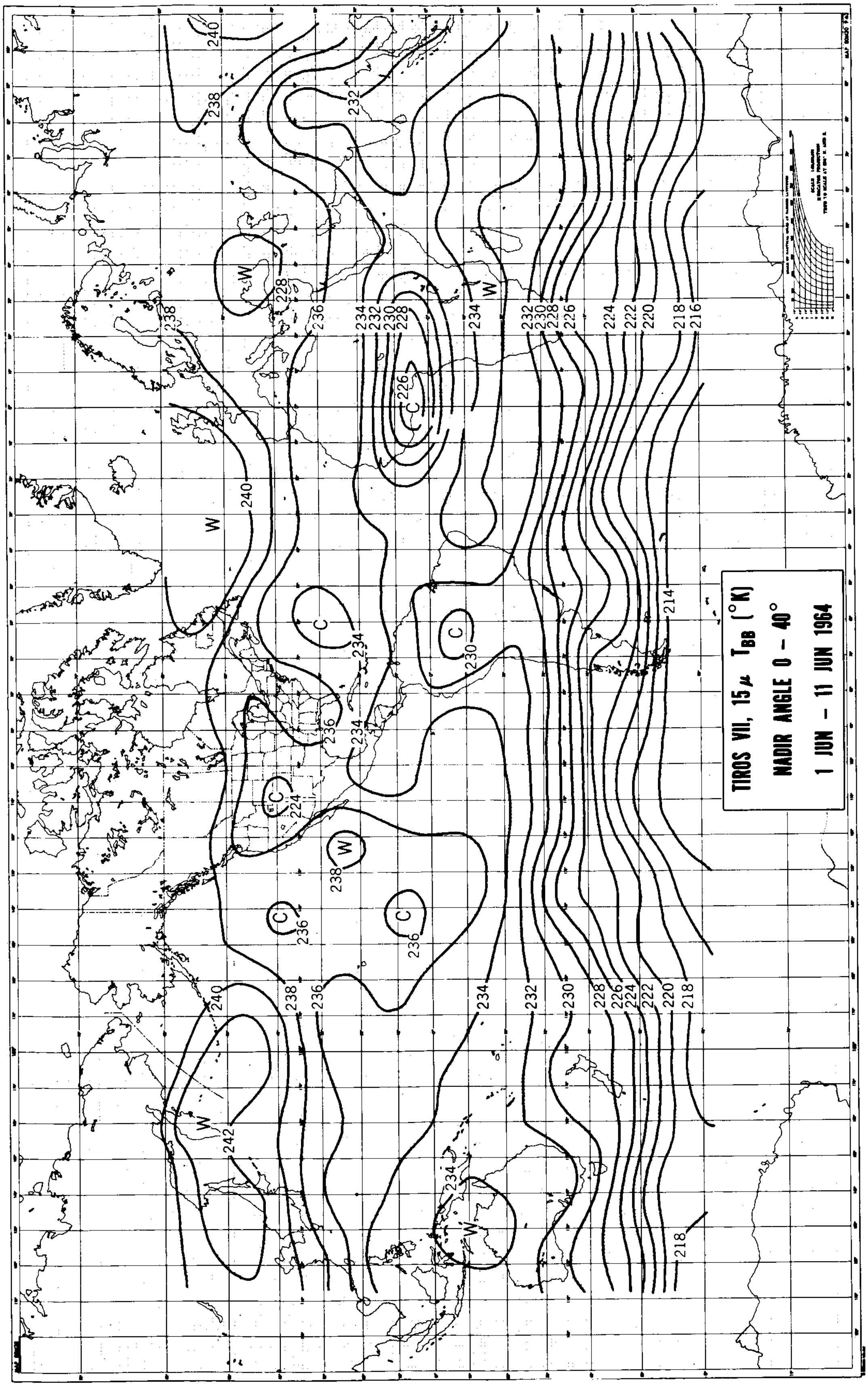
TIROS VII, 15μ T_BB (°K)
NADIR ANGLE 0 – 40°
1 JUN – 11 JUN 1964

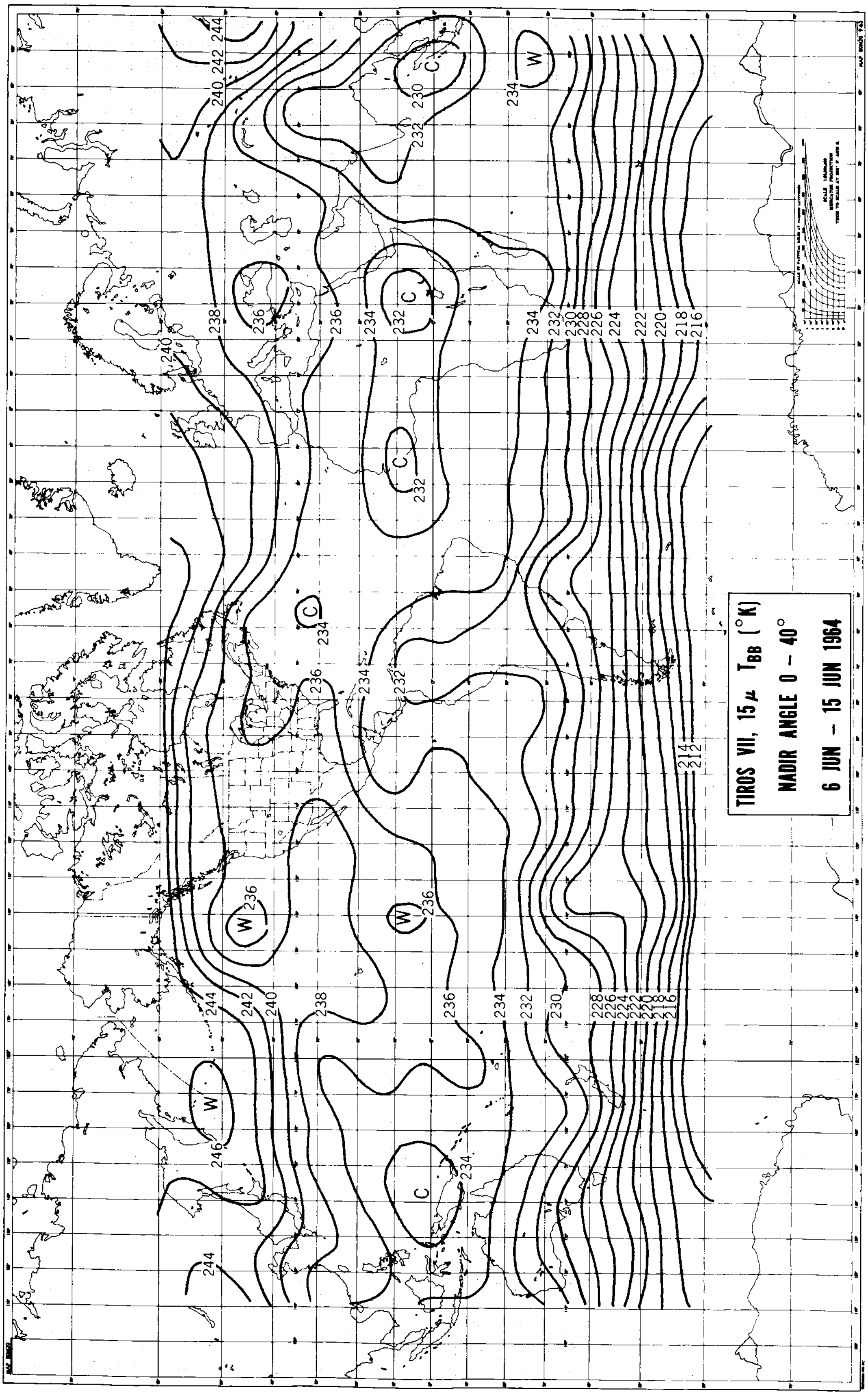
TIROS VII, 15 μ T$_{BB}$ (°K)
NADIR ANGLE 0 – 40°
6 JUN – 15 JUN 1964

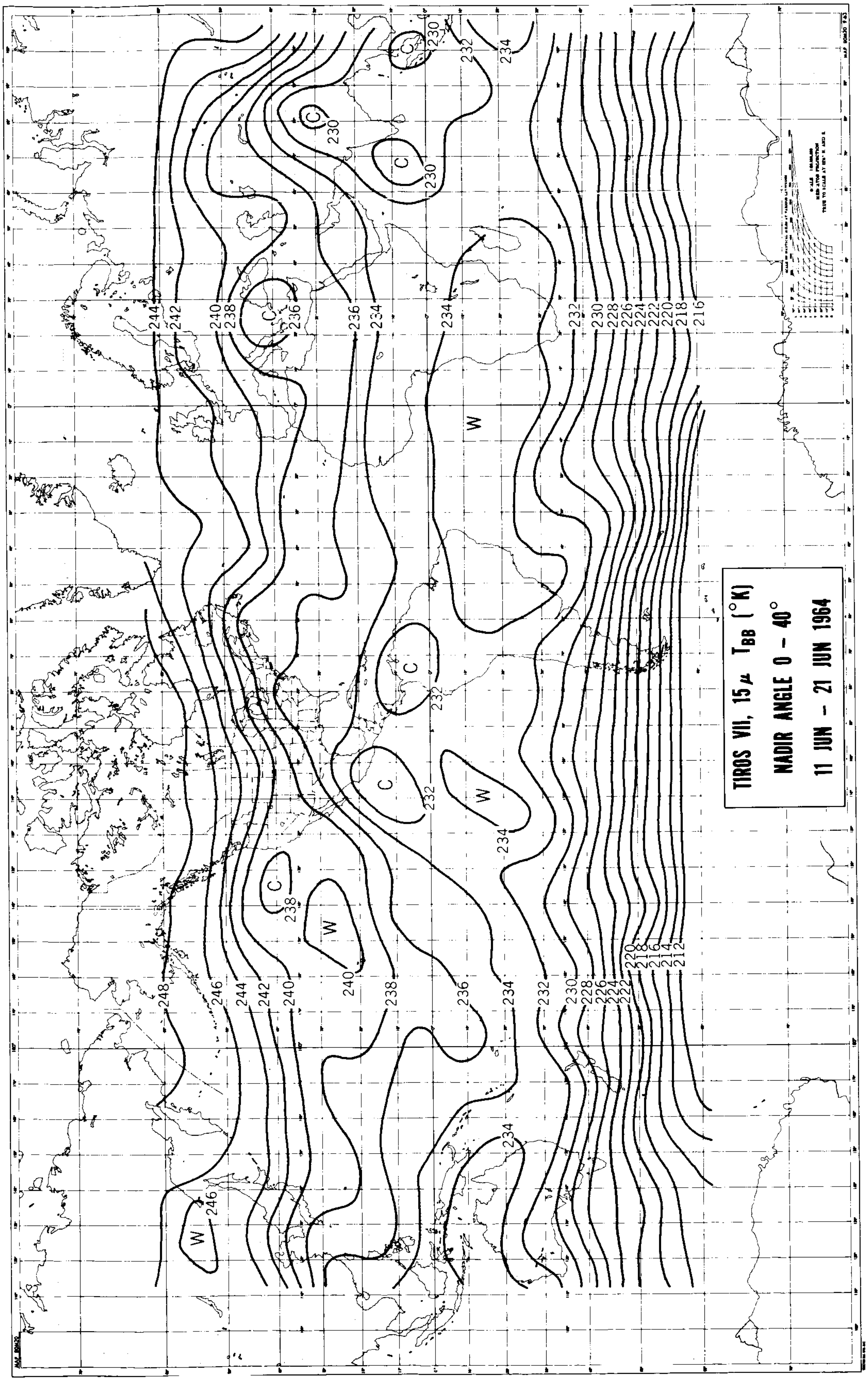
TIROS VII, 15 μ T$_{BB}$ (°K)
NADIR ANGLE 0 – 40°
11 JUN – 21 JUN 1964

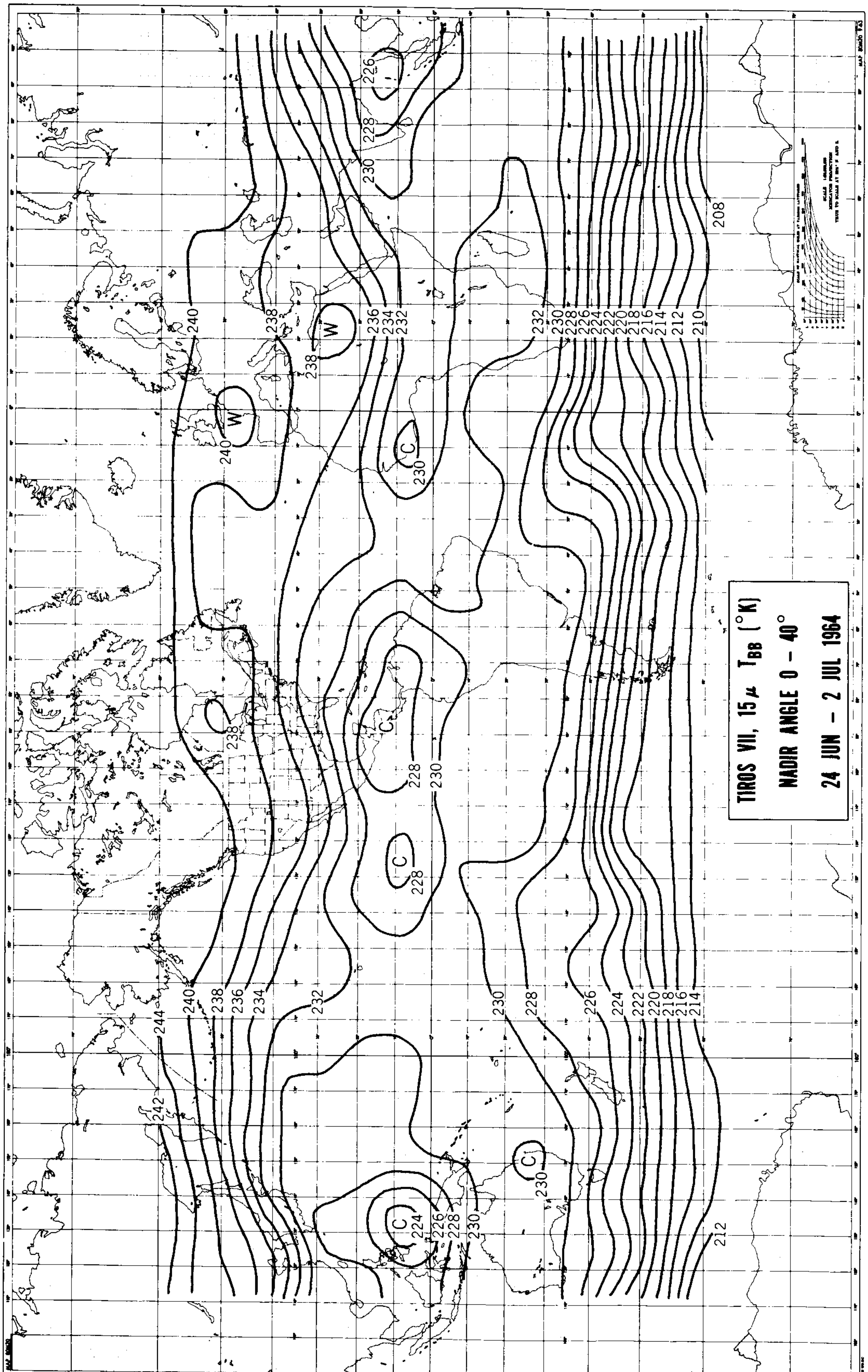
TIROS VII, 15 μ T_BB (°K)
NADIR ANGLE 0 - 40°
24 JUN - 2 JUL 1964

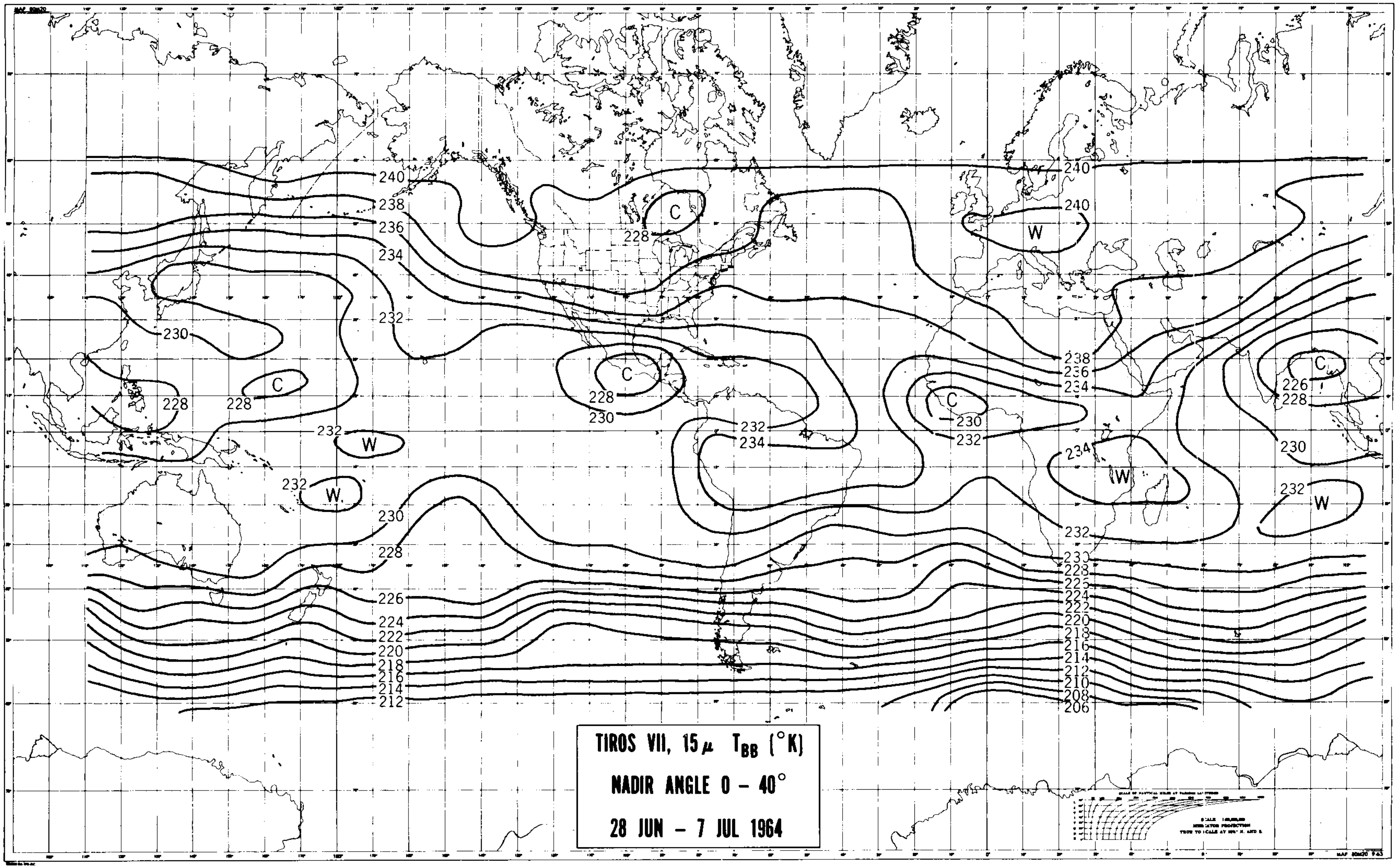
TIROS VII, 15μ T_{BB} (°K)
NADIR ANGLE 0 – 40°
28 JUN – 7 JUL 1964

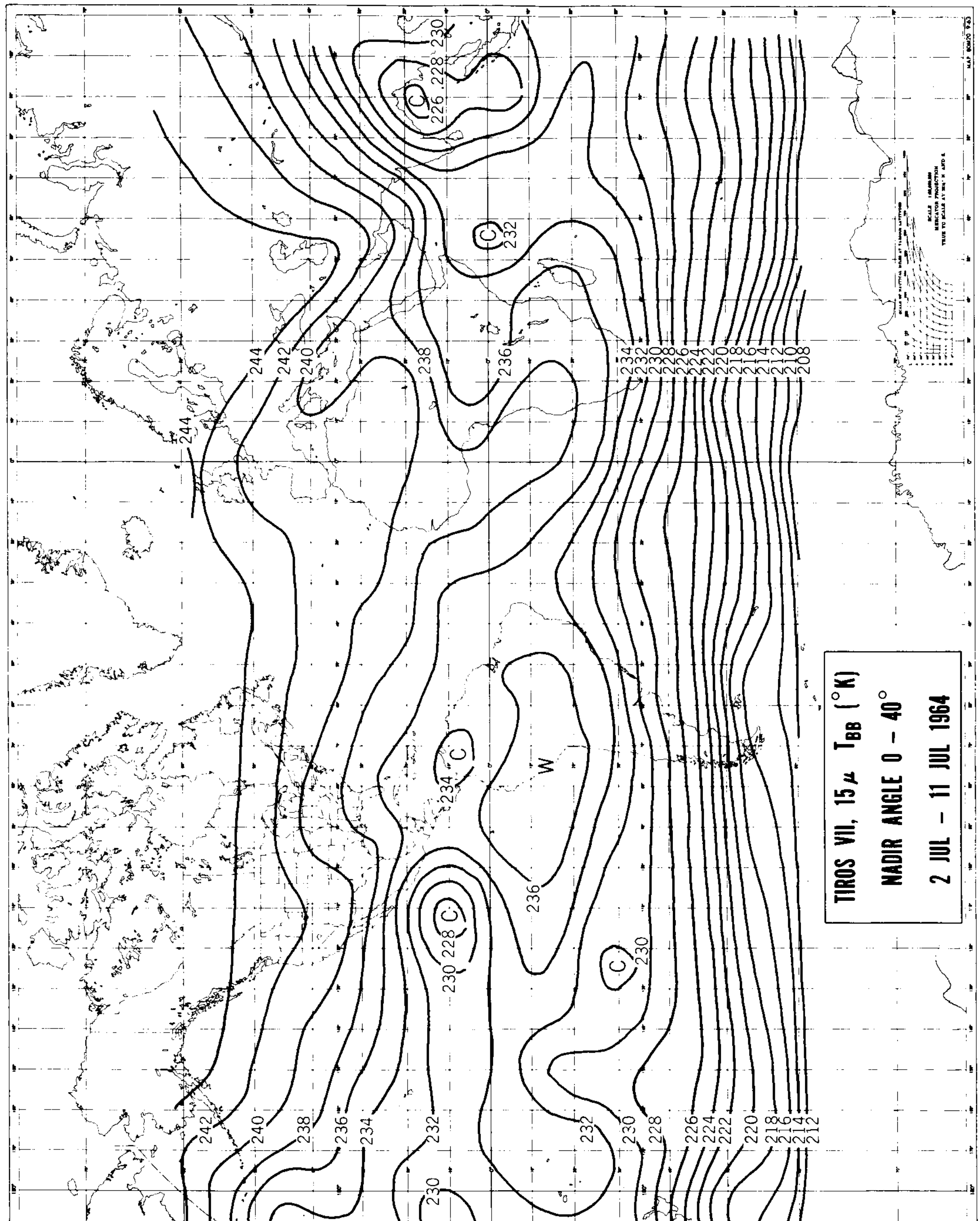
TIROS VII, 15μ T_{BB} (°K)
NADIR ANGLE 0 – 40°
2 JUL – 11 JUL 1964

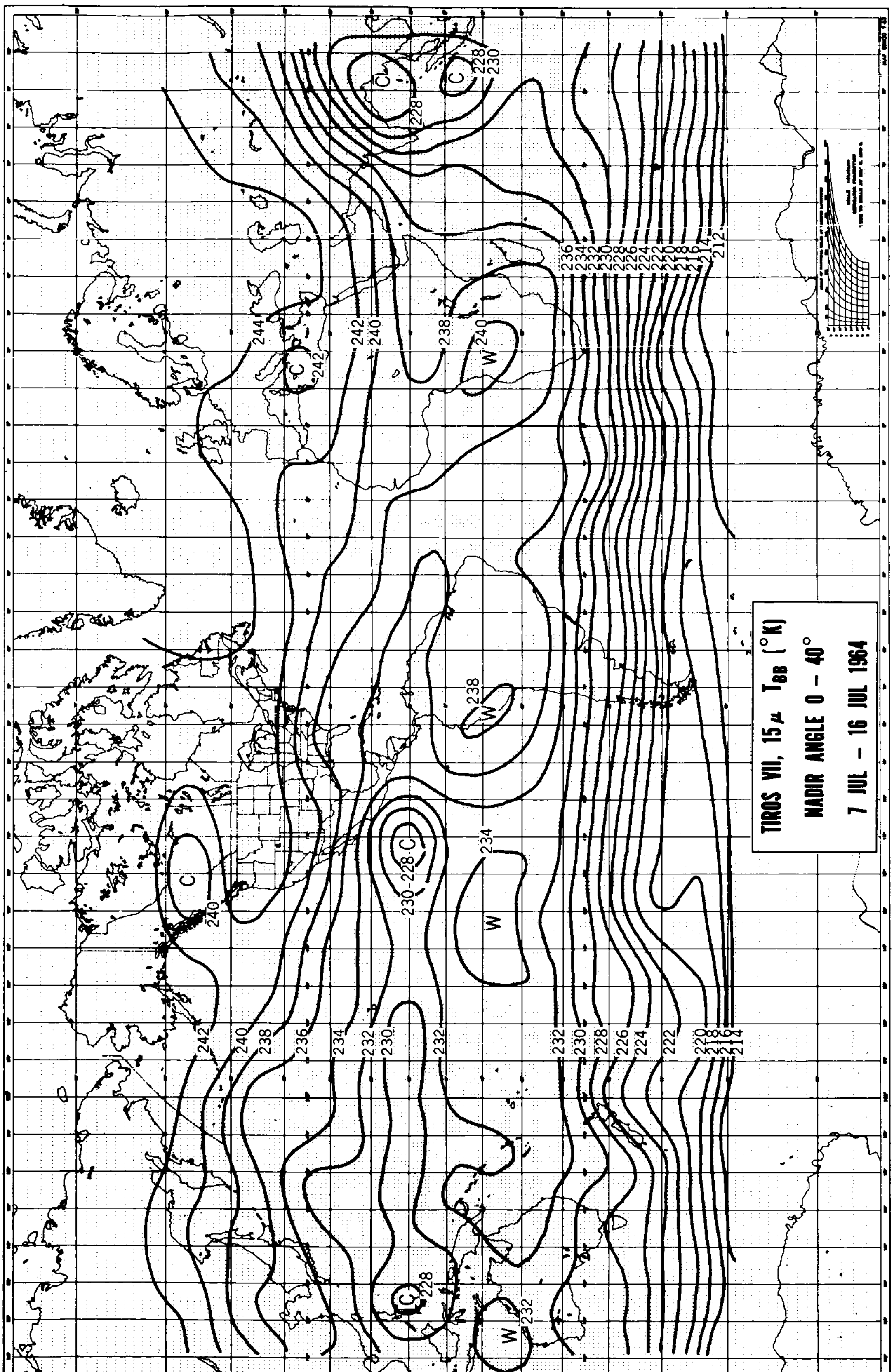
TIROS VII, 15 μ T_BB (°K)
NADIR ANGLE 0 – 40°
7 JUL – 16 JUL 1964